A Szilikátipari Tudományos Egyesület lapja

építőanyag

Journal of Silicate Based and Composite Materials

A TARTALOMBÓL:

2018/2


TUNGSRAM
Innovation is our heritage
EST.1896
INNOVATUNGSRAM
Tungsram returns to the market as an innovative, premium brand with design, development and manufacturing in Europe and a commitment to continue and expand its outreach.
tungsram.com

építőanyag

Journal of Silicate Based and Composite Materials

2018/2

TARTALOM

CONTENT

A finomkerámia-, üveg-, cement-, mész-, beton-, tégla- és cserép-, kő- és kavics-, tűzállóanyag-, szigetelőanyag-iparágak szakmai lapja
Scientific journal of ceramics, glass, cement, concrete, clay products, stone and gravel, insulating and fireproof materials and composites

A folyóiratot referálja · The journal is referred by:
Cambridge Scientific Abstracts
ProQuest

A folyóiratban lektorált cikkek jelennek meg.
All published papers are peer-reviewed.
Kiadó · Publisher: Szilikátipari Tudományos Egyesület (SZTE)
Elnök · President: ASZTALOS István
1034 Budapest, Bécsi út 122–124.
Tel.: +36-1/201-9360 ▪ E-mail: epitoanyag@szte.org.hu
Tördelő szerkesztő · Layout editor: NÉMETH Hajnalka
Címlapfotó · Cover photo: KÓSA Luca Kornélia

WWW.EPITOANYAG.ORG.HU
EN.EPITOANYAG.ORG.HU

Online ISSN: 2064-4477
Print ISSN: 0013-970x
INDEX: 2 52 50 ▪ 70 (2018) 33–72

Vol. 70, No. 2

Pre-surface preparation features when applying wear resistant composite sprayed coatings

Jüri OLT ▪ Institute of Technology, Estonian University of Life Sciences ▪ jyri.olt@emu.
Viacheslav V. MAKSAROV ▪ Department of Mechanical Engineering, Saint-Petersburg Mining University ▪ maks78.54@mail.ru
Victor A. KRASNYY ▪ Department of Mechanical Engineering, Saint-Petersburg Mining University ▪ vikras1955@yandex.ru

Érkezett: 2017. 11. 14. ▪ Received: 14. 11. 2017. ▪ https://doi.org/10.14382/epitoanyag-jsbcm.2018.7

Abstract

In this paper we consider the use of composite metal sprayed coatings for the improvement of the abrasion resistance levels in the working surfaces of friction couples. It is noted that pre-surface preparation, which provides the proper surface roughness that improves the adhesion of the coating to the base, is an important processing step prior to applying such coatings. As a method which enhances the adhesion strength of the sprayed coating, we consider the jet-abrasive (shot-blasting) treatment to be ideal. The object of our research was the compression piston rings the internal combustion engine with a composite steel-molybdenum coating. Such coatings provide high abrasion resistance for the rings of a good many large-sized engines. The research that has been carried out allowed the conclusion to be reached that the surface roughness depends on abrasive blasting modes, and that it impacts upon the strength of adhesion between the coating and the base. We proposed the jet-abrasive processing modes, which provide the required roughness to the working surface of the piston ring before spraying.

Keywords: composite coatings, wear resistant sprayed coating, surface roughness, adhesive strength, abrasive jet machining, piston rings.
Kulcsszavak: kompozit bevontok, kopásálló szórt bevonat, felületi érdesség, tapadószilárdság, abrazív vízsugaras megmunkálás, dugattyúgyűrű.

Jüri OLT, DSc.
Professor at Estonian University of Life Sciences. His main research areas are fundamentals of production enginering, materials cutting and design of technological machinery.

Viacheslav V. MAKSAROV, DSc.
Professor at Saint-Petersburg Mining University, Head of Department of Mechanical Engineering since 2012 and Dean of Electromechanical Faculty since 2015. Spezializes in the field of dynamics of machining technological systems.

Victor A. KRASNYY, PhD.
Associate professor at Saint-Petersburg Mining University. Specializes in the field of technological methods of increasing wear resistance of machinery parts.

1. Introduction

Improving the reliability of modern machinery, reducing maintenance costs, ensuring competitiveness, extending useful life, and also carrying out machinery refurbishment by restoring units to like-new operating condition with the help of state-of-the-art technology are the priority trends in technology development.

The utilisation of protective and wear-resistant-coating application technologies, of which gas-thermal and plasma flame processes are preferred choices, is one of the radical methods available when it comes to solving this problem. Current coating equipment, materials, and technologies permit us to significantly reduce or exclude the effect of such factors as erosion, corrosion (including hot corrosion), cavitation, etc on the wear and tear of parts [1].

a) *b)*

Fig. 1. Gas-thermal (a) and plasma (b) spraying
1. ábra Gázlángos (a) és plazma (b) szórás

Gas-thermal and plasma flame composite coatings (*Figs. 1.a* and *1.b*) are used for equipment repair and hardening the working faces of new parts. Depending on the purpose of a coating and its operating conditions, the requirements can change for strict adherence to the principal parameters of a coating (ie. in terms of its composition, thickness, density, and adhesion) [2, 3].

Gas-thermal coatings are used extensively in the manufacture and repair of a number of essential combustion engine components, primarily in terms of cylinder-piston group parts (pistons and piston rings), crankshaft main and rod journals, and a number of other parts.

Abrasive jet machining of the base surface is used extensively as a preparatory operation before applying the spray coating. Such preparation work cleans the surface and upsets its thermodynamic equilibrium with the environment, breaking the chemical bonds of the base surface atoms: i.e. it is activated chemically. However, base surface activity reduces rapidly due to the chemical absorption of gases from the atmosphere and also thanks to oxidation. Besides this, machining roughens the surface, causing a temperature increase in the contact surfaces of deposited particles and roughness peaks, and serving to increase the total area of the applicable welded surfaces. A rough surface has a larger area than a smooth one; this fact also contributes to increasing adhesion strength. Another factor which helps to determine the adhesion efficiency of roughness in the target surface is the volume of roughness cavities which ensures the necessary value of deposited layer shrinkage during cooling [2, 4].

The objective of this work is to study the relationship between the adhesion strength of the piston rings' gas-thermal wear-

resistant composite coating on the working surface's roughness following abrasive jet machining which, in turn, depends upon its prevailing conditions (the distance between the working surface and the nozzle exit, the number of passes, the operating air pressure, and the shot changing frequency).

In industrially advanced countries, the replacement of 'dirty' electrodepositing gas-thermal spraying is viewed as a solution to environmental problems. Many Russian and foreign authors propose various methods of applying protective and wear-resistant coatings, including the development and improvement of methods which involve spraying on various vital parts. The thermal spraying process diagram is shown in *Fig. 2.*

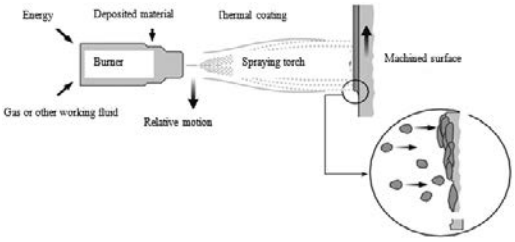

Fig. 2. Schematic diagram gas-thermal coating deposition
2. ábra Gázlángos szórás sémája

The process of applying coatings includes the following operations: preliminary preparation of the target surface in order to obtaining the firm adhesion of the material to be deposited; material preparation; coating application; and machining the coating after its application [1, 2].

When coatings more than 1.0 mm thick are deposited on load-bearing parts, special machining is also used. Such machining can be grouped into types as follows: knurling, notching, grooving, and 'ragged' thread cutting. Threads and grooves should not be deep. Excessive depth leads to excessive porosity and the blistering of fused coatings.

The target surface must be roughened in order to improve coating adhesion. Abrasive jet machining, etching, and electrosparking methods are all used for that purpose. Depositing an intermediate layer which consists of materials which have good levels of adhesion to the base metal is a method that has been used increasingly in recent years.

Abrasive jet machining is the most versatile method. Its advantages are connected with the capabilities involved even in the machining of large areas and oxide film removal from the target surface. Roughness levels depend upon the abrasive type, air pressure, the equipment used, and the surface hardness.

Primary machining of base surface is an important factor in ensuring firm adhesion of the deposited coating to the target surface, because in most cases the deposited coating has bonded with the base surface as a result of mechanical adhesion. Therefore the base surface must be rough enough so that the deposited particles that strike the base surface and are distorted are be bound rigidly to the surface asperities.

The increase in terms of mechanical adhesion strength is connected with the increase of the base surface area and making the base surface more active. This is also important for other types of adhesion. Therefore the intense roughening of the base surface is an important requirement.

Another method of machining the surface before applying the coating is shot blasting.

Shot blasting roughens the target surface. *Fig. 3* shows surfaces after shot blasting (a) and after applying the coating (b).

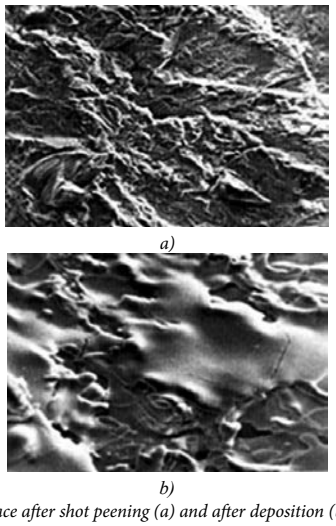

a)

b)

Fig. 3. The surface after shot peening (a) and after deposition (b)
3. ábra Előkészített felület felületdurvítást követően (a) és bevonat felhordást követően (b)

2. Piston ring surface machining for applying a wear-resistant coating

Operational experience regarding combustion engines demonstrates that their reliability depends to a large extent on the wear rate of the top piston rings as determined by their vibration and stress-strain behaviour, as well as on the composition and technology of the application of a wear-resistant coating which permits their structural composition to be controlled.

Coatings are deposited onto the working surfaces of piston rings in order to improve their terminological behaviour. This is an area in which improving wear resistance and ensuring lubrication and sealing under extreme operating conditions are to the foreground. The composite coating material must match the materials used in the construction of the piston ring and the cylinder wall, and also the engine oil. Coating the working surfaces of the piston rings has become widely used. Piston rings in mass produced engines are often coated with chrome, molybdenum, and ferric oxide.

One of the principal reliability factors is the limit to the service life which depends upon the wear resistance of friction couples. It is well known that the friction in piston rings amounts to as much as 50% of overall engine friction, with the work put in by the top compression ring providing the highest figure within this percentage. This is connected to the ring having to work under great temperatures (up to 200°C) and in a semi-suspended condition. However, the actual service life so far of the top piston rings has been much lower than the service life of other combustion engine cylinder-piston group parts. For example, the extensively used galvanic method of coating the working surfaces of piston rings with chrome reduces the wear rate by only 30% when compared to the figures exhibited by uncoated rings. This is manifestly insufficient, especially under

great combustion pressures in cylinders which are typical for high-power combustion engines. As the compression intensity increases in combustion engines, previously used technologies which involved depositing porous chrome coatings onto the piston rings meet increasingly stringent requirements for coatings under higher temperatures and pressures to a lesser extent.

In coatings which are based on the use of deposited molybdenum and its compounds, these are often deposited on the top compression rings in the manufacture of piston rings for larger-sized engines used in haulage lorries, diesel locomotives, etc. (*Figs. 4.a* and *4.b*). Molybdenum ensures high thermal resistance thanks to its high melting point (2,620°C). Besides, by using this method of applying the coating it is possible to obtain a porous structure in the material. Motor oil can remain in microcavities on the working surfaces of the rings (*Fig. 4.b*), thereby preventing scouring under extreme operating conditions. Under these circumstances the coating thickness reaches between 0.5–1 mm and even more.

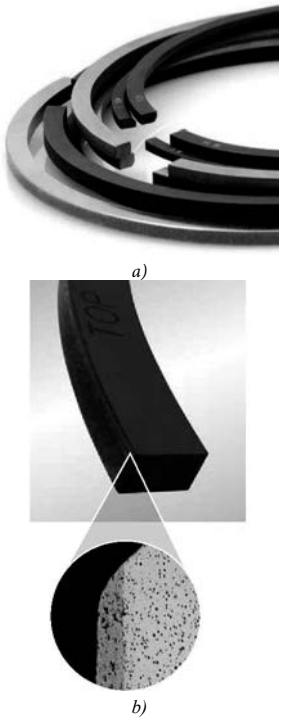

a)

b)

Fig. 4. Design types of top compression piston ring (a) and molybdenum coating ring (b)
4. ábra Dugattyúgyűrűk tervezési formái (a) és molibdén bevonatos gyűrű (b)

Coating to base bonding strength is doubtlessly a condition of the normal operation of rings that are coated with wear-resistant coatings. As a piston ring operates in an engine, tensions linked to external forces are being applied to the rings and high temperatures arise in the adhesion contact area. Therefore the adhesive strength of the wear-resistant coating is a very important operational characteristic of piston rings in combustion engines. To a large extent, this characteristic depends upon the base surface pre-machining method. Shot blasting is used prior to the application of gas-spray coatings (in particular, the molybdenum coatings) on piston rings of large-sized combustion engines. The task of ensuring the necessary surface micro-relief and shot-blasting conditions prior to the application of the wear-resistant gas-thermal coating is critical.

3. A discussion of the research findings

Our work considered a composite steel-molybdenum coating which was obtained from molybdenum wire and steel wire and deposited by using the gas-thermal method on the working surface of piston rings of a 210 mm diameter.

Prior to applying the coating, a total of twenty rings were placed on a mandrel, and a trapezoid groove was turned on the working surface of each of them. Afterwards, the rings were shot-blasted and coated with a gas-thermal coating on the same mandrel.

Adhesion strength was determined by the twist angle α at which the coating on finished rings sagged. The relationship between twist angle α and roughness parameter R_z was determined by the use of the indirect method. At first, the relationship between R_z and α and the shot change frequency n was discovered, and then their mutual dependence was assessed.

Abrasive jet machining was carried out under the following conditions:

- distance between the working surface and nozzle exit: 130 mm;
- operating air pressure: 0.4 MPa;
- number of passages: 2;
- mandrel rotation frequency: 17 min^{-1};
- nozzle's angle of attack: 80°.

The shot was changed after the machining of 35, 40, and 43 mandrels with rings. The roughness of the ring specimens was measured on a model 201 profilograph/profilometer.

At first, we determined the relationship between the ring specimens' roughness R_z and the shot change frequency n as represented in *Fig. 5.a*. It is evident that the roughness ensured by the newer shot is higher than it is in the older version.

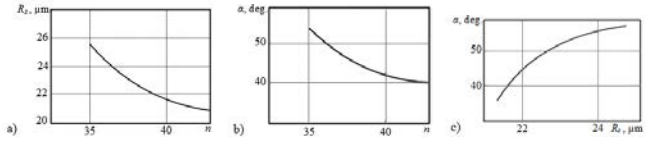

Fig 5

Fig. 5. Relationship between roughness Rz (a) and twisting angle α (b) and shot changing frequency and between and twisting angle α and surface roughness R_z after abrasive jet machining (c)
5. ábra Összefüggés a felületi érdesség Rz (a) és az elfordulási szög α (b) között valamint a lövési frekvencia és az elfordulási szög α és a felületi érdesség R_z között abrazív vízsugaras megmunkálást követően (c)

The results of tests aimed at determining the twist angle α at which the coating would delaminate depending on the shot change frequency are shown in *Fig. 5.b*. The twist angle varied from 57° at n = 35 to 39° at n = 43.

A study of the results presented in *Figs. 5.a* and *5.b* means that the relationship between twist angle α and roughness R_z (*Fig. 5.c*) can be obtained. It can be seen that, within the roughness variation range being studied, the aforementioned relationship is approximated as a virtually linear one, i.e. adhesion strength increases as surface roughness increases.

Therefore, when taking into account the fact that as operational experience shows, the piston rings operate normally when the coating separates at twist angles exceeding 35°, so that one can conclude that shot must be changed after

machining a maximum of forty mandrels. The minimum roughness in this case would be limited to $R_z \geq 22$ μm.

In the second series of tests which were aimed at ensuring the required surface roughness following abrasive jet machining, various conditions for such machining were studied and their relationship with roughness parameters were uncovered. In each set of experiments, one of the machining parameters varied: the distance between the working surface and the nozzle exit, the number of passages, or the operational air pressure, while two other characteristics remained unchanged.

In the first set of experiments, the distance between the working surface and the nozzle exit varied (70 mm, 90 mm, 110 mm, 130 mm, and 150 mm). Machining was carried out in two passes at a 0.4 MPa operational air pressure. *Fig. 6.*a demonstrates that 110 mm should be used as the optimum distance between the working surface and the nozzle exit both for the new shot method and for shots after machining a total of forty mandrels.

In the second set of experiments, the number of passages varied (k = 1, 2, 3). The distance between the working surface and the nozzle exit was set at 110 mm and the operational air pressure was at 0.4 MPa. As illustrated in *Fig. 6.b*, k = 2 should be considered as being the optimum value.

In the third series, the operation air pressure varied (P = 0.35 MPa, 0.40 MPa, and 0.45 MPa). The number of passes was set at two and the distance between the working surface and the nozzle exit was 110 mm. P = 0.4 MPa should be considered as being the optimum figure with regard to obtaining the necessary roughness (*Fig. 6.c*).

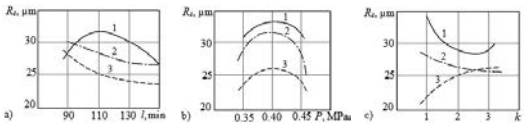

Fig. 6. Relationship between surface roughness and abrasive jet machining conditions: distance between Workpiece and Nozzle Exit (a), number of passages (b), operation air pressure (c): 1 – new shot; 2 – shot after machining 20 mandrels; 3 – shot after machining 40 mandrels

6. ábra Összefüggés a felületi érdesség és az abrazív vízsugaras megmunkálás körülményei között: távolság a munkadarab és a fúvóka között (a), ismétlésszám (b), működési levegőnyomás (c): 1 – első lövés; 2 – lövés 20 tüske megmunkálás után; 3 – lövés 40 tüske megmunkálás után

It can be seen that our studies resulted in the discovery of the relationship between the adhesion strength of the gas-thermal wear-resistant coating on the piston rings and the roughness of the working surface following abrasive jet machining and establishing machining conditions which ensure the optimum levels of roughness: operational air pressure - 0.4 MPa; number of passages - two; distance between the working surface and the nozzle exit – 110 mm. The shot must be changed following the abrasive jet machining of a maximum of forty mandrels with rings.

4. Conclusions

1. Surface roughness obtained as a result of abrasive jet machining exerts a considerable level of impact upon the adhesion strength of coating as obtained by gas-thermal and plasma flame spraying.

2. Spray coatings based on molybdenum and its compound are extensively used in the manufacture of piston rings for large-size combustion engines. Coating adhesion to the base surface is closely associated with obtaining the necessary levels of roughness and abrasive jet machining conditions.

3. We have proposed the use of abrasive jet machining conditions (operation air pressure: 0.4 MPa, distance between working surface and nozzle exit – 110 mm, number of passages – two, shot change needed after machining forty mandrels), which ensure the required roughness levels in the piston ring's working surface (Rz ≥ 22 μm) prior to applying the coating.

References

[1] Drozdov, Y. N. – Yudin, E. G. – Belov, A. I. (2010): Applied tribology (friction, wear and lubrication) Eco-Press. Moscow. 604 pp.

[2] Suslov, A. G. – Fedorov, B. N. – Gorlenko, O. A. (2006): Technological support and enhance the operational properties of parts and their connections. *Mechanical Engineering*, Moscow, 448 pp.

[3] Maksarov, V. – Krasnyy, V. (2017): The formation of surface roughness of piston rings for the purpose of improving the adhesion of wear-resistant coatings. *Key Engineering Materials*, Vol. 736, pp. 73–78. https://doi.org/10.4028/www.scientific.net/KEM.736.73

[4] Krasnyy, V. – Maksarov, V. – J. Olt. (2016): Increase of wear and fretting resistance of mining machinery parts with regular roughness patterns. *Annals of DAAAM and Proceedings of the International DAAAM Symposium*. Vol. 17, Issue 1, pp. 151–156. https://doi.org/10.2507/27th.daaam.proceedings.023

[5] Holmberg, K. – Matthews, A. (2009): Coatings Tribology – Properties, Mechanisms, Techniques and Applications in Surface Engineering, Tribology and Interface Engineering Series 56, Elsevier, Amsterdam, 560 pp.

[6] Musil, J. (2000): Hard and super hard nanocomposite coatings. *Surface and Coatings Technology.* Vol. 125, Issue 13, pp. 322–330. https://doi.org/10.1016/S0257-8972(99)00586-1

[7] Agarwala, R.C. – Agarwala, V. (2003): Electroless alloy/composite coatings. A review. *Sadhana – Academy Proceedings in Engineering Sciences*, Vol. 28, Issue 3-4, pp. 475–493.

[8] Kamo, L. – Saad, P. – Saad, D. – Bryzik, W. – Mekari, M. H. (2007): Diesel Engine Cylinder Bore Coating for Extreme Operating Conditions, *SAE Technical Paper*, 2007-01-1439, https://doi.org/10.4271/2007-01-1439

[9] Shaffer, S. J. – Rogers, M. J. (2007): Tribological performance of various coatings in unlubricated sliding for use in small arms action components – A case study. *Wear*, Vol. 263, Issue 7-12, pp. 1281–1290. https://doi.org/10.1016/j.wear.2007.01.115

[10] Donnet, C. – Erdemir, A. (2003): Historical developments and new trends in tribological and solid lubricant coatings. Saint-Etienne, France: Elsevier B.V.

[11] Loomis, W. (1985): New Directions in Lubrication, Materials, Wear, and Surface Interactions. Park Ridge, New Jersey: Noyes Publications.

[12] Sigmund, P. (1987): Mechanisms and theory of physical sputtering by particle impact. *Nuclear Instruments and Methods in Physics Research*, Section B, Beam Interactions with Materials and Atoms 27: 1. https://doi.org/10.1016/0168-583X(87)90004

[13] Krasnyy, V. A. – Maksarov, V. V. – Olt, J. (2015): The use of polymer composite materials in the friction nodes downhole oil pumps. *Notes of the Mining Institute*. 2015. Vol. 211, pp. 71–79.

[14] Krasnyy, V. – Maksarov, V. – Olt, J. (2016): Improving fretting resistance of heavily loaded friction machine parts using a modified polymer composition. *Agronomy Research*, Vol. 14, Special Issue 1, pp. 1023–1033.

Ref.:

Olt, Jüri – **Maksarov**, Viacheslav V. – **Krasnyy**, Victor A.: *Pre-surface preparation features when applying wear resistant composite sprayed coatings*

Építőanyag – Journal of Silicate Based and Composite Materials, Vol. 70, No. 2 (2018), 34–37. p.

https://doi.org/10.14382/epitoanyag-jsbcm.2018.7

Rheological parameters of some soil samples before and after H_2O_2 treatment

Dolgor KHAYDAPOVA ▪ Department of Soil Science, Lomonosov Moscow State University ▪ dkhaydapova@yandex.ru
Liesl WIESE ▪ Department of Soil Science, Stellenbosch University
Andrei ROZANOV ▪ Department of Soil Science, Stellenbosch University
Evgeny MILANOVSKIY ▪ Department of Soil Science, Lomonosov Moscow State University

Érkezett: 2017. 11. 19. ▪ Received: 19. 11. 2017. ▪ https://doi.org/10.14382/epitoanyag-jsbcm.2018.8

Abstract
The effect of soil organic matter (SOM) on formation of inter-particle bonds was studied in soils with high organic and no mineral carbon content in the top (A1, Ap) layers of different origin and under various land uses. The first set of soil samples was collected in the Alekhin Central Chernozem Reserve (Kursk region, Russia): under native steppe vegetation and under 67-year-old bare fallow. The second set of samples was sourced from the Midlands of Kwa-Zulu Natal, South Africa: under pine plantation and under long-term maize monoculture. Soil organic matter was removed by of 30% hydrogen peroxide (H_2O_2) treatment for 20-40 days. The rheological behaviour of the capillary-wetted soil pastes was characterized by amplitude sweep test with the modular compact rheometer MCR-302 (Anton-Paar, Austria). The storage modulus in linear viscous-elasticity range (LVE-range) and crossover of storage modulus and loss modulus were determined. The samples treated with H_2O_2 in all cases except the Ferralsol under pine plantation, increased the storage modulus in the LVE-range. It shows more rigid particle interaction due to loss of SOM. The peculiarity of soil under pine plantation is very high resistance to stress in native state and loss of this resistance upon SOM oxidation or removal. We connect this with significant change in particle size distribution upon the H_2O_2 treatment. In contrast to other samples, this soil shows significant reduction in coarse silt fraction (from 44.5 to 23.2%) and an increase in clay content (from 10.8 to 36.5). We connect the observed differences to the type of organic matter inputs. Unlike the herbaceous vegetation, pine plantations lead to significant accumulation of plant litter on the soil surface. The dissolved organic matter (DOM) is leached out of the litter layer by percolating water. The sorption of DOM (ligand exchange, cation bridges, hydrophobic interactions) on the mineral surfaces contributes to particle aggregation.
Keywords: soil, structure, organic matter, rheology, amplitude sweep test
Kulcsszavak: talaj, szerkezet, szervesanyag, reológia, változó frekvenciájú nyírásvizsgálat

Dolgor KHAYDAPOVA
Associate professor at the M. V. Lomonosov Moscow state University, Department of Soil Science. Specializes in the study of soil structure, soil physics, soil rheology.

Evgeny MILANOVSKIY
Leading researcher at M. V. Lomonosov Moscow state University, Department of Soil Science. Specializes in the study of soil organic matter, soil structure, soil physics.

Liesl WIESE
Ph.D. student, Stellenbosch University, Department of Soil Science. Specializes in the study of soil organic matter.

Andrei ROZANOV
Senior lecturer, Stellenbosch University, Department of Soil Science. Specializes in the study of soil.

1. Introduction

Study of rheological properties of soils are very important for the assessment of soil structure, its resistance to slaking in water and to mechanical stress. The soil structure in turn determines: 1) the structure of the soil pore space as the condition for the optimal development of the plant root system; 2) the soil reaction to compaction under the influence of heavy agricultural machinery; 3) the preservation of organic carbon in occluded form and prevention of its emission into the atmosphere. The soil organic matter represents one of the largest carbon pools in terrestrial ecosystems and affects all soil functions. The formation and stability of soil aggregates is largely due to the presence of the humic substances as "adhesive" [1,4]. Hence, the soil organic carbon (SOC) content strongly affects the soil aggregate stability [10].

Rheological approach to study of the soil structure in recent years has become actively used by researchers as a promising method of quantifying the inter-particle interactions [2,3,5,6,7,8]. Baumgarten and Horn [5] were the first to apply the method of amplitude sweep on a rheometer MCR to study soil structure.

In this work we attempt to identify the role of soil organic matter derived from different plant communities on the rheological behaviour of soils of different genesis. The dependence of soil organic matter (SOM) in the top soil horizons of different genesis and under different land use on formation of interpartial structural bonds is analyzed.

2. Materials

The first set of soil samples is from the Alekhin Central Chernozemic Reserve (Kursk region, Russia): 1a – Chernozem under native steppe vegetation (51°34'19.6"N 36°05'37.3"E) and 1b – Chernozem under bare fallow since 1947 (51°34'12.6"N 36°05'22.3"E). According to the WRB (2006) both soils are Chernozem pachic voronic (Fig.1).

The second set of samples is from the Midlands of Kwa-Zulu Natal, South Africa [11]: 2a – Umbric Ferralsol under pine plantation (Location GPS coordinates S29.23062° *E030.32897*°), 2b – cultivated Plinthic Ferralsol under long-term maize (Location GPS coordinates monoculture*S29.19399*° *E030.50589*° (*Fig. 1*). The texture of voronic chernozem pachic can be characterized as silt loam, Humic Haplustox under

forestry plantation – as silt loam and Plinthic Haplustox of farming – as silty clay loam. The studied examples of soil do not contain carbonate salts or lime.

1 a) 1 b)

2 a) 2 b)

Fig. 1. Objects of research; 1a) - chernozem under native steppe vegetation; 1b) - chernozem old (since 1947) bare fallow; 2a) - Umbric Ferralsol under pine plantation; 2b) - cultivated Plinthic Ferralsol under long-term maize

1. ábra A kutatás témái; 1a) – Csernozjom természetes sztyeppe vegetáció alatt; 1b) – Öreg csernozjom (1947 óta) parlagon fekvő ugar; 2a) - Umbric Ferralsol fenyő növényzet alatt; 2b) - Művelt Plinthic Ferralsol kukorica alatt

3. Methods of research

Particle size distribution was determined by laser diffraction (Analysette 22 Comfort, Fritsch, Germany) after the dispersion of soil suspension in water by ultrasound for 5 min. Content of total carbon was determined with a CHN analyzer (Vario EL, Elementar). Organic matter was removed by sample treatment with 30% hydrogen peroxide (H_2O_2) for 20-40 days. Rheological properties of capillary-moistened soil pastes were determined by amplitude sweep test on a modular compact rheometer MCR-302 (Anton-Paar, Austria) [3,5,9]. The following parameters of rheological behavior were obtained: Storage Modulus in the range of linear viscoelasticity (LVE range), the range of linear viscoelasticity, the point of crossover of Storage Modulus and Loss Modulus, which describes the destruction of the elastic structure of the substance (*Fig. 2*). The studies were conducted in three replicates, average values are presented in this work

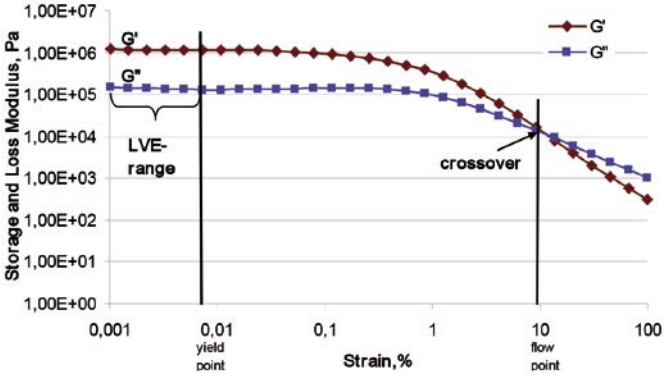

Fig.2. Amplitude sweep test

2. ábra. Változó frekvenciájú nyírásvizsgálat

4. The obtained results

The soil organic matter (SOM) content before and after H_2O_2 treatment is presented in *Table 1*. The SOM content after oxidation significantly decreased.

The content of organic matter (%) before and after oxidation

Sample Name	Content of organic matter in initial samples,%	Content of organic matter after oxidation,%
Chernozem under native steppe vegetation	6.7	0.52
Chernozem old (since 1947) bare fallow	3.14	0.08
Umbric Ferralsol under pine plantation	12.5	2.55
Cultivated Plinthic Ferralsol under long-term maize	2.9	0.42

Table 1. Organic matter content of samples

1. táblázat. Minták szervesanyag tartalma

In Chernozem under steppe vegetation after treatment with hydrogen peroxide the content of coarse silt slightly decreased and fine silt and medium silt increased. In Chernozem under long term bare fallow after treatment the content of fine silt increased, but that of coarse silt decreased. In Plintic Ferrasol under long-term maize after treatment the contents of coarse silt decreased and that of medium silt increased slightly.

In contrast to other samples, the soil from pine plantation shows significant reduction in coarse silt fraction (from 44.5 to 23.2%) and an increase in clay content (from 10.8 to 36.5). In the latter case the coarse silt fraction (50-10μm fraction) of untreated sample consists to a large extent of clay-SOM-clay micro-aggregates resistant to 400 J ml^{-1} of ultrasonic dispersion energy (Branson Ultrasonics, USA). SOM oxidation leads to disaggregation and changes in particle size distribution (*Fig. 3.c*). We see that in all cases (*Fig. 3*) there was a decrease in the content of coarse silt, which shows the removal of organic matter caused the destruction of microaggregates and the increase in the proportion of the finer fractions.

In all samples after removal of OM the storage modulus in the LVE-range increased, except for the ferralitic soil from the pine forest (*Fig. 4*).

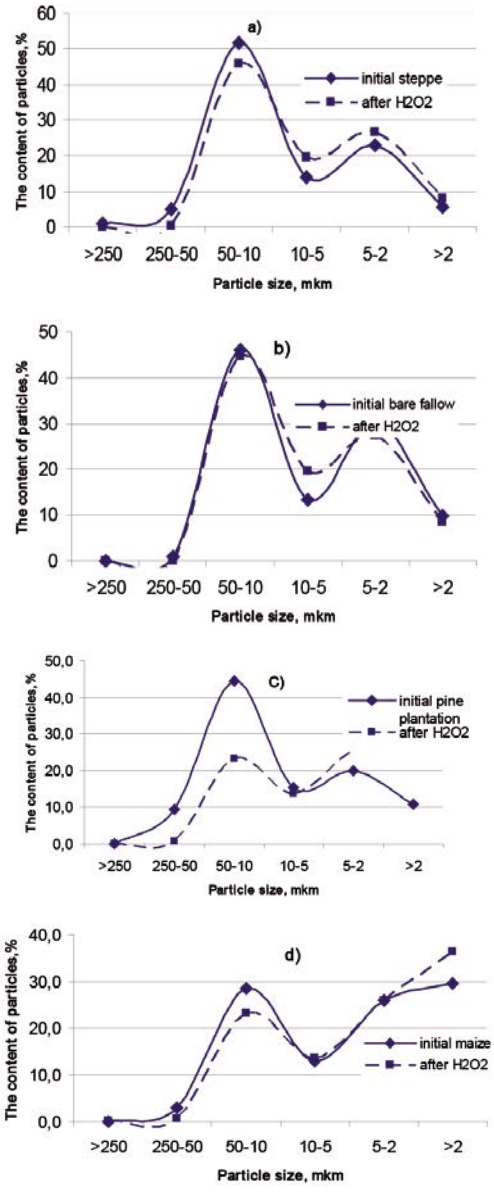

Fig. 3. Particles size distributions before and after oxidation of organic matter; a) in Chernozem under steppe vegetation; b) in Chernozem under long term bare fallow; c) in Ubric ferralsol under pine plantation; d) in Plinthic ferralsol under long term miaze.

3. ábra Szemcseméret eloszlás a szervesanyag oxidálása előtt és után; a) – Csernozjom természetes sztyeppe vegetáció alatt; b) – Öreg csernozjom (1947 óta) parlagon fekvő ugar; c) - Umbric Ferralsol fenyő növényzet alatt; d) - Művelt Plinthic Ferralsol kukorica alatt

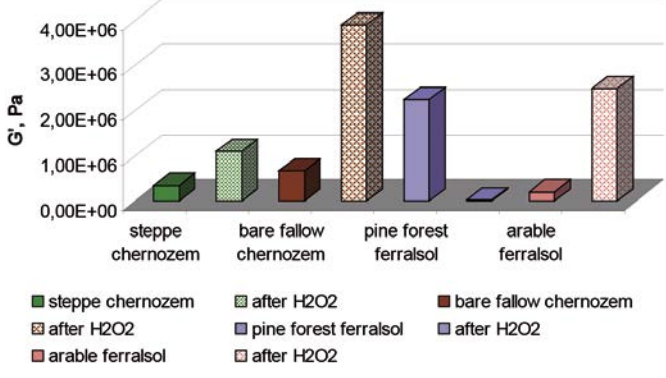

Fig. 4. Storage modulus before and after H_2O_2 treatment in Chernozems and Ferralsols

4. ábra Storage modulus H_2O_2 kezelés előtt és után Csernozjom és Ferralsol mintákban

Possible strengthening of inter-particle contacts in all the samples, except the soil from pine forest occurred due to the development of direct contacts between the rigid particles in the absence of SOM. The decrease of storage modulus in the soil from the pine plantation may be due to a significant increase in the content of the fine silt and clay fractions after removal of SOM. It accordingly absorbs more water and reduces strength of inter-particle contacts. A significant increase in the modulus of elasticity in the arable soils likely associated with a significant decrease in the content of SOM after oxidation or removal. The increase in the strength of bonds between soil particles probably causes block-like soil structure.

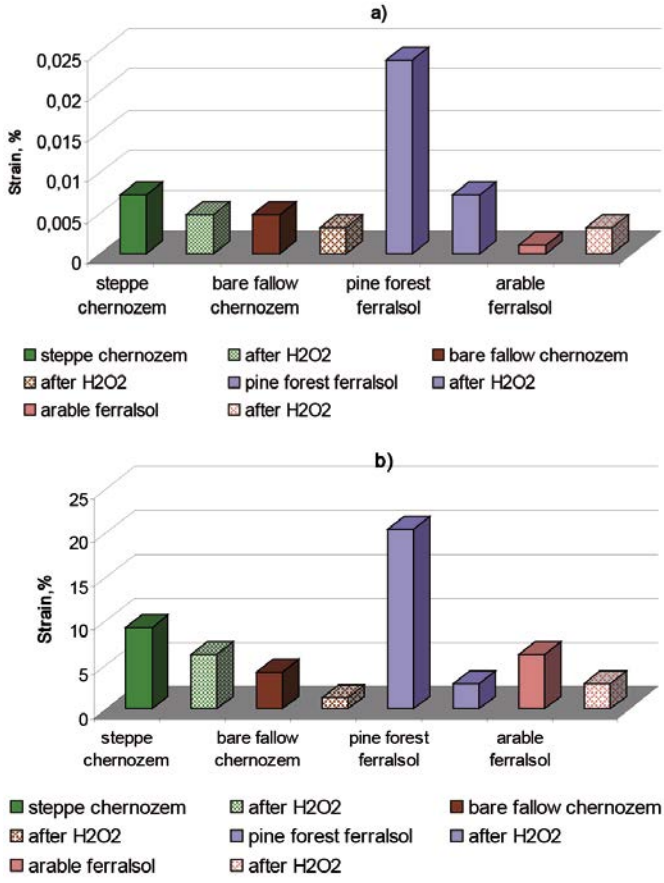

Fig. 5. Linear viscoelastic (LVE) range – a) and crossover – b) of soils before and after treatment H_2O_2

5. ábra Lineárisan viszkoelasztikus (LVE) tartomány – a) és crossover – b) H_2O_2 kezelés előtt és után

The values of LVE-range in all variances of soils after removal OM went down, also as well as crossover. This means that the soil structure after the SOM removal became less resistant to stress.

The soil under pine forests is characterized by high values for all measured rheological parameters.

We connect the observed differences to the type of organic matter inputs. Unlike the herbaceous vegetation, pine plantations lead to significant accumulation of plant litter on the soil surface. The dissolved organic matter (DOM) is leached out of the litter layer by percolating water. The sorption of DOM (ligand exchange, cation bridges, hydrophobic interactions) on the mineral surfaces contributes to particle aggregation.

5. Conclusions

The increase in the strength of bonds between soil particles probably causes block-like soil structure. In the absence of SOM in interaction between soil particles is more rigid, samples of soil types become less plastic, destruction of structural bonds happens at smaller loadings.

The distinct rheological behavior of soil from pine plantations is manifested as very high resistance to loadings in its initial state and significant loss of stability after SOM oxidation.

The quality of organic matter due to different plant origin has an effect on the processes of micro-aggregation and consequently on the rheological behaviour of soils. The established differences in the rheological behavior of the studied soils from different locations and land uses may be associated with the type of organic inputs.

6. Acknowledgments

The study was supported by Russian Fond of Basic Research – project № 16-04-01111 The laboratory work utilized the equipment purchased by the MSU Development Program. The sampling in South Africa was funded by the South African National Research Foundation (NRF) through the Department of Science and Technology/NRF Green Landscapes project, the Applied Centre for Climate & Earth Systems Science (ACCESS) programme, as well as the NRF Thuthuka programme. The funding sources had no involvement in the study design, collection, analysis and interpretation of data, writing the report, or submitting the article for publication.

References

[1] Voronin, A. D.: Strukturno-funktsionalnay gidrofizika pochv (1984), *Izdatelstvo* MGU, p.204.

[2] Khaydapova, Dolgor – Yurevich Milanovskiy, Evgeny – Victorovich Shein, Evgeny (2013): Impact of Antropogenic Load on Rheologocal Properties of Typical Chernozems (Kyrsk Region, Russia). *Advances in geoecology* 42: Soil Degradation, Catena Verlag GMBH, Reiskirchen, Germany, pp. 62-71.

[3] Khaidapova, D. D. – Chestnova, V. V. – Shein, E. V. – Milanovskii, E. Yu.: Rheological properties of typical chernozems (Kursk Oblast) under different land uses, *Eurasian Soil Sci.*, 2016, vol. 49, no. 8, p. 890. https://doi.org/10.1134/S1064229316080044

[4] Kachinskiy, N. A.: Soil physics (1965) *Visshaya shkola*, Moscow, p.323.

[5] Markgraf, W. – Horn, R. – Peth, S. (2006): An Approach to Rheometry in Soil Mechanics: Structural Changes in Bentonite, Clayey and Silty Soils. *Soil and Tillage Research.* No 91, pp. 1-14. https://doi.org/10.1016/j.still.2006.01.007

[6] Markgraf, W. – Watts, C. W. – Whalley, W. R. – Hrkac, T. – Horn, R.: Influence of organic matter on rheological properties of soil. *Applied Clay Science*. 2012, V. 64, P. 25–33. https://doi.org/10.1016/j.clay.2011.04.009

[7] Pertile, P. – Reichert, J. M. – Gubiani, P. I.: Rheological parameters affected by water tension in subtropical soils, *Rev. Bras. Cienc Solo,* 2016, vol. 40, p. e0150286 https://doi.org/10.1590/18069657rbcs20150286

[8] Baumgarten, W. – Horn, R. (2013): Assessing soil degradation by using a scale-spanning soil mechanical approach: A review. *Advances in geoecology* 42: Soil Degradation, Catena Verlag GMBH, Reiskirchen, Germany, pp. 1-61.

[9] Mezger, T. (2011): The Rheology Handbook – For users of rotational and oscillatory rheometers. 3rd revised edition, *Vincentz*, Hannover, Germany, 252 p.

[10] Tisdall J. M. – Oades J. M. (1982): Organic matter and water-stable aggregates in soils. *Journal of Soil Sci*. V.33,p.141-163 https://doi.org/10.1111/j.1365-2389.1982.tb01755.x

[11] Wiese, Liesl – Ros, Ignacio – Rozanov, Andrei – Boshoff, Adriaan – Clercq, Willem de – Seifert, Thomas (2016): An approach to soil carbon accounting and mapping using vertical distribution functions for known soil types. *Geoderma* 263, pp. 264–273 https://doi.org/10.1016/j.geoderma.2015.07.012

Ref.:
Khaydapov, Dolgor – **Wiese**, Liesl – **Rozanov**, Andrei – **Milanovskiy**, Evgeny: *Rheological parameters of some soil samples before and after H_2O_2 treatment*
Építőanyag – Journal of Silicate Based and Composite Materials, Vol. 70, No. 2 (2018), 38–41. p.
https://doi.org/10.14382/epitoanyag-jsbcm.2018.8

New approach for investigation of reinforcement in polymer nanocomposites using oscillatory shear flow data

Milan KRACALIK ▪ Institute of Polymer Science, Johannes Kepler University Linz ▪ Milan.Kracalik@jku.at

Érkezett: 2017. 12. 19. ▪ Received: 19. 12. 2017. ▪ https://doi.org/10.14382/epitoanyag-jsbcm.2018.9

Abstract

Polymer nanocomposites exhibit complex rheological behaviour due to physical and also possibly chemical interactions between individual phases. Up to now, rheology of polymer nanocomposites has been usually described by evaluation of viscosity curve (shear thinning phenomenon), storage modulus curve (formation of secondary plateau) or plotting information about damping behaviour (e.g. Van Gurp-Palmen-plot, Cole-Cole plot). On the contrary to evaluation of damping behaviour, new approach – based on evaluation of rigidity behaviour – was tested, where the values of cot δ were calculated and called as „storage factor", analogically to loss factor. Afterwards, values of storage factor were integrated over specific frequency range and called as "cumulative storage factor". In this contribution, LDPE-ZnO-clay nanocomposites with different polyethylene matrices and dispersion grades (physical networks) have been prepared and characterized by both conventional as well as novel analysis approach. Next to cumulative storage factor, further cumulative rheological parameters like cumulative complex viscosity, cumulative complex modulus or cumulative storage modulus have been introduced.

Keywords: shear flow, oscillatory shear, polymer, clay, nanocomposites

Kulcsszavak: nyírási folyás, változó amplitúdójú nyírás, polimer, agyag, nanokompozitok

Prof. Dr. Milan KRACALIK

is assistant professor at the Institute of Polymer Science, Johannes Kepler University Linz. His field of expertise covers in particular polymer rheology, polymer composites and nanocomposites, polymer recycling, study of structure-properties relationship in polymer materials and management associated with technological processes and products. He studied Technology & Management at the Brno University of Technology, Czech Republic (MSc.: 2000), at Tomas Bata University in Zlin and Institute of Macromolecular Chemistry, Academy of Sciences of the Czech Republic (Ph.D.: 2006) associated with praxis in marketing department of Podravka-Lagris Inc., Czech Republic. Between 2006 and 2012 he was post-doc researcher & project leader at the Department of Polymer Engineering and Science of the University of Leoben, Austria. Between 2012 and 2014 he was research manager at the Department Research and Development of the ISOVOLTAIC AG, Austria. He has also lectured on Technology & Management at several European universities such as Albert Ludwigs University Freiburg, Budapest University of Technology and Economics, Chemical Research Centre / Hungarian Academy of Sciences, University of Zagreb and Department of Technical Sciences / Croatian Academy of Sciences and Art.

1. Introduction

Nanocomposites using organically modified clays have been intensively investigated due to enhancement of processing as well as application properties of polymer matrix. Using nanoparticles is an interesting way for preparation of tailored materials, possibly also with recycled polymers. The enhancement of material properties because of nanoparticles addition has usually been analyzed using a combination of morphological (X-ray diffraction (XRD), transmission electron microscopy (TEM)), mechanical (tensile testing) and rheological (rotational rheometry) measurements. Using 2-5% of organoclay, significant enhancement of material properties has been reported: higher elastic modulus, tensile strength, thermal resistivity, lower gas and liquid permeability, reduced flammability and improved rheological properties (increased melt strength) compared to the unfilled polymer matrix. High reinforcement due to addition of the layered silicates results from their large surface area (in the case of montmorillonite 700-800 m2/g) [31, 33, 38]. In the case of highly dispersed systems, a three dimensional physical network is achieved, formed due to interactions between silicate platelets and the polymer chains. This phenomenon can be investigated by analysis of the melt elasticity using rotational rheometry [1-47]. These studies are mainly based on evaluation of viscosity curve shape (shear thinning phenomenon), storage modulus curve at low frequencies (formation of secondary plateau), phase homogeneity (Cole-Cole plot) or plotting information about damping behaviour (e.g. Van Gurp-Palmen-plot, comparison of loss factor tan δ). In order to enable simple comparison of nanocomposites reinforcement in the shear flow, new way to analyze data of the shear flow has been tested [18]. The storage modulus G′ reflects the elastic part while the loss modulus gives information about the viscous part of the dynamic shear flow. The relation of G′′/G′ is defined as tan δ and describes damping behaviour of the polymer system. On the contrary, to our knowledge, the G′/G′′ ratio (cot δ) has not been used for rheological evaluation of nanocomposites up to now. Compared to tan δ (loss factor), cot δ (named as storage factor, SF) reflects melt rigidity, which can be associated with reinforcement effect of nanostructured filler (combination of chain elasticity with silicate layers rigidity in the polymer melt). In order to reduce the values of storage factor to one representative magnitude for one nanocomposite sample, G′ as well as G′′ curves have been integrated over the measured frequency range as following:

$$CSF = \int_{0.1rad/s}^{628rad/s} G' \Big/ \int_{0.1rad/s}^{628rad/s} G'' \qquad (1)$$

In this way, cumulative storage factor (CSF) and some further cumulative rheological parameters (e.g. cumulative complex viscosity CCV, cumulative complex modulus CCM, cumulative storage modulus CSM) were introduced [16]. It was proven that values of CSF can be correlated with values of melt strength, i.e. the reinforcement in polymer nanocomposites can be assessed and compared in both, shear as well in elongational flow [18]. In this paper, LDPE-ZnO-clay nanocomposites with different dispersion grades (physical networks) are reported. It is shown that nano-scaled ZnO can be used not only as UV stabilizer but also as reinforcement and dispersion agent, respectively. The obtained data is analysed in this paper using typical rheological approaches as well as cumulative rheological parameters like CSF or CCV.

2. Materials

Two low-density polyethylene grades: low melt viscosity CA9150 (MFR (190°C/2.16 kg): 15 g/10 min, Borealis Inc., Linz, Austria) and high melt viscosity Lupolen 2420 D (MFR (190°C/2.16 kg): 0.25 g/10 min, LyondellBasell Industries Inc., Rotterdam, Netherlands) have been used for the preparation of nanocomposites. The used nanoclay Cloisite20 (Cl20) as well as masterbatch with nano-scaled ZnO (Nanobyk, dispersion of 30% zinc oxide nanoparticles in low-molecular weight polyethylene) were supplied by BYK-Chemie Ltd, Wesel, Germany / POLYchem Ltd, Markt Allhau, Austria, respectively.

3. Experimental

Nanocomposites have been prepared using laboratory compounder MiniLab II Haake Rheomex CTW5 (Thermo Fisher Scientific, Germany). Performance of 8 different compositions (pure PE matrices, 5wt.% of Cl20, 5wt.% of ZnO, 2.5/2.5 wt.% of Cl20/ZnO) have been compared. Rheological properties in the shear flow were analyzed using a Physica MCR 502 rheometer (Anton Paar Ltd., Graz, Austria) with the cone-plate geometry of 25 mm diameter and measuring gap of 43 μm.

4. Results and discussion

The nanocomposites structure has been usually assessed by analysis of viscosity curve (shear-thinning effect) in combination with evaluation of the storage modulus curve (G´ secondary plateau). In *Fig. 1.a* and *1.b*, magnitudes of complex viscosity for nanocomposites based on both LDPE matrices in dependency on angular frequency have been plotted. Addition of nanoparticles to CA9150 resulted to significant differences in the viscosity of mixtures. On the other hand, no substantial differences between viscosity values of systems filled in Lupolen (*Fig. 1.b*) can be seen. This is because dispersion process of polymer nanocomposites based on layered silicates (delamination) requires enough chain mobility so that molten polymer chains are able to penetrate into interlayer space of silicate. In high viscosity / high melt strength polymers, chain mobility is rather reduced and, consequently, it is difficult to achieve high dispersion grade. This is confirmed in *Figs. 1.a, 1.b, 2.a, 2.b*, where mixtures based on Lupolen showed typical pseudoplastic behaviour (*Fig. 1.b*) with viscoelastic feature (*Fig. 2.b*), while 2 nanocomposites based on CA9150 (5% Cl20, 2.5% Cl20/2.5% ZnO) revealed pronounced shear-thinning behaviour (*Fig. 1.a*) concomitant with rubber-like behaviour at low frequencies (*Fig. 2.a*), indicating high dispersion grade. Lower viscosity values of nanocomposites with 5% ZnO and 2.5% Cl20/2.5% ZnO comparing with pure LDPE matrices (*Fig. 1a, 1b*) can be explained by significantly lower viscosity of PE matrix used for preparation of ZnO masterbatch. It was not possible to measure MFR value of ZnO masterbatch at 190°C/2.16 kg, but the value 404 g/10 min measured by 100 °C/2,16 kg confirms a significant "dilution" effect in used LDPE matrices. The higher admixture of ZnO masterbatch to CA9150 or Lupolen matrix results to higher "dilution" of CA9150 or Lupolen matrix, respectively, i.e. the average molecular weight in such polymer blends will be lowered.

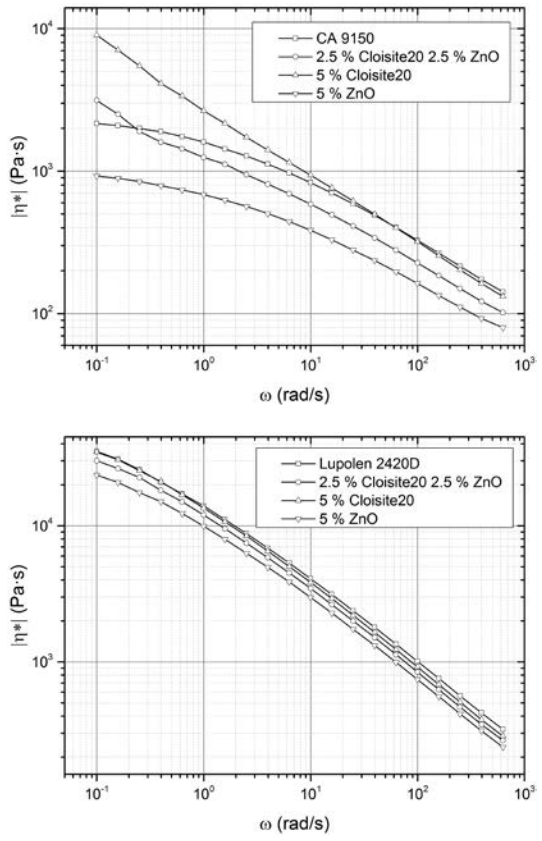

Fig. 1. Complex viscosity of nanocomposites
1.ábra Nanokompozitok komplex viszkozitása

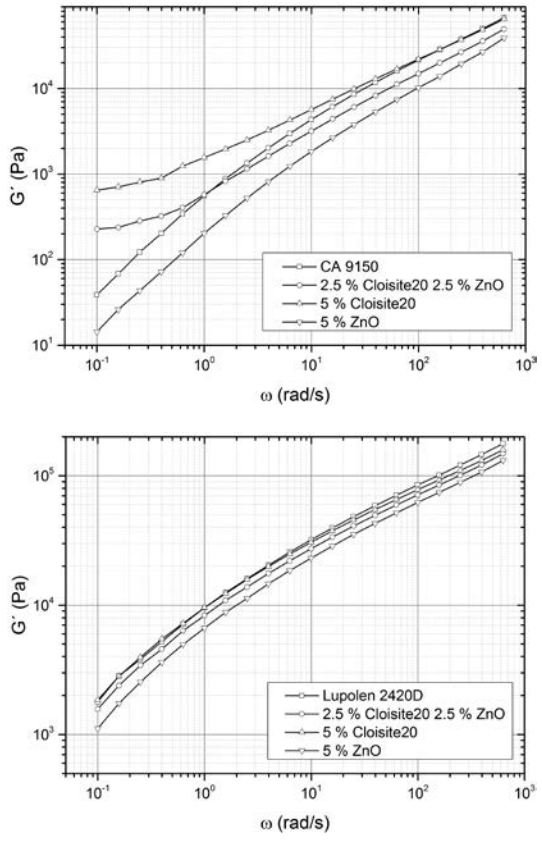

Fig. 2. Storage modulus of nanocomposites
2. ábra Nanokompozitok tárolási modulusa

The van Gurp-Palmen (vGP) plot as a dependency of loss angle δ on complex modulus |G*| has been usually used in order to evaluate the topological structures of polymers. The vGP plot is temperature invariant and can be used to check for the time temperature superposition principle [48-52]. In *Figs. 3.a* and *3.b*, this kind of dependency is plotted for prepared samples. For the polymers with rather linear chain structure, a continuous shaped curve has been published. On the contrary, long chain branched (LCB) polymers revealed a developed bump between the |G*| minimum and the 90° plateau [50, 51]. As can be seen in *Fig. 3.a*, systems prepared with Cl20 and Cl20/ZnO in CA9150 show topological structure similar to mentioned LCB polymers with even two bumps or peaks (Cl20), indicating 3D physical network made of silicate layers and polymer chains. The pure CA9150 matrix and nanocomposite with 5% ZnO showed behaviour associated with linear chain structure. It can be seen in *Fig. 3.b* that Lupolen matrix as well as nanocomposites based on it exhibited continuous shaped curve, i.e. the physical network formed in nanocomposites using Lupolen matrix was rather weak and could not be characterized from vGP plot.

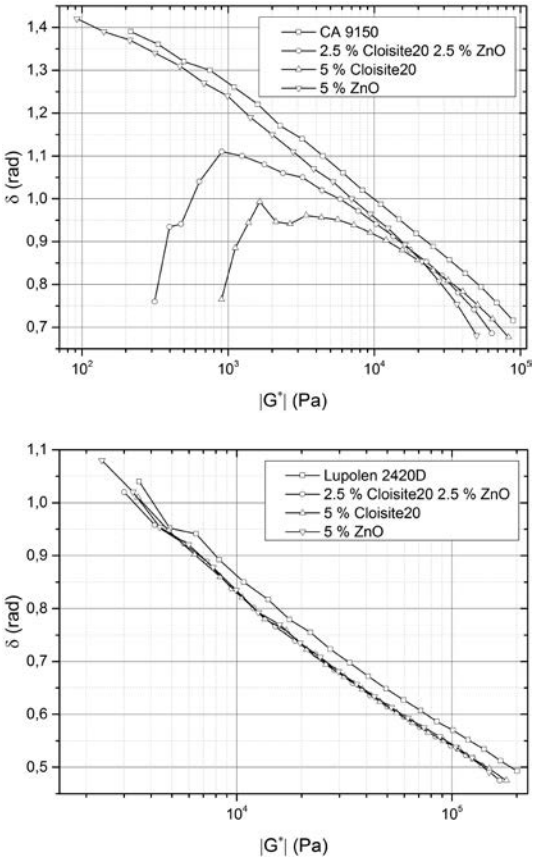

Fig. 3. Van Gurp-Palmen plot of nanocomposites
3. ábra Nanokompozitok Van Gurp-Palmen diagramja

In order to provide additional information about viscoelastic damping behaviour of the prepared samples, phase angle δ in dependency on angular frequency has been plotted (*Figs. 4.a* and *4.b*). The curves for nanocomposites with CA9150 as well as Lupolen matrix are similar to those of vGP plot. Mixtures using CA9150 polymer matrix (*Fig. 4.a*) confirm formation of differently organized structures (specific combination of agglomerated, delaminated and exfoliated structure in nanocomposites) depending on 3D microstructure. Samples using Lupolen matrix (*Fig. 4.b*) exhibit similar damping behaviour.

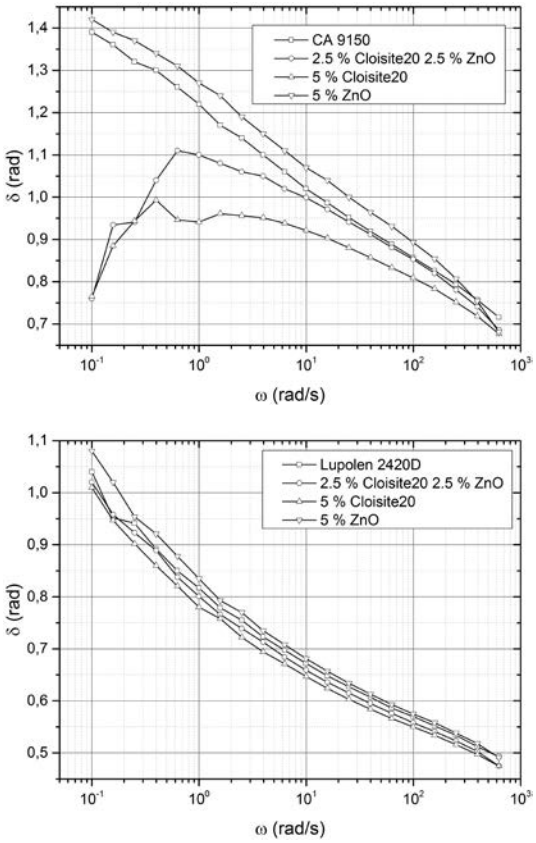

Fig. 4. Phase shift in dependency on angular frequency.
4. ábra Fáziseltolódás a körfrekvencia függvényében

Other approach for description of viscoelastic damping behaviour is "Cole-Cole" figure, where imaginary part of complex viscosity is plotted over the real part. This plot has been usually used to assess miscibility/homogeneity of polymer blends and composites in the way that a smooth, semi-circular shape can be interpreted by better compatibility and homogeneity [53, 54]. As shown in *Fig. 5.a*, the CA9150 matrix and nanocomposite with 5% ZnO showed semi-circle shapes, reflecting high homogeneity of the system. However, for the analysis of polymer nanocomposites performance, not only homogeneity but also mechanical reinforcement should be addressed. Using Cole-Cole plot, it seems that systems prepared with Cl20 and Cl20/ZnO revealed deviation from semi-circle shape and, therefore, are rather not homogeneous. However, no information about reinforcement level can be obtained from this figure. The Cole-Cole plot for nanocomposites using Lupolen matrix showed semi-circle shapes for all samples and, therefore, it cannot be used for analysis of differencies between pure polymer matrix and filled systems.

Using previously introduced analysis based on "melt rigidity" behaviour [16, 18], there is possibility to analyse reinforcement level as result of 3D physical network between polymer chains and filler particles and, consequently, to obtain some

information hidden in analysis based on damping behaviour (vGP, Cole-Cole plot) or typical evaluation of viscosity or storage modulus curves. The cumulative storage factor plotted over cumulative complex viscosity in *Figs. 6.a* and *6.b* show clearly other trend as trends obtained from figures analysed previously in this paper.

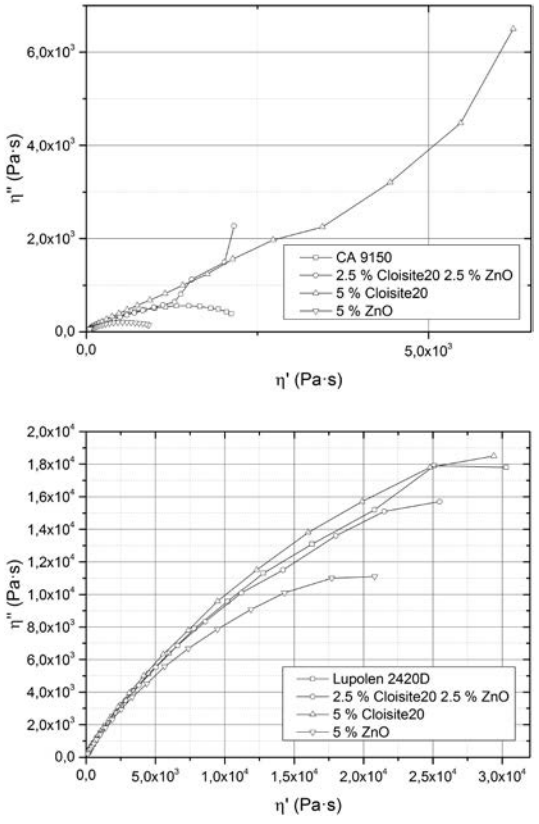

Fig. 5. Cole-Cole plot
5. ábra Cole-Cole diagram

For CA9150 matrix (*Fig. 6.a*) it can be seen that viscosity value is high, but reinforcement level (comparing to all nanocomposites) is low. Comparing to CA9150, the nanocomposite with 5% of ZnO revealed lower value of viscosity (due to admixture of low-viscous PE masterbatch carrier), but higher value of reinforcement, followed by nanocomposite with 2.5/2.5 wt.% of Cl20/ZnO and finally followed by nanocomposite with 5wt.% of Cl20 showing the highest reinforcement and approximately same level of viscosity as CA9150 (as in this case, no "dilution" effect was caused). In this way, it was possible to recognize effect of "internal reinforcement" coming from internal friction (change in viscosity coming from mixture of two polyethylenes with different MFR values) – described by CCV – and "external reinforcement" coming from 3D physical network between polymer chains and nanofiller particles – described by CSF. These two effects were not possible to be separated using evaluation methods based on damping behaviour.

It is also interesting to compare the values of CCV of CA9150/Lupolen matrices and corresponding nanocomposites filled with 5% of ZnO. It can be clearly seen that dilution effect in low-viscosity matrix (CCV of mixture with 5% ZnO is about two-times lower than CCV of CA9150) is much higher than that in high-viscosity matrix (CCV of mixture with 5% ZnO is about 25% lower than CCV of Lupolen).

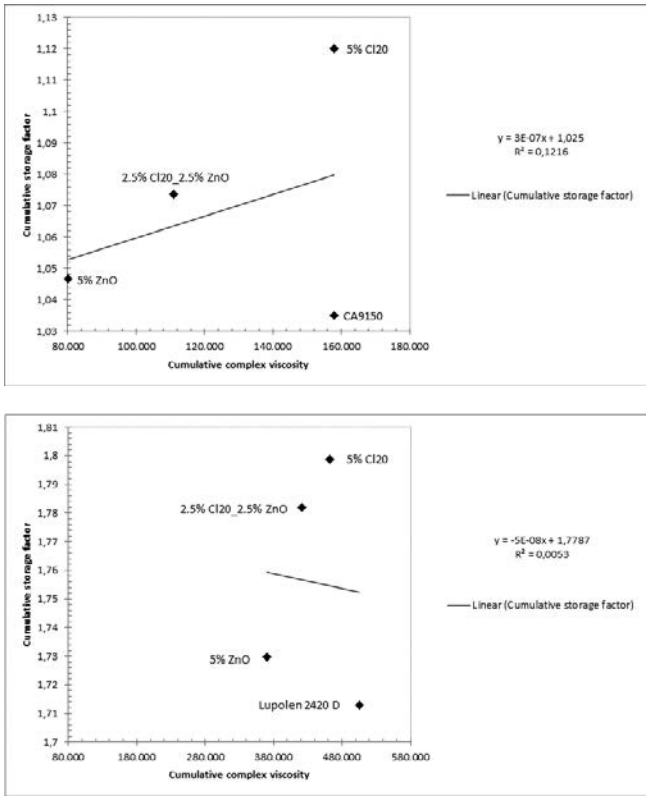

Fig. 6. Cumulative storage factor.
6. ábra Összegzett tárolási tényező

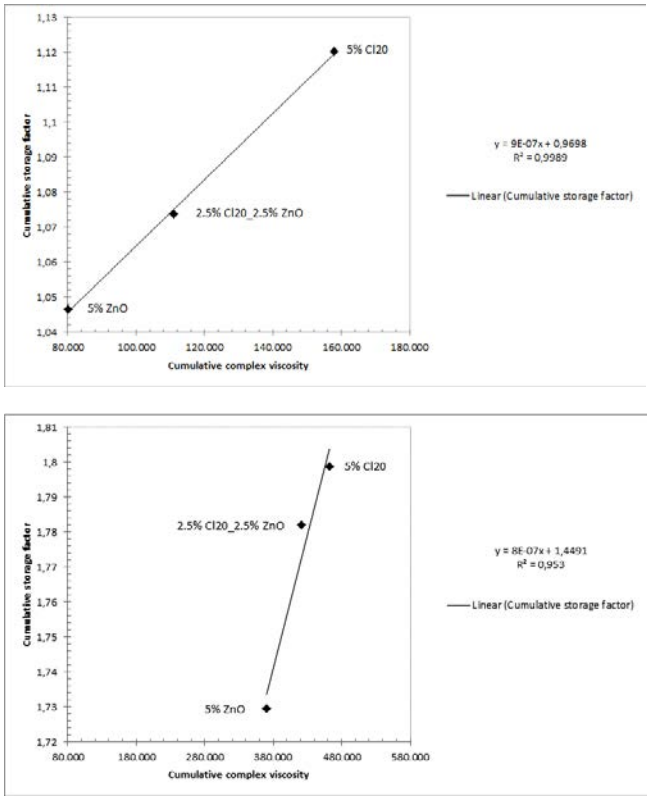

Fig. 7. Cumulative storage factor of nanocomposites without neat matrix
7. ábra Ágyazóanyag mentes nanokompozitok összegzett tárolási tényezője

Comparing to *Fig. 6.a*, coefficient of linear regression in *Fig. 7.a* (without polymer matrix) is very high. It means, if only polymer nanocomposites are compared, there is high correlation between CSF and CCV values, giving possibility to compare previously described "external reinforcement" not only in cases of nanocomposites using one polymer matrix, but also in cases of nanocomposites based on polymer blends. This is proved in *Fig. 8,* where all nanocomposites using low-viscous CA9150 as well as high-viscous Lupolen are compared in one data set with high correlation coefficient.

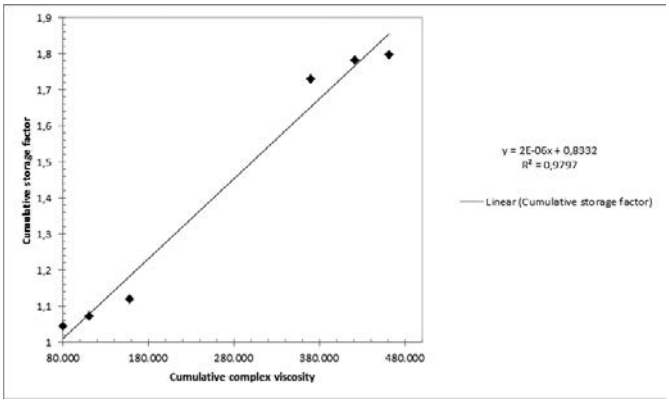

Fig. 8. Cumulative storage factor of nanocomposites with both LDPE matrices
8. ábra LDPE ágyazóanyagú nanokompozitok összegzett tárolási tényezője

5. Conclusions

Polymer nanocomposite blends with different melt viscosity polyethylenes and clay/ZnO nanoparticles were prepared and analysed by conventional as well by new rheological approach. Using novel approach based on melt rigidity analysis (cumulative storage factor) the reinforcement caused by 3D physical network between polymer chains and nanofiller particles could be separated from that coming from internal friction (associated with polymer melt viscosity). In this way, new insight into structure/property relation description of polymer nanocomposites has been introduced.

References

[1] Abdel-Goad, M. (2011): Rheological characterization of melt compounded polypropylene/clay nanocomposites, *Composites Part B* 42 (2011) 1044–1047. https://doi.org/10.1016/j.compositesb.2011.03.025

[2] Aghjeh, M. R. – Asadi, V. – Mehdijabbar, P. – Khonakdar, H. A. – Jafari, S. H. (2015): Application of linear rheology in determination of nanoclay localization in PLA/EVA/Clay nanocomposites: Correlation with microstructure and thermal properties, *Composites Part B* (2015) 273–284. https://doi.org/10.1016/j.compositesb.2015.09.064

[3] Ahmed, J. – Auras, R. – Kijchavengkul, T. – Varshney, S. K. (2012): Rheological, thermal and structural behavior of poly (e-caprolactone) and nanoclay blended films, *Journal of Food Engineering* (2012) 580–589. https://doi.org/10.1016/j.jfoodeng.2012.03.014

[4] Allahbakhsh, A. – Mazinani, S. – Kalaee, M. R. – Sharif, F. (2013): Cure kinetics and chemorheology of EPDM/graphene oxide nanocomposites, *Thermochimica Acta* 563 (2013) 22–32. https://doi.org/10.1016/j.tca.2013.04.010

[5] Al-Saleh, M. H. – Sundararaj, U. (2010): Processing-microstructure-property relationship in conductive polymer nanocomposites, *Polymer* 51 (2010) 2740–2747. https://doi.org/10.1016/j.polymer.2010.03.022

[6] Al-Samhan, M. – Samuel, J. – Al-Attar, F. – Abraham, G. (2017): Comparative Effects of MMT Clay Modified with Two Different Cationic Surfactants on the Thermal and Rheological Properties of Polypropylene Nanocomposites, *Hindawi* (2017). https://doi.org/10.1155/2017/5717968

[7] Anderson, B. J. – Zukoski, C. F. (2010): Rheology and microstructure of polymer nanocomposite melts: Variation of polymer segment-surface interaction, *Langmuir* 26 (2010) 8709–8720. https://doi.org/10.1021/la9044573

[8] Ayyer, R. K. – Leonov, A. I. (2004): Comparative rheological studies of polyamide-6 and its low loaded nanocomposite based on layered silicates, *Rheologica Acta* 43 (2004) 283–292. https://doi.org/10.1007/s00397-003-0343-6

[9] Block, C. – Watzeels, N. – Rahier, H. – van Mele, B. – van Assche, G. (2011): Rheology of nanocomposites, *Journal of thermal analysis and calorimetry* 105 (2011) 731–736. https://doi.org/10.1007/s10973-011-1417-9

[10] Cassagnau, P. (2008): Melt rheology of organoclay and fumed silica nanocomposites, *Polymer* 49 (2008) 2183–2196. https://doi.org/10.1016/j.polymer.2007.12.035

[11] Chambon, F. – Winter, H. H. (1987): Linear viscoelasticity at the gel point of a crosslinking PDMS with imbalanced stoichiometry, *Journal of Rheology* 31 683–697. https://doi.org/10.1122/1.549955

[12] Chevallier, C. – Becquart, F. – Taha, M. (2013): Polystyrene/polycarbonate blends compatibilization: Morphology, rheological and mechanical properties, *Materials Chemistry and Physics* (2013) 616–622. https://doi.org/10.1016/j.matchemphys.2013.02.006

[13] Filippone, G. – Carroccio, S. C. – Curcuruto, G. – Passaglia, E. – Gamarotti, C. – Dintcheva, N. Tz. (2015): Time-resolved rheology as a tool to monitor the progress of polymer degradation in the melt state Part II: Thermal and thermo-oxidative degradation of polyamide 11/organo-clay nanocomposites, *Polymer* (2015) 102–110. https://doi.org/10.1016/j.polymer.2015.07.042

[14] Ghanbari, A. – Heuzey, M.-C. – Carreau, P. J. – Ton-That, M.-T. (2013): Morphological and rheological properties of PET/clay nanocomposites, *Rheologica Acta* (2013) 59–74. https://doi.org/10.1007/s00397-012-0667-1

[15] Goffin, A.-L. – Raquez, J. M. – Duquesne, E. – Siqueria, G. – Habibi, Y. – Dufresne, A. – Dubois, P. (2011): Poly(e-caprolactone) based nanocomposites reinforced by surface-grafted cellulose nanowhiskers via extrusion processing: Morphology, rheology, and thermo-mechanical properties, *Polymer* 52 (2011) 1532–1538. https://doi.org/10.1016/j.polymer.2011.02.004

[16] Kracalik, M. (2015): Rheology of multiphase polymer systems using novel "melt rigidity" evaluation approach, in: AIP Publishing LLC, 2015, p. 40002.

[17] Kracalik, M. – Laske, S. – Holzer, C. (2011): Extensional Rheology as Effective Tool for Characterization of Polymer Nanocomposites, *Novel Trends in Rheology* IV 1375 (2011). https://doi.org/10.1063/1.3604480

[18] Kracalik, M. – Laske, S. – Witschnigg, A. – Holzer, C. (2011): Elongational and shear flow in polymer-clay nanocomposites measured by on-line extensional and off-line shear rheometry, *Rheologica Acta* (2011) 937–944. https://doi.org/10.1007/s00397-011-0545-2

[19] Kracalik, M. – Pospisil, L. – Slouf, M. – Mikesova, J. – Sikora, A. – Simonik, J. – Fortelny, I. (2008): Effect of glass fibers on rheology, mechanical properties of recycled thermal and PET, *Polymer Composites* 29 (2008) 915–921. https://doi.org/10.1002/pc.20467

[20] Kracalik, M. – Pospisil, L. – Slouf, M. – Mikesova, J. – Sikora, A. – Simonik, J. – Fortelny, I. (2008): Recycled poly(ethylene terephthalate) reinforced with basalt fibres: Rheology, structure, and utility properties, *Polymer Composites* 29 (2008) 437–442. https://doi.org/10.1002/pc.20425

[21] Krishnamoorti, R. – Banik, I. – Xu, L. (2010): Rheology and processing of polymer nanocomposites, *Reviews in Chemical Engineering* 26 (2010) 354.

[22] Laske, S. – Kracalik, M. – Gschweitl, Michael M. – Feuchter, M. – Maier, G. – Pinter, G. – Thomann, R. – Friesenbichler, W. – Langecker, G. R. (2009): Estimation of Reinforcement in Compatibilized Polypropylene Nanocomposites by Extensional Rheology, *Journal of Applied Polymer Science* 111 (2009) 2253–2259. https://doi.org/10.1002/app.29163

[23] Laske, S. – Witschnigg, A. – Mattausch, H. – Kracalik, M. – Pinter, G. – Feuchter, M. – Maier, G. – Holzer, C. (2012): Determining the ageing of polypropylene nanocomposites using rheological measurements, *Applied Rheology* (2012). https://doi.org/10.3933/ApplRheol-22-24590

[24] Le Losq, C. – Neuville, D. R. (2013): Effect of the Na/K mixing on the structure and the rheology of tectosilicate silica-rich melts, *Chemical Geology* 346 (2013) 57–71. https://doi.org/10.1016/j.chemgeo.2012.09.009

[25] Li, J. – Zhou, C. – Wang, G. – Zhao, D. (2003): Study on rheological behavior of polypropylene/clay nanocomposites, *J. Appl. Polym. Sci.* 89 (2003) 3609–3617. https://doi.org/10.1002/app.12643

[26] Li, Z. – Liu, F. – Xu, G. – Zhang, J. – Chu, C. (2014): A kinetics-controlled coating method to construct 1D attapulgite @ amorphous titanium oxide nanocomposite with high electrorheological activity, *Colloid and Polymer Science* 292 (2014) 3327–3335. https://doi.org/10.1007/s00396-014-3384-8

[27] Liu, Q. – Chen, D. (2008): Viscoelastic behaviors of poly(ε-caprolactone)/attapulgite nanocomposites, *European Polymer Journal* 44 (2008) 2046–2050. https://doi.org/10.1016/j.eurpolymj.2008.04.035

[28] Miltner, H. E. – Watzeels, N. – Block, C. – Gotzen, N.-A. – van Assche, G. – Borghs, K. – van Durme, K. – van Mele, B. – Bogdanov, B. – Rahier, H. (2010): Qualitative assessment of nanofiller dispersion in poly(ε-caprolactone) nanocomposites by mechanical testing, dynamic rheometry and advanced thermal analysis, *European Polymer Journal* 46 (2010) 984–996. https://doi.org/10.1016/j.eurpolymj.2010.01.002

[29] Mishra, J. K. – Hwang, K.-J. – Ha, C.-S. (2005): Preparation, mechanical and rheological properties of a thermoplastic polyolefin (TPO)/organoclay nanocomposite with reference to the effect of maleic anhydride modified polypropylene as a compatibilizer, *Polymer* 46 (2005) 1995–2002. https://doi.org/10.1016/j.polymer.2004.12.044

[30] Nobile, M. R. – Simon, G. P. – Valentino, O. – Morcom, M. (2007): Rheological and Structure Investigation of Melt Mixed Multi-Walled Carbon Nanotube/PE Composites, *Macromol. Symp.* 247 (2007) 78–87. https://doi.org/10.1002/masy.200750110

[31] Paul, D. R. – Robeson, L. M. (2008): Polymer nanotechnology: Nanocomposites, *Polymer* 49 (2008) 3187–3204. https://doi.org/10.1016/j.polymer.2008.04.017

[32] Pötschke, P. – Fornes, T. D. – Paul, D. R. (2002): Rheological behavior of multiwalled carbon nanotube/polycarbonate composites, *Polymer* 43 (2002) 3247–3255. https://doi.org/10.1016/S0032-3861(02)00151-9

[33] Ray, S. S. – Okamoto, K. – Maiti, P. – Okamotoa, M. (2002): New Poly(butylene succinate)/Layered Silicate Nanocomposites: Preparation and Mechanical Properties, *Journal of Nanoscience and Nanotechnology* 2 (2002) 171–176. https://doi.org/10.1166/jnn.2002.086

[34] Sadeghipour, H. – Ebadi-Dehaghani, H. – Ashouri, D. – Mousavian, S. – Hashemi-Fesharaki, M. – Gahrouei, M. S. (2013): Effects of modified and non-modified clay on the rheological of high density polyethylene, *Composites: Part B* (2013) 164–171. https://doi.org/10.1016/j.compositesb.2013.04.010

[35] Samakande, A. – Sanderson, R. D. – Hartmann, P. C. (2009): Rheological properties of RAFT-mediated poly(styrene-co-butyl acrylate)–clay nanocomposites [P(S-co-BA)-PCNs]: Emphasis on the effect of structural parameters on thermo-mechanical and melt flow behaviors, *Polymer* 50 (2009) 42–49. https://doi.org/10.1016/j.polymer.2008.10.050

[36] Samyn, F. – Bourbigot, S. – Jama, C. – Bellayer, S. – Nazare, S. – Hull, R. – Castrovinci, A. – Fina, A. – Camino, G. (2008): Crossed characterisation of polymer-layered silicate (PLS) nanocomposite morphology: TEM, X-ray diffraction, rheology and solid-state nuclear magnetic resonance measurements, *European Polymer Journal* 44 (2008) 1642–1653. https://doi.org/10.1016/j.eurpolymj.2008.03.021

[37] Százdi, L. – Ábrányi, Á. – Pukánszky, B. – Vancso, J. G. (2006): Morphology Characterization of PP/Clay Nanocomposites Across the Length Scales of the Structural Architecture, *Macromol. Mater. Eng.* 291 (2006) 858–868. https://doi.org/10.1002/mame.200600026

[38] Thomas, S. – Muller, R. – Abraham, J. (2016): Rheology and Processing of Polymer Nanocomposites, *John Wiley & Sons, Inc,* Hoboken, NJ, USA, 2016.

[39] Vermant, J. – Ceccia, S. – Dolgovskij, M. K. – Maffettone, P. L. – Macosko, C. W. (2007): Quantifying dispersion of layered nanocomposites via melt rheology, *Journal of Rheology* 51 (2007) 429–450. https://doi.org/10.1122/1.2516399

[40] Wagener, R. – Reisinger, T. J. G. (2003): A rheological method to compare the degree of exfoliation of nanocomposites, *Polymer* 2003 7513–7518. https://doi.org/10.1016/j.polymer.2003.01.001

[41] M. Wang, – X. Fan, – Thitsartarn W., – He C., (2014): Rheological and mechanical properties of epoxy/clay nanocomposites with enhanced tensile and fracture toughnesses, *Polymer* (2014) 43–52. https://doi.org/10.1016/j.polymer.2014.12.042

[42] Wood-Adams, P. M. – Dealy, J. M. – deGroot, A. W. – Redwine, O. D. (2000): Effect of Molecular Structure on the Linear Viscoelastic Behavior of Polyethylene, *Macromolecules* 33 (2000) 7489–7499. https://doi.org/10.1021/ma991533z

[43] Wu, D. – Wu, L. – Sun, Y. – Zhang, M. (2007): Rheological properties and crystallization behavior of multi-walled carbon nanotube/poly(ε-caprolactone) composites, *Journal of Polymer Science: Part B: Polymer Physics* 45 (2007) 3137–3147. https://doi.org/10.1002/polb.21309

[44] Zhang, X. – Yang, G. – Lin, J. (2006): Synthesis, Rheology, and Morphology of Nylon-11/Layered Silicate Nanocomposite, *Journal of Polymer Science: Part B: Polymer Physics* 44 (2006) 2161–2172. https://doi.org/10.1002/polb.20881

[45] Zhao, J. – Morgan, A. B. – Harris, J. D. (2005): Rheological characterization of polystyrene-clay nanocomposites to compare the degree of exfoliation and dispersion, *Polymer* 2005 8641–8660. https://doi.org/10.1016/j.polymer.2005.04.038

[46] Zhao, Y. – Huang, H.-X. (2008): Dynamic rheology and microstructure of polypropylene/clay nanocomposites prepared under Sc-CO2 by melt compounding, *Polymer Testing* 27 (2008) 129–134. https://doi.org/10.1016/j.polymertesting.2007.11.006

[47] Zhong, Y. – Zhu, Z. – Wang, S.-Q. (2005): Synthesis and rheological properties of polystyrene/layered silicate nanocomposite, *Polymer* 46 (2005). https://doi.org/10.1016/j.polymer.2005.02.014

[48] Lohse, DJ – Milner, ST – Fetters, LJ – Xenidou, M. – Hadjichristidis, N. – Mendelson, RA. – Garcia-Franco, CA – Lyon, MK (2002): Well-defined, model long chain branched polyethylene. 2. melt rheological behaviour. *Macromolecules* 35:3066-3075 https://doi.org/10.1021/ma0117559

[49] Schulze, D. – Trinkle, S. – Mulhaupt, R. – Friedrich, C. (2003): Rheological evidence of modifications of polypropylene by β-irradiation. *Rheol Acta* 42:251-258 https://doi.org/10.1007/s00397-002-0282-7

[50] Trinkle, S. – Friedrich, C. (2001): Van Gurp-Palmen plot: a way to characterize polydispersity of linear polymers. *Rheol Acta* 40:322-328 https://doi.org/10.1007/s003970000137

[51] Trinkle, S. – Walter, P. – Friedrich, C. (2002): Van Gurp-Palmen plot II – classification of long chain branched polymers by their topology. *Rheol Acta* 41:103-113 https://doi.org/10.1007/s003970200010

[52] Van Gurp, M. – Palmen, J. (1998): Time-temperature superposition for polymeric blends. *Rheol Bull* 67:5-8

[53] Aklonis, JJ. – Macknight, WJ.: Introduction to viscoelasticity. New York: *Wiley*; 1983.

[54] Utracki, LA. (1999): Polymer blends handbook. Netherlands: *Kluwer Academic Publishers*

Ref.:
Kracalik, Milan: *New approach for investigation of reinforcement in polymer nanocomposites using oscillatory shear flow data*
Építőanyag – Journal of Silicate Based and Composite Materials, Vol. 70, No. 2 (2018), 42–47. p.
https://doi.org/10.14382/epitoanyag-jsbcm.2018.9

Preliminary Corrosion Testing of Steel Rebar Samples in 3.5%NaCl Solution with and without a Green Inhibitor

Shaymaa Abbas ABDULSADA ▪ Faculty of Materials Science and Engineering, University of Miskolc ▪ qkosha86@uni-miskolc.hu
Tamás I. TÖRÖK ▪ Faculty of Materials Science and Engineering, University of Miskolc ▪ fektt@uni-miskolc.hu
Éva FAZAKAS ▪ Department of Surface Technology, Bay Zoltán Nonprofit Ltd. for Applied Research ▪ eva.fazakas@bayzoltan.hu
Érkezett: 2017. 12. 30. ▪ Received: 30. 12. 2017. ▪ https://doi.org/10.14382/epitoanyag-jsbcm.2018.10

Abstract
The applicability of a new organic inhibitor extracted from a cheap organic waste of orange peel (so-called „green" inhibitor) was studied in a laboratory system where the steel rebar samples obtained from a steel mill operating in Hungary were investigated in several sets of experiments to reveal their major corrosion properties in aqueous solutions containing sodium chloride salt. The initial corrosion rates were determined by a standard electrochemical polarisation technique on active (scale and rust free) steel specimen while being immersed in 3.5% NaCl aqueous solutions containing the methanol extract of the chosen green inhibitor in a preliminary test run of 24 hours. Due to the inhibitor's active groups identified by FTIR spectroscopy, this new green inhibitor (with concentrations tested at 1 and 3%) showed promising surface adsorptive and corrosion mitigating effects examined also by scanning electron microscopy (SEM) combined with EDS surface analysis. These SEM-EDS surface analyses were performed on the given rebar samples after an immersion (i.e. corroding) period of one month.
Keywords:, Steel reinforcement, orange peels, corrosion properties, SEM EDS analysis.

Shaymaa Abbas ABDULSADA
PhD student in Faculty of Materials Science and Engineering, University of Miskolc, Hungary. Lecturer at Faculty of Engineering, University of Kufa, Iraq.
Research Interests: Corrosion Engineering, Metallurgy Engineering, Heat Treatment of Metals, Casting of Metals.

Tamás I. TÖRÖK
Professor of Chemical Metallurgy and Surface Technologies at University of Miskolc, Hungary. First Secretary of HUNKOR, the Hungarian Corrosion Society, and former President of ASM International Hungary Chapter.
Recent Research Interests: Corrosion Phenomena, Protective Coatings, Metals Surface Treatments and Surface Engineering.

Éva FAZAKAS
Head of Department in Bay Zoltán Nonprofit Ltd. for Applied Research, Budapest.
As the head of the department I am in charge of arranging and realizing the professional development works of the department, as well as organizing and co-ordinating the industrial and R&D projects related to their fields of competence.
Research interest: Corrosion Engineering, Material Science, Structural analysis of metals, Heat treatment of Metals, Casting and mechanical alloying of metals.

1. Introduction

As it is stated in many relevant publications, the corrosion of steel reinforcement is a major problem influencing the long-term performance of reinforced concrete structures. It typically occurs due to onslaught of aggressive agents such as chloride ions from marine environment, deicing salt or chloride contaminated aggregate. In the subsistence of chloride, the protective passive stratum of steel is locally destroyed and the unprotected steel areas starts dissolve. The formation of corroding products (rust) involves a substantial volume increase, i.e. the volume of corrosion products is greater than that of original steel bar. Therefore expansive stresses are induced around corroded steel bars causing possible cracking, spalling of concrete cover and loss of bond between steel/concrete, and thus reducing the serviceability of concrete structures [1-6].

Cracking of the concrete cover is a critical limit state and this is often modelled as a two-stage process that consists of a) an initiation phase, defined as the time taken for corrosion to commence, and b) propagation phase (*Fig. 1*), where the accumulation of corrosion products induces expansive stresses and damage. Until recently, most research has focused on the time up to corrosion initiation, while the propagation phase leading to failure remains poorly understood as it is stated in a recent report of Wong et al. [7].

Anyhow, as a preventive measure against steel rebar corrosion, it is highly recommended by many corrosion experts [e.g. 8-11] studying the mechanism of the reinforcing steel corrosion in concretes, that inhibitors added to the fresh concrete mixtures can effectively defer the initiation phase of corrosion as well as decrease its rate during the propagation phase.

As it is well known, the corrosion inhibitors are chemical substances that when added in small amount to concrete mix decrease or slow down corrosion rate by changing the surface condition of the reinforced steel [12]. Most of the corrosion inhibitors are classified as organic and inorganic ones according to their chemical nature as well as anodic, cathodic or mixed inhibitors according to the electrochemical reaction on the steel surface with its environment [13]. Considering their material sources and varieties, recently the popularity and use of synthetic chemical compounds as corrosion inhibitors is diminishing due to the strict environmental regulations and toxic effects of many synthetic compounds on human and animal life. Consequently, there exists the need to develop a new class of corrosion inhibitors with low toxicity, eco-friendliness and good efficiency. Throughout the ages, plants have been used by human beings for their basic needs such as production of food-stuffs, shelters, clothing, fertilizers, flavors and fragrances, medicines and last but not least, as corrosion inhibitors. The use of natural products as corrosion inhibitors can be traced back to the 1930's when plant extracts of *Chelidonium majus* (Celandine) and other plants were used for the first time in H_2SO_4 pickling baths [14,15].

Extracts of plants materials contain a wide variety of organic compounds [16]. The natural constituents of these extracts contain N, O, and S containing heterocyclic macromolecules, which when reaching the steel surface by diffusion and got adsorbed at the steel concrete interface by secondary molecular interaction with the metal and metal oxide they

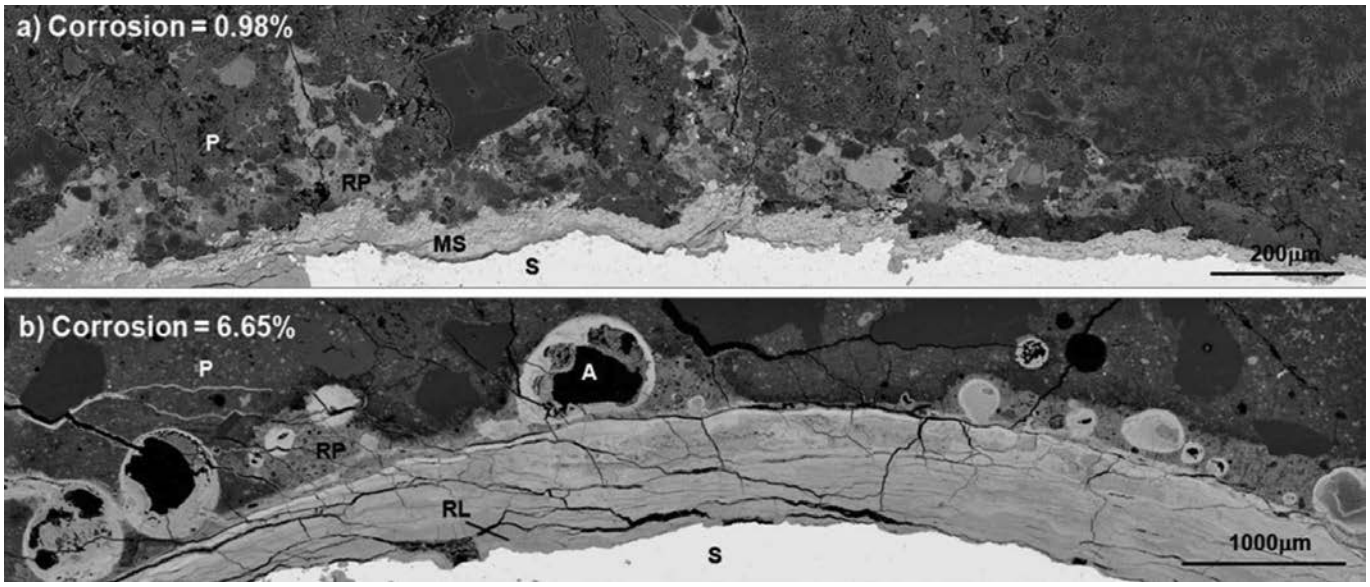

Fig. 1. BSE images of samples with different degrees of corrosion, showing rust accumulating at the steel-concrete interface and migrating into the cement paste, cracks and air voids (S: Steel, MS: Millscale, RL: Rust layer, RP: Rust-filled paste, P: Unaffected Paste) [7]

1. ábra Elektronmikroszkópos (BSE) felvételek különböző mértékű korróziós károsodásokról vasbetonban: az acélbetét és a beton határfelületén keletkezett és felszaporodott rozsda bepréselődött a cemetpépbe, a repedésekbe és a légüregekbe (Jelölések az ábrán: S: acél, MS: reve, RL: rozsdaréteg, RP: rozsdával penetrálódott cementkő, P: nem károsodott cementkő (megkötött cementpép). [7]

can form protective layers to repeal water molecules and inhibit ingression of destructive species like Cl^-, SO_4^{2-}, and CO_2 which are responsible for the depassivation of steel during the initiation phase of corrosion [17].

Getting motivated by the above described new tendencies and continued need of further research in this field, the main purpose of this study was to perform experimental laboratory tests to reveal the major corrosion related properties of steel rebar samples immersed in sodium chloride solution in contact with air. This approach is well justified as such or similar situations might also arise during the real and long service life of steel reinforced concrete structures and must be addressed in order to mitigate the risk of their degradation in such harsh (e.g. close to the see) environmental conditions. And, towards that aim, testing the potential of a new green inhibitor can be an important step forward in this respect.

2. Materials and methods

The steel rebar samples were obtained from a secondary steel making factory (Ózd Steelworks Ltd.), which produces different hot rolled rod and wire products. The hot rolled and ribbed reinforcing steel bar samples with diameter of about 8 mm were cut to 10 cm long pieces. The steel quality was in compliance with the standard EN 10080 [18] and contained about 0.2 wt.% C, somewhat over 1% Mn, and about 0.3 % Si as the main alloying elements. The as-received rod samples surface was covered with a thin layer of mill scale (iron oxide) which for some further corrosion testing experimental sets was removed by standard acid pickling in HCl solution.

In order to detect the active compounds of the powder of the ground dry orange peel, their FTIR spectra were also recorded. This test provides information about the chemical bonding or molecular structure of materials; determines the chemical types of components in the mixture, and whether they are organic or inorganic. The BRUKER type FTIR spectroscope (IRAffinity-1S) was equipped with a diamond crystal, and always a clean, empty diamond crystal was used for the collection of background spectrum.

The inhibitor tested in these experiments was a methanol extract of fine ground dry orange peel. The Soxhlet-extraction was made for 6 hours, then the methanol was evaporated under reduced pressure (60 mbar) at 40°C and the extract was dispersed/dissolved in distilled water. This aqueous suspension of the orange peel extract was then used as an inhibitor stock solution/suspension and was added in different percentages to the corrosion test electrolyte solutions of NaCl.

To estimate the initial corrosion rates, the properly prepared steel samples were put in the NaCl test solutions both without and with added orange peel extract as the inhibitor. During the polarization measurements the (steady-state open circuit) corrosion potentials (*E*/V) were recorded referenced to a saturated calomel electrode (SCE), then the electrode potential was scanned with a constant rate of 10 mV/min „down" to more negative (i.e. so-called cathodic) polarisation potentials of -2.5 V_{SCE}. Then the potential was reversed and scanned with the same rate through the *E*/V corrosion potential up to about +2.0 V_{SCE} more positive value than that of the corrosion potential. In this way a total potential range of almost 4.5 V were scanned. This procedure was then repeated in the same manner after longer periods of immersion times of 1 h, 3h, 5h, 7h, and 24 hours.

In the other sets of experiments both the initial surface state (i.e. mill-scale covered / as-received one) and the corroded surface conditions were characterized by scanning electron microscopy (SEM) coupled with energy-dispersive X-ray spectroscopic micro-analyser (EDS). Before the SEM-EDS testing the samples were left corrode for one month in NaCl solutions in contact with air both without and with green inhibitors of only 1 % and 3%, respectively.

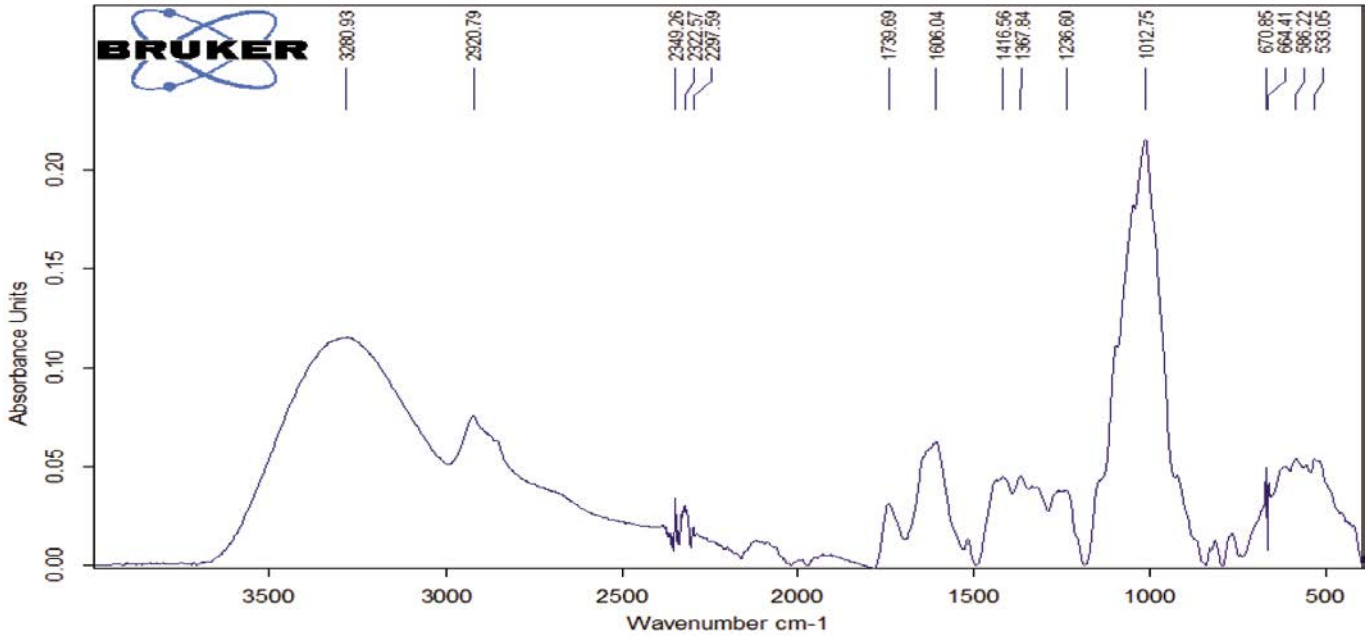

Fig. 2. Fourier transform infrared spectrum (FTIR) of the dry orange peel powder depicting its IR absorbance peaks in the function of wavenumber with the most significant values indicated above the peaks

2. ábra Szárított narancshéj por Fourier-transzformációs infravörös (FTIR) spektruma; a legjellemzőbb abszorpciós csúcsokhoz rendelhető hullámszám értékekkel is jellemezve

3. Results and discussion

3.1 Analysis of the Powdered Orange Peel

The dry and ground orange peel sample was first studied by recording its FTIR spectrum (*Fig. 2*) in order to detect its most probable IR active functional groups. In accordance with the relevant literature [19] our chosen natural organic material should also contain chemical constituents like organic fats, pectins, lignin, reducing and non-reducing sugars all of which have many active functional groups (carboxyl, hydroxyl, aldehyde, etc.) which make it a good candidate to show surface modifying properties if its water soluble components are properly extracted from it and used afterwards as an adsorptive type bio-based inhibitor.

The typical functional /active/ groups and the corresponding IR signals are also summed up in *Table 1.*

The above presented FTIR data have confirmed our supposition that the extract of orange peel should be an effective green inhibitor to be used in steel reinforced concrete structures.

A somewhat similar approach was considered and taken by Zapata, Balmaseda, Fregoso-Israel and Torres-García [20] when they studied the chemical structure of orange peel by FTIR technique as shown in *Fig.3.* Where we found most of the groups that appeared in our examination are similar to the groups that appeared in their analysis, for example, in the high energy region at (3280.93)cm^{-1} is due to a large amount of OH groups of the carbohydrates and those of lignin. Also at (1045) cm^{-1} corresponds to the link C–O–H or C–O–R (alcohols or esters) while the distinctive band at (2925)cm^{-1} is related to the presence of C–H stretching vibration together with bending vibrations around (1428)cm^{-1} of aliphatic chains (–CH_2– and –CH–) forming the basic structure of this lignocellulosic materials.

Active Group	Positive Number
OH	(3280.93) cm^{-1}
CH	(2920.79) cm^{-1}
P-H	(2349.26) cm^{-1}
C = O	(1739.69) cm^{-1}
C = C	(1606.04) cm^{-1}
-CH_2	(1416.56) cm^{-1}
-CH_3	(1367.84) cm^{-1}
CH-OH	(1236.60) cm^{-1}
C–O-H or C–O-R	(1012.75) cm^{-1}
= CH	(670.85) cm^{-1}
C-Br	(664.41) cm^{-1}
O-N≡O	(586.22) cm^{-1}
S – S	(533.05) cm^{-1}

Table 1. The IR active groups and positive numbers of the FTIR tested orange peel powder

1. táblázat A vizsgált narancshéj por mintában detektált IR aktív csoportok és a hozzájuk rendelt hullámszámok

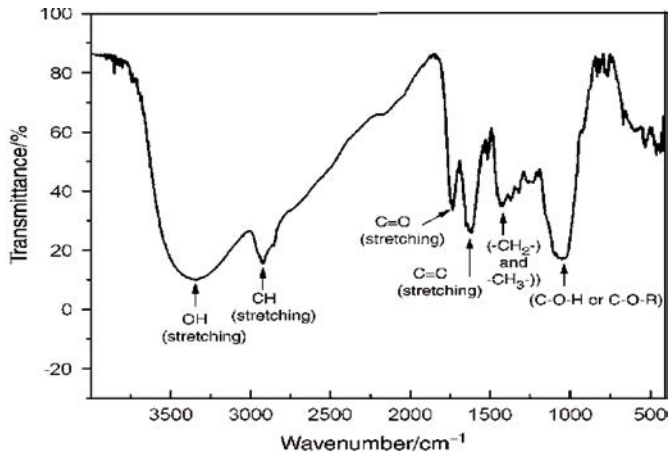

Fig. 3. FTIR spectrum of the dried orange peel sample [20]

3. ábra Szárított narancshéj minta [20] FTIR spektruma

Time	E (V) for samples in 3.5%NaCl solution	E (V) for samples in 3.5%NaCl solution + green inhibitor	i_{corr} ($\mu A/cm^2$) for samples in 3.5%NaCl solution	i_{corr} ($\mu A/cm^2$) for samples in 3.5%NaCl solution + green inhibitor	CR (mm/year) for samples in 3.5%NaCl solution	CR (mm/year) for samples in 3.5%NaCl solution + green inhibitor
0h	-0,942	-0,857	3,116	2,681	0,0362	0,0312
1h	-0,895	-0,808	2,588	2,511	0,0300	0,0292
3h	-0,895	-0,837	2,542	2,371	0,0300	0,0276
5h	-0,914	-0,895	2,572	2,411	0,0300	0,0280
7h	-0,972	-0,885	2,429	2,402	0,0282	0,0279
24h	-0,867	-0,875	2,572	2,208	0,0299	0,0257

Table 2. Initial corrosion properties of the steel specimen measured in the first 24 hours
2. táblázat A vizsgált betonacél mintákon az első 24 órában mért korróziós jellemzők

3.2 Corrosion Properties Obtained from Electrochemical Polarization Experiments

The adsorptive properties of the chosen green inhibitor can be indirectly sized up relatively easily from the polarization curves which technique is widely used by electrochemists working in the field of corrosion studies. In our case a computer controlled (ZAHNER type potentiostat was used to record the current – potential data which were then converted to corrosion rates according to standard procedures described in ASTM STP 908 [21]. The so obtained corrosion properties (*E*/V, i_{corr}, and CR values) are all summarised in *Table 2* and the corrosion rates (CR) are depicted also in *Fig. 4*.

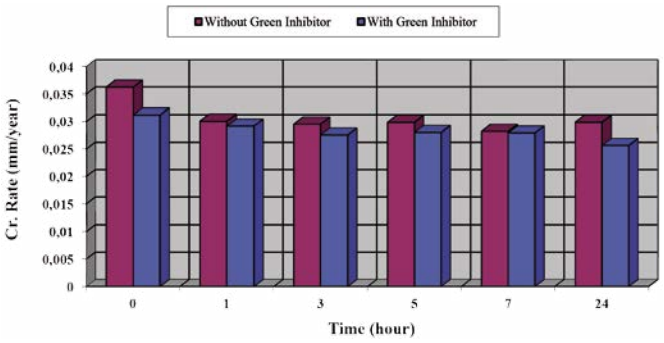

Fig. 4. Calculated initial corrosion rates of the given steel specimen being immersed in 3.5%NaCl solution in contact with air in the first 24 hours
4. ábra Levegővel érintkező és 3,5 % NaCl tartalmú vizes oldatban tesztelt acélminták számított korróziósebesség adatai az első 24 órában

As it is seen in *Figure 4*, the tendency of the corrosion rates is diminishing with time of immersion during the tested first short period of 24 hours, and the rates are always somewhat lower in cases when the NaCl solution contained the extract of the orange peel inhibitor. As the start of chemical attack (i.e. initiation of surface rusting) on the surface of such freshly prepared (cleaned and mechanical polished) steel specimen is always rather slow in such neutral and stagnant aqueous salt solutions in contact with air, the observed tendency should be evaluated accordingly. It means that the inhibitive effect of the chosen and so tested green inhibitor is really plausible and promising.

3.3 Results of SEM and EDS Analysis

In addition to testing the initial corrosion behaviour of the given steel material by the above described electrochemical testing techniques, several sets of the steel rods of about 10 cm long (half having their as-received original surface condition and half acid pickled) were put and kept in three different NaCl solutions for 30 days. One set was the blank (without inhibitor) and the two other sets contained 1 or 3% inhibitors as well.

After 30 days the corroded samples surfaces were examined by scanning electron microscopy (SEM) and the scanned surface areas were also EDS analysed to detect the observable chemical elements in the close to surface zones in depth of about 1 μm.

The first SEM image (*Fig. 5*) shows the as-received surface condition of the reinforcing steel rebar sample obtained from a steel works (ÓAM Ltd., Ózd). Its oxide cover was identified as some kind of mill-scale with an average chemical composition close to that of FeO (wüstite). This surface product is due to the high temperature metal forming technology (hot rolling in air), and it seems to be well adhered, but shows several cracks and distorted areas at higher magnification (*Fig. 5*).

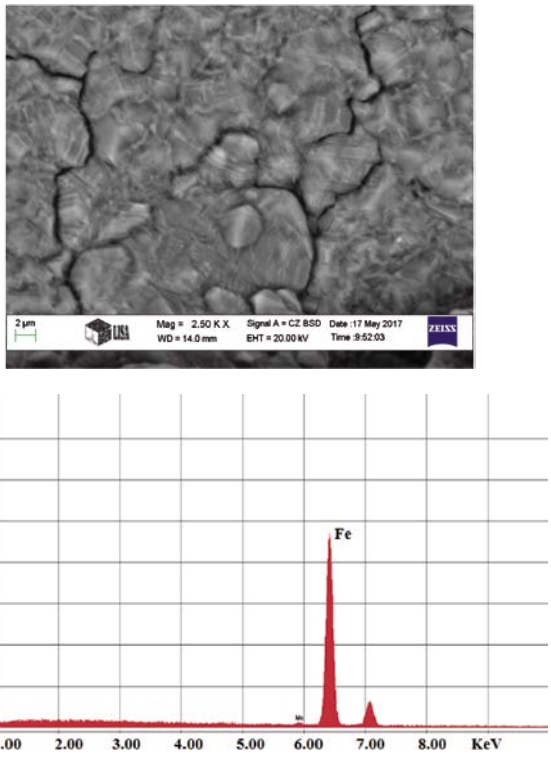

Fig. 5. SEM image and EDS analysis of the steel rebar as recieved from the steel mill
5. ábra Az acélgyártól kapott betonacél minta felületének elektronmikroszkópos (SEM) képe és kémiai elemi összetétele EDS (elektronmikroszondás) elemzéssel meghatározva

After 30 days immersion in the testing NaCl solutions, the corroded surfaces of the steel rebar samples showed quite varied surface morphologies as it is demonstrated in a randomly selected SEM image shown in *Figure 6*.

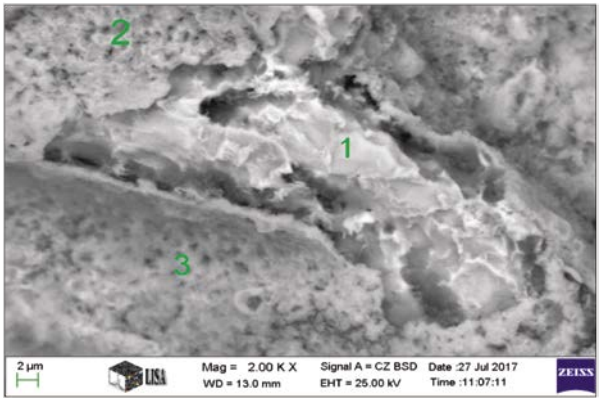

Fig. 6. SEM image of a small rusted surface region of a steel rebar sample first HCl acid pickled to remove the mill-scale then kept in 3.5 % NaCl solution with 3% inhibitor in air for one month. EDS spot analysis showed approximate Fe and O atomic percentages at Point 1: Fe ~89 at%, O ~9 at%; at Point 2: Fe ~54 at%, O ~44 at%; and at Point 3: Fe ~49 at%, O ~50 at%.

6. ábra Sósavas pácolással revétlenített, majd egy hónapig 3,5 % NaCl-ot és 3% inhibitort is tartalmazó, s levegővel is érintkező vizes oldatban korrodálódott betonacél minta rozsdás felületének kicsiny részlete (SEM felvétel), és a jelölt három pontban elvégzett EDS mikroszondás elemzések eredménye (közelítő Fe és O atomszázalékos értékek): az 1 pontban: Fe ~89 at%, O ~9 at%; a 2 pontban: Fe ~54 at%, O ~44 at%; és a 3 pontban: Fe ~49 at%, O ~50 at%.

Although the exact identification of the most probable corrosion products was not aiming at in this research, but their approximate average surface coverage was estimated based on the EDS area analysis taking into consideration the limitations of this technique while trying to analyse such rather thin and heterogeneous surface layers of various and loose corrosion products. Therefore, for the correct interpretation of the EDS analysis one should always remember the important fact that the EDS microanalysis (using the given apparatus type ZEISS) provides information only from the outermost surface zone with a maximum depth of about 1 µm. Moreover, the elementary composition obtainable from such a close to surface volume does not contain the amount of hydrogen, which element is not detectable by this technique. Hence, the atomic percentages given below the SEM images (i.e. in *Figures 6-7*) do provide only some approximate average ratios of Fe and O present in the surface oxide-hydroxide layers plus that of mostly Fe in the zone (i.e. in the bulk steel) underneath the oxide-hydroxide cover.

Knowing that the oxide-hydroxide corrosion products formed in such circumstances on such type of steels are different iron oxide-hydroxides like Lepidocrocite (γ-FeOOH), Akaganeit (β-FeOOH), and Goethite (α-FeOOH), it follows that in all these phases the atomic ratios of Fe to O is 1:2 (i.e. ~33 at.% to ~66 at.%), disregarding the presence of H. Based on such a comprehension, and evaluating the EDS detected Fe to O atomic percentages given in *Figure 7*, it can be concluded with high certainty, that the oxide-hydroxide corrosion layer formed on the surfaces of the steel rebar samples exposed for one month to the corrosion attack of inhibited stagnant NaCl aqueous test solutions in contact with air, could not develop/grow as thick as in the case without inhibitor.

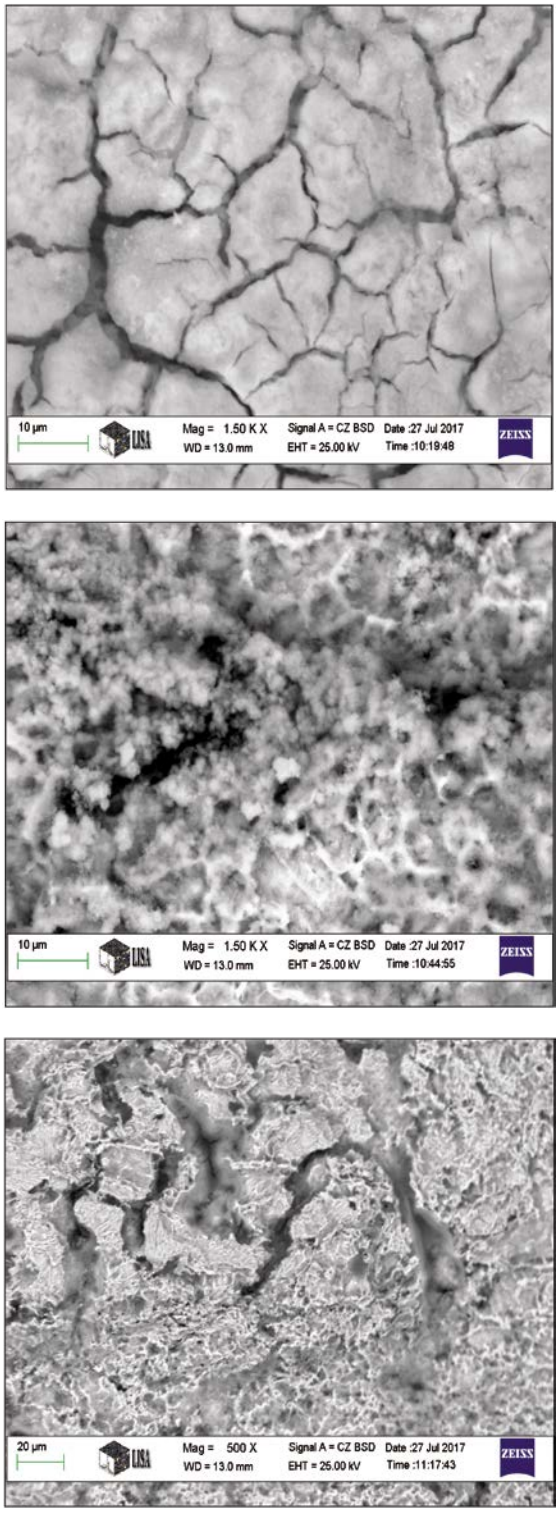

Fig. 7. SEM images with the results of EDS area analysis of the as received steel rebar samples kept in stagnant NaCl solutions without (a-), with 1% (b-), and 3% (c-) inhibitor for one month. Approximate Fe and O concentrations detected in the close to surface thin corroded zones were as follows: a) Fe ~52.6 at.%, O~44.3 at.%; b) Fe ~61.2 at.%, O~35.7 at.%; and c) Fe ~66 at.%, O~18 at.%. (Other minor detected elements are not listed.)

7. ábra Egy hónapig stagnáló (nem kevert) NaCl-os vizes oldatban egy hónapig korrodálódott betonacél minták felületének SEM felvételei és ezeken a korrodálódott felületrészeken EDS mikroszondás elemzéssel meghatározott Fe és O atomszázalékos koncentrációk (a kis mennyiségben detektált egyéb elemek nélkül). Jelölések: (a-) inhibitor nélkül; (b-) 1% inhibitorral; és (c-) 3% inhibitorral. Fe és O tartalmak a vizsgált minták felületközeli tartományaiban: a) Fe ~52.6 at.%, O~44.3 at.%; b) Fe ~61.2 at.%, O~35.7 at.%; and c) Fe ~66 at.%, O~18 at.%.

4. Concluding remarks

During our laboratory experiments the tested orange peel extract has shown promising positive effect on inhibiting the corrosion rate of iron in close to neutral aqueous NaCl solutions in contact with air.

In the future the new orange peel extract inhibitor will also be tested as an admixture of freshly prepared concrete laboratory specimens reinforced with steel rebars in order to explore its potential applicability in the building industry.

5. Acknowledgements

We would like to thank everyone who helped us to complete this research; especially Árpád Kovács working in the SEM laboratory at the Institute of Physical Metallurgy, Metal Forming and Nanotechnology, and the technician from the BorsodChem extraction laboratory.

We must also not forget the efforts of the Institute of Metallurgy in providing all the possibilities available to us in order to make this research successful.

References

[1] Abosrra, L. – Ashour, A. F. – Youseffi, M. (2011): Corrosion of Steel Reinforcement in Concrete of Different Compressive Strengths, *Journal of Construction and Building Materials*, Vol.25, No.10, pp. 3915–3925. https://doi.org/10.1016/j.conbuildmat.2011.04.023

[2] Talbot, D. – Talbot, J. (1998): Corrosion Science and Technology, CRC Press, Taylor & Francis, ISBN 9781138745896.

[3] Bentur, A. – Diamond, S. – Berke, N. S.(1997): Steel Corrosion in Concrete: Fundamentals and Civil Engineering Practice, CRC Press, Taylor & Francis, ISBN 9780419225300.

[4] Bertolini, L. – Elsener, B. – Pedeferri, P. – Redaelli, E. – Polder, R.B. (2014): Corrosion of Steel in Concrete: Prevention, Diagnosis, Repair, 2nd Edition, Wiley, ISBN: 978-3-527-33146-8.

[5] ACI Committee 222 (2005): Protection of Metals in Concrete Against Corrosion, ACI 222R-01, ACI Manual of Concrete Practice.

[6] Broomfield, J. P. (2007): Corrosion of Steel in Concrete: Understanding, Investigation and Repair, Second Edition, CRC Press, Taylor & Francis, London, ISBN 9780415334044.

[7] Wong, H. S. – Karimi, A. R. – Buenfeld, N. R. – Zhao, Y. X. – Jin, W. L. Microstructure of corroded steel-concrete interface, on the web: http://www.imperial.ac.uk/structural-engineering/research/structural-materials/microstructure/

[8] Zhao, Y. X. – Karimi, A. R. – Wong, H. S. – Hu, B. Y. – Buenfeld, N. R. – Jin, W. L. (2011): Comparison of Uniform and Non-uniform Corrosion Induced Damage in Reinforced Concrete Based on a Gaussian Description of the Corrosion Layer, *Corrosion Science*, Vol.53, No.9, pp.2803-2814. https://doi.org/10.1016/j.corsci.2011.05.017

[9] Sagoe-Crentsil, K. K. – Glasser, F. P. (1989): Steel in Concrete: Part I. A Review of the Electrochemical and Thermodynamic Aspects, *Magazine of Concrete Research*, Vol.41, No.149, pp.205– 212. https://doi.org/10.1680/macr.1989.41.149.205

[10] Glasser, F. P. – Sagoe-Crentsil, K. K. (1989): Steel in Concrete: Part II. Electron Microscopy Analysis, *Magazine of Concrete Research*, Vol.41, No.149, pp.213–220. https://doi.org/10.1680/macr.1989.41.149.213

[11] Sagoe-Crentsil, K. K. – Glasser, F. P. (1993): Green Rust, Iron Solubility and the Role of Chloride in the Corrosion of Steel at High pH, *Cement and Concrete Research*, Vol.23, No.4, pp.785–791. DOI: 10.1016/0008-8846(93)90032-5

[12] Burubai, W. – Dagogo, G.(2007): Comparative Study of Inhibitors on the Corrosion of Mild Steel Reinforcement in Concrete, Agricultural Engineering International: the CIGR Ejournal, Vol.9, pp.1-10.

[13] Mahdi, A. S.(2014): Urea Fertilizer as Corrosion Inhibitor for Reinforced Steel in Simulated Chloride Contaminated Concrete Pore Solution, *International Journal of Advanced Research in Engineering and Technology*, Vol.5, No.5, pp.30-39.

[14] Al-Otaibi, M. S. – Al-Mayouf, A. M. – Khan, M. – Mousa, A. A. – Al-Mazroa, S. A. – Alkhathlan, H. Z.(2014): Corrosion Inhibitory Action of Some Plant Extracts on the Corrosion of Mild Steel in Acidic Media, *Arabian Journal of Chemistry*, Vol.7, No.3, pp.340–346. https://doi.org/10.1016/j.arabjc.2012.01.015

[15] Sanyal, B. (1981): Organic Compounds as Corrosion Inhibitors in Different Environments — A review, Progress in Organic Coatings, Vol.9, No.2, pp.165-236. https://doi.org/10.1016/0033-0655(81)80009-X

[16] Sangeetha, M. – Rajendran, S. – Muthumegala, T. S. – Krishnaveni, A. (2011): Green Corrosion inhibitors-An Overview, Zaštita Materijala, Vol.52, No.1, pp.3-19. http://www.sitzam.org.rs/zm/2011/No1/ZM_52_1_3.pdf

[17] Kundu, M. – Prasad, S. K. – Kumar, V. (2016): A Review Article on Green Inhibitors of Reinforcement Concrete Corrosion, *International Journal of Emerging Research in Management &Technology*, Vol.5, No.1, pp.42-46. https://www.ermt.net/docs/papers/Volume_5/1_January2016/V5N1-125.pdf

[18] EN 10080 (2005): Steel for the Reinforcement of Concrete, European Commission mandate, 23 December 2005.

[19] Sastri, V. S.(2011): Green Corrosion Inhibitors: Theory and Practice, John Wiley & Sons, Inc, ISBN: 978-0-470-45210-3.

[20] Zapata, B. – Balmaseda, J. – Fregoso-Israel, E. – Torres-García, E. (2009): Thermo-kinetics study of orange peel in air, *Journal of Thermal Analysis and Calorimetry*, Vol.98, pp.309–315. https://doi.org/10.1007/s10973-009-0146-9

[21] Moran, G. C. – Labine, P. (1984): ASTM STP 908: Corrosion Monitoring in Industrial Plants Using Nondestructive Testing and Electrochemical Methods, Canada, 22-24 May 1984, ISBN-EB: 978-0-8031-4974-8.

Ref.:
Abdulsada, Shaymaa Abbas – **Török**, Tamás I. – **Fazakas**, Éva: *Preliminary Corrosion Testing of Steel Rebar Samples in 3.5%NaCl Solution with and without a Green Inhibitor*
Építőanyag – Journal of Silicate Based and Composite Materials, Vol. 70, No. 2 (2018), 48–53. p.
https://doi.org/10.14382/epitoanyag-jsbcm.2018.10

Acélbetétek korróziós vizsgálata 3,5% NaCl oldatban zöld inhibitor alkalmazásával és anélkül

Olcsó szerves hulladéknak minősülő narancshéjból új inhibitor anyagot (ún. „zöld" inhibitort) vontunk ki, melynek acélbetétek korrózióvédelmi célra történő alkalmazhatóságát többféle kísérleti módszerrel laboratóriumi körülmények között vizsgáltuk. Az egyik magyarországi acélgyártól kapott betonacél minták több sorozatát (eredeti revés és revétlenített állapotukban egyaránt) vizes 3,5 %-os nátrium-klorid oldatokba merítettük és a szokásos elektrokémiai polarizációs méréstechnikát alkalmazva meghatároztuk a metanolos extrakcióval kinyert inhibitort is esetenként (1, illetve 3 %-ban) tartalmazó vizes közegben kialakuló kezdeti korróziós sebességeket az első 24 órában. Az új „zöld" inhibitor aktív csoportjait FTIR spektrometriásan identifikáltuk, mely aktív csoportoknak köszönhetően ezen új inhibitor felületszorpciós hatása által képes volt jól érzékelhetően csökkenteni a vizsgált acél minták korróziósebességét. Az egy hónapos korróziós hatásnak kitett mintákat pásztázó elektronmikroszkópos (SEM) és EDS mikroszondás felületanalitikai módszerekkel is elemeztük.
Kulcsszavak: acélbetét vasbetonhoz, narancshéj, korróziós tulajdonságok, SEM EDS elemzés

Alagúttüzek hatása az alagútfalazat és kőzetkörnyezet teherbírására

CSANÁDY Dániel ▪ BME Építőanyagok és Magasépítés Tanszék ▪ csanady.daniel@epito.bme.hu
FENYVESI Olivér ▪ BME Építőanyagok és Magasépítés Tanszék ▪ fenyvesi.oliver@epito.bme.hu
LUBLÓY Éva Eszter ▪ BME Építőanyagok és Magasépítés Tanszék ▪ lubloy.eva@epito.bme.hu
MEGYERI Tamás ▪ Mott MacDonald Magyarország Kft. ▪ tamas.megyeri@mottmac.com
Érkezett: 2018. 01. 05. ▪ Received: 05. 01. 2018. ▪ https://doi.org/10.14382/epitoanyag-jsbcm.2018.11

Effects of tunnel-fire on load bearing capacity of tunnel-lining and surrounding rock mass
The effect of tunnel-fire can causes significant changes in strength of the tunnel-lining and the rock environment. Different concrete specimens which modelled the closer and further part of the lining from the fire were tested after different heating and cooling treatments. Diagrams and reducing factors recommended by the standard MSZ EN 1991-1-2:2005 were investigated by different conditions according to hydrocarbon fire curve. The reason of differences between the test results and standard curve were investigated. The reasons of failures were analysed due to the breaking surfaces and failure shape of specimens and processes during heating and cooling. The resulted differences were investigated to apply particular numerical model which can handle the temperature changes. The change of compressive strength and Young's modulus were measured and compared with the standard values. The Young's modulus which was calculated from measured compressive strength was also compared with the measured values. Temperature has been determined where the measured and calculated curves fit correctly and the required reducing factors also.
The test results showed that in case of tunnel fires the reducing factors depends on heating and cooling rates. The calculated Young's modulus values are accurate until a certain limit and beyond this limit Young-modulus can be considered as zero. Starting from the test results, the possibility of creating a fast and efficient routine method was investigated. This method is able to predict the conditions of load-bearing structure of fire-loaded tunnels, after fire.
Keywords: Tunnel-fire, standard fire curve, high temperature, concrete, compressive strength, modulus of elasticity
Kulcsszavak: Alagúttűz, szabványos tűzgörbe, magas hőmérséklet, beton, nyomószilárdság, rugalmassági modulus

CSANÁDY Dániel
Okl. építőmérnök, doktorandusz a BME Építőanyagok és Magasépítés Tanszékén. Fő érdeklődési körök: építőanyagok (kiemelten beton) tűzzel szembeni viselkedése, környezetbarát építőanyagok, biomimetika, hőszigetelés, hangszigetelés, új építőanyagok fejlesztése.

Dr. FENYVESI Olivér
Dr. Fenyvesi Olivér (1981), okl. építőmérnök (BME 2005), PhD (BME 2012), műemlékvédelmi szakmérnök (BME 2017), adjunktus a BME Építőanyagok és Magasépítés Tanszékén. Fő kutatási területei: betonok korai (autogén+száradási) zsugorodása, korai zsugorodási repedések normál és könnyűbetonokban, szálerősített betonok, szálerősített könnyűbetonok, könnyűbetonok tartóssága, önterülő könnyűbetonok, épületdiagnosztika, épített örökség védelme. A Szilikátipari Tudományos Egyesület Beton Szakosztályának titkára illetve Kő és kavics szakosztályának tagja, a *fib* (Nemzetközi Betonszövetség) Magyar Tagozatának tagja, a Magyar Mérnöki Kamara tagja.

Dr. LUBLÓY Éva
Dr. Lublóy Éva (1976) okl. építőmérnök (BME Építőmérnöki Kar 2001), adjunktus a BME Építőanyagok és Magasépítés Tanszékén (2008). Fő érdeklődési területei: vasbetonszerkezetek viselkedése tűz hatására, tűzkárok mérnöki tanulságai. A *fib* Magyar Tagozatának tagja.

MEGYERI Tamás
Okl. Építőmérnök (Mott MacDonald Magyarország Kft. 2007), alagutak és földmegtámasztó szerkezetek tervezésével foglalkozó geotechnikus mérnök.

1. Bevezetés

Cikkünk a Szilikátipari Tudományos Egyesület által 2016-ban meghirdetett diplomapályázaton II. helyet elnyert diplomamunka témáját mutatja be.

Az alagúttüzekből származó hőhatás jelentős változásokat eredményezhet az alagútfalazat és a kőzetkörnyezet szilárdsági és merevségi tulajdonságaiban, esetlegesen teljesen tönkre is teheti a szerkezeti elemeket (*Sarma, Ramana, 1979, Rideg, 2014)*. Külön-külön már számos vizsgálat készült a kőzetkörnyezet (Görög 2007a, Görög 2007b) és az alagútfalazat vizsgálatáról (Parkinson, Ékes 2008). E mellett több szerző foglalkozott a falazat és kőzetkörnyezet egymásra hatásával is (Gál, Görög 2013, Oreste 2003). A hő hatására történő szilárdságváltozás mind a kőzetkörnyezet, mind a falazat szempontjából fontos. Gránitos kőzetek esetén a hő hatására történő szilárdságváltozásról *Török et al (2015)* írt, alagútfalazat betonjának vizsgálatát tűz hatására például Hertz (2003) végezte. A tűzből és tönkrement szerkezetből való mentés és a helyreállítás során az életvédelem a legfontosabb szempont. Az anyagi kár nyilvánvalóan annál nagyobb minél tovább van üzemen kívül egy alagút. Az említett veszélyek és károk minimalizálása érdekében vizsgáltuk azt, hogy a szabványban megadott szilárdságcsökkentő tényezők alagúttüzek esetén való alkalmazása megfelelően pontos eredményeket adnak-e a tervezéshez.

2. Célkitűzések

Munkánk során alapvetően a tűz anyagjellemzőkre gyakorolt hatásával foglalkoztunk, kiemelve a vasbeton alagútfalazatban a beton anyagjellemzőinek változását visszahűlt állapotban. A diplomamunkában, a kőzetkörnyezetben hő hatására bekövetkező változásokra is kitértünk, de ez nem képezi jelen cikk témáját. Egy gyors és egyszerű eszközökkel végrehajtható, hőterhelés utáni maradó szilárdság/merevség becslési módszer megalkotásának lehetőségét is vizsgáltuk. Alagúttűz esetén, ha a tűz időtartama, maximális hőmérséklete ismert és azonos maximális hőmérsékletig, azonos időtartamig tartó hőterheléssel előállíthatók a sérült beton tulajdonságaival közel azonos tulajdonságú próbatestek, megállapítható, hogy körülbelül milyen mértékű károsodást szenvedett az alagútfalazat. Eltérő felfűtési sebességgel a tűzfészekhez közeli vagy távolabbi falazatrészek modellezhetők és az eltérő hűtési módokkal szimulálható a különbség a falazat oltásakor hirtelen, vízzel lehűtött, illetve oltást követően a levegőn lehűlt részei között. A próbatestek csökkent szilárdságából következtetni tudunk arra, hogy a falazat különböző átmelegedésű zónáiban mekkora a szilárdságcsökkenés. A hőterhelt és az etalon (hőterhelés nélküli) próbakockák szilárdsági értékeinek viszonyszámából következtetni lehet a rugalmassági modulus változására is.

3. Tűz hatása beton/vasbeton falazatra

A hőmérséklet emelkedésével a beton szilárdsági jellemzői romlanak *(1. ábra)*. A beton a lehűlés során részlegesen sem nyeri vissza eredeti tulajdonságait, jellemzőit, mivel a hőterhelés hatására a beton szerkezetében irreverzibilis folyamatok mennek végbe, a beton anyagszerkezete megbomlik, és végezetül tönkremegy (Lublóy, 2008).

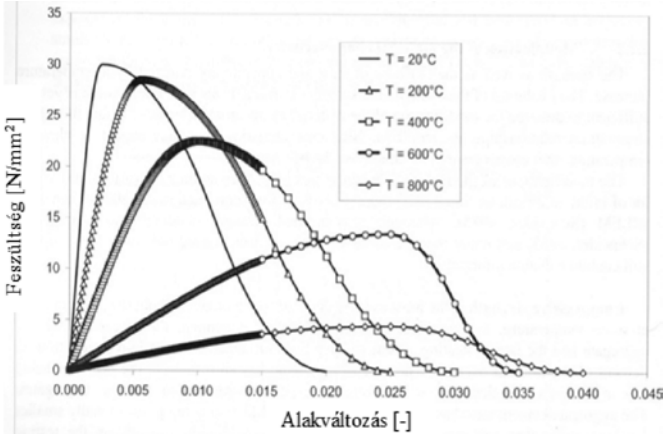

1 ábra A beton nyomószilárdságának változása a hőmérséklet függvényében (fib bulletin 38, 2007.)
Fig. 1. Compressive strength of concrete on different temperatures

2 ábra Száladagolás nélkül készült alagútelem 1200°C-os hőterhelés után (fent) és 2 kg/m³ polipropilén száladagolással készült alagútelem 1200°C-os hőterhelés után (lent) (Mörth, et al., 2005)
Fig 2. Tunnel element made without fibres after fire loading on 1200 °C (above) and tunnel element made with 2 kg/m³ of polypropylene fibres after fire loading on 1200 °C (below)

Alagutak esetén fontos, hogy a betonfelületek réteges leválása tűz esetén ne következzen be. Számos kísérlet igazolta, hogy ennek veszélye műanyagszálak alkalmazása esetén lényegesen kisebb, mivel a szálváz kiégése során létrejövő pórusszerkezet a szétrepedés veszélyét csökkenti. (Mörth, et al., 2005). Alagútelemekkel végzett kísérlek igazolták, hogy a polipropilén szálerősítésű betonok felületének réteges leválása a tűz hatására (1200 °C) nem következett be (2. ábra). Ausztriában egy kutatócsoport (Walter, et al., 2005) vasbeton födémeket tesztelt, melyeket gépekkel terheltek, majd kétórás tűzterhelésnek vetettek alá. A betontakarás rétegesen levált a szálerősítés nélküli födémeknél, azonban az 1-3 V% polipropilén szállal készült tábláknál réteges leválás nem volt tapasztalható. Általánosságban kijelenthető, hogy a kis átmérőjű, kis hosszúságú polipropilén szálak kedvező hatással vannak a betonra tűzteher esetén, mivel a réteges leválást akadályozzák (Horiguchi, Suhaendi, 2005, Lublóy, 2016).

A réteges leválás egyik kiváltó oka a megnövekedett pórusgőz-nyomás. A gőz és gázok által kifejtett nyomás a keresztmetszet mentén változik, de nem a tűzzel terhelt felület környezetében a legnagyobb. A felületközeli rétegekben a nyílt pórusrendszer a nyomást hatékonyan csökkenti. Ugyanakkor kis mélységben, ahol már a pórusok kiegyenlítő hatása nem érvényesül, létrejön egy „vízgőz-gát"(3. ábra).

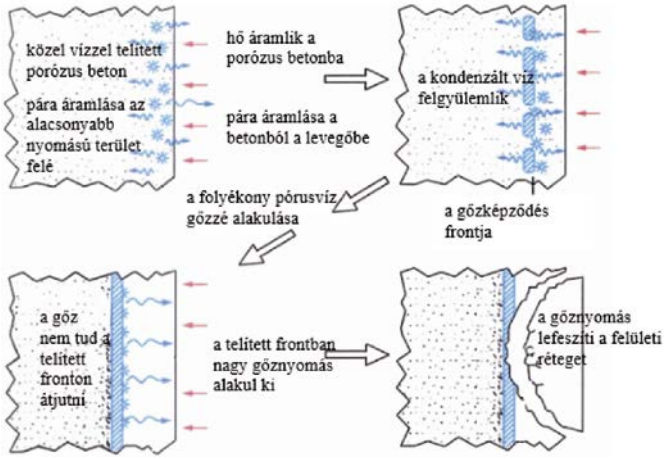

3. ábra A betonfelület réteges leválása gőznyomás hatására (Winterberg, Dietze, 2004)
Fig. 3. Spalling of concrete surface due to vapour pressure

A betonacélok szilárdsága 400 °C-os hőmérséklet felett kezd rohamosan csökkeni. 1000 °C környezetében a vasalás teherbírása gyakorlatilag nullára csökken. Különbséget kell tenni a melegen hengerelt és a hidegen húzott betonacélok hőhatásra való méretezése között (*MSZ EN-1992-1-2*).

4. Kőzetkörnyezet viselkedése magas hőmérsékleten

Gránitoknál a kezdeti hőmérséklettartományban (~300 °C-ig) a nyomószilárdság 80%-kal megnő, majd magasabb, 600°C-os hőmérsékleten 15%-os szilárdságcsökkenés tapasztalható a 22 °C-os állapothoz képest *(Török,* Török, *2013)*.

A húzószilárdság értéke a magas hőmérséklet hatására csökken, 550 °C -nál a húzószilárdság értékében hirtelen esés ész-

lelhető *(Sarma, Ramana, 1979)*. A vizsgálati tapasztalatok szerint a húzószilárdság a nyomószilárdság értékének 10%-a körül van. A pillanatnyi rugalmassági modulus értéke a hőmérséklet és a nyomás függvénye. A hőmérséklet emelkedésével a gránit minták rendre veszítenek a rugalmasságukból, 300 °C-nál pedig a rugalmassági modulus (kőzettömb) a felére csökken *(Sarma, Ramana, 1979)*. Ezeket az eredményeket Török, Török (2013) ausztriai gránitokon végzett vizsgálatai is alátámasztották. Rideg (2014) számítással igazolta, hogy alagutakban már csekély hőmérsékletváltozás is okozhat elmozdulásokat.

5. Laboratóriumi vizsgálatok

A vizsgálatok során két betonösszetételt alkalmaztunk (1. táblázat). A betonok mindkét esetben kvarckavics és kvarchomok adalékanyaggal és CEM I 42,5 N típusú cementel készültek, szilárdsági osztályuk C55/67. A két betonösszetételnek a víz-cement tényezője tért el (és ebből adódóan a folyósító adalékszer mennyisége). Meg kell jegyeznünk, hogy a CEM III heterogén cementek kedvezőbben viselkednek a tűzzel szemben, de jelen esetben nem a teljesítmény maximalizálása hanem a teljesítmény változásának vizsgálata volt a cél. Mindkét összetétel esetén két fajta próbatest készült, 150 mm élhosszúságú, szabványos próbakocka és 70 mm x 70 mm x 250 mm-es kisméretű hasáb.

Minden próbatest tömörítése vibroasztalon történt, (beton lövellő gép nem ált rendelkezésünkre) kizsaluzás után a próbatesteket az *MSZ EN 1992-1-1:2010* szabványnak megfelelően tároltuk. A próbakockákat 8 darab részre vágtuk, így átlagosan 75 mm élhosszúságú, kisméretű kockákat kaptunk (később „kisméretű kocka"). A kisméretű kockák alkalmazását indokolta, hogy ezekből egyszerre több helyezhető a kemencébe és gyorsabban érik el teljes térfogatukban a kívánt hőmérsékletet, így a vizsgálat gyorsabb. A kisméretű kockákon mért értékek átszámíthatók szabványos nyomószilárdsági értékekre, a hőterhelt kisméretű kockákon mért szilárdsági értékeket, azonos méretű, 20°C-on mért szilárdsági értékekhez viszonyítottuk, így kiejthető a próbatest méretének hatása. A kapott hányadossal beszorozva a szabványos próbatestek 20 °C-on mért szilárdsági értékét megkapjuk a szabványos (*MSZ EN 1992-1-1:2010*) szilárdságot. A kísérleteket a BME Építőanyagok és Magasépítés Tanszékének anyagvizsgáló laboratóriumában végeztük.

4. ábra Próbatestek hőterhelés (fent) és nyomószilárdság vizsgálat után (lent)
Fig 4. Specimens after heat (without naked flame) load (above) and compressive strength test (below)

A kemencét szabadon fűtöttük fel (megelőző hőmérsékleti lépcsők nélkül) és a benne lévő próbatesteket hőn tartottuk 1 órán keresztül, a próbatesteket lánghatás nem érte, kizárólag a

C 55/67							
Anyag	**Fajta vagy frakció**		**Tömeg [kg/m³]**	**Térfogat [l/m³]**	**Keverés 50 l [kg]**	**Víztartalom [kg]**	**Korrekció**
Adalékanyag	0/4 mm frakció	45%	833,40	315,09	41,67	1,67	43,34
	4/8 mm frakció	25%	463,00	175,05	23,15	-	-
	8/16 mm frakció	30%	555,60	210,03	27,78	0,41	28,19
	Összesen	100%	1852,00	700,19	92,60	-	-
Cement	CEM I 42,5 N		390,00	125,80	19,50	-	-
Víz	m/mc=	0,41	160,00	160,00	8,00	-	5,92
Adalékszer cem m %	Glenium 323	1,00%	3,90	3,90	0,20	-	-
Levegő			-	10,00	-	-	-
Összesen			2406	1000	-	-	-

1. táblázat Az első betonösszetétel
Table 1. The first concrete mixture

kemencében lévő magas léghőmérséklet hatására melegedtek fel (*4. ábra*).

A kisméretű kockákat és a hasábokat négy hőmérsékleten terheltük, 300 °C, 500 °C, 800 °C, 1000 °C -on. Az első keverékből származó hasábok és próbakockák hőterhelése négy fajtára bontható:

- **LL jelű:** 20 °C-os hasáb és kisméretű kocka 20 °C-os kemencébe helyezve, T °C-ra felfűtve, 1 órán át hőn tartva, majd laborlevegőn lehűtve. Ezen próbatestek a falazat tűzfészektől távolabb lévő, lassabban felmelegedő és oltás közben vízzel nem érintkezve, lassan lehűlő részeit modellezik.
- **HS jelű:** 20 °C-os hasáb és kisméretű kocka 20 °C-os kemencébe helyezve, T °C-ra felfűtve, 1 órán át hőn tartva, majd vízbe lehűtve. Szintén a lassabban felmelegedő falazatrészeket modellezi, amelyek oltás közben vízzel érintkezve gyorsan hűlnek le.
- **LL+ jelű:** 20°C-os hasáb és kisméretű kocka T °C-os kemencébe helyezve, 1 órán át hőn tartva, majd laborlevegőn lehűtve. Ezek a próbatestek a tűzfészek közelében lévő, szénhidrogének égése esetén fellépő, nagyon gyors léghőmérséklet emelkedésnek kitett és oltás közben vízzel nem érintkezve, lassan lehűlő falazatrészeket modellezik.
- **HS+ jelű:** 20 °C-os hasáb és próbakocka T °C-os kemencébe helyezve, 1 órán át hőn tartva, majd vízbe lehűtve. Ezek a próbatestek a tűzfészek közelében lévő, szénhidrogének égése esetén fellépő nagyon gyors léghőmérséklet emelkedésnek kitett és oltás közben vízzel érintkezve, hirtelen lehűlő falazatrészeket modellezik.

Az első keverésből készült próbatesteket az összes említett hőterhelési módon vizsgáltuk, majd kiválasztottuk azt a két esetet, melyeknél a legnagyobb szilárdságcsökkenést tapasztaltuk, és ami a valósághoz legközelebb áll. Ez a két eset az LL+ és a HS+ jelű hőterhelési mód volt, ahogy az *5. ábrán* is látható, ez a két hőterhelési mód roncsolja legjobban a próbatesteket. A második kísérleti sorozatból származó próbatesteket már csak a két választott módon hőterheltük.

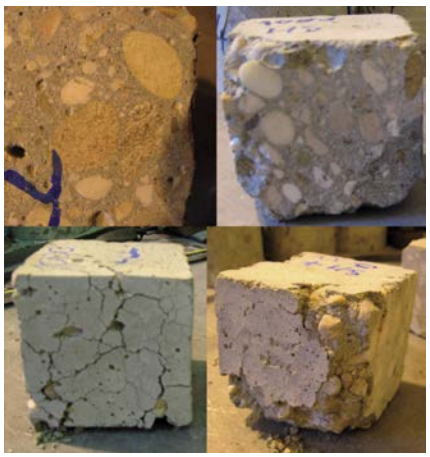

5. ábra Próbakockák 1000°C-os hőterhelés után (jel szerint balról jobbra: felső sor: LL, HS, alsó sor: LL+, HS+)
Fig. 5. Specimens after heat load on 1000 °C (signs from left to right: top row: LL, HS, bottom row: LL+, HS+)

Az alagútfalazat modellezésének és erőtani méretezésének szükséges, de nem feltétlenül elégséges bemenő adata a beton hőterhelés utáni maradó nyomó, hajlító-húzó szilárdságára és rugalmassági modulusa.

Hőmérsékleti lépcsőnként, minden hőterhelés típusból kapott eredményt három próbatest vizsgálatával határoztunk meg. A nyomószilárdsági vizsgálatokat a próbatest kis mérete miatt 2,7 kN/s terhelési sebességgel végeztük Form+Test Alpha4 típusú hidraulikus törőgép használatával.

A beton rugalmassági modulusának változása arányos a nyomószilárdság megváltozásával, így a rugalmassági modulus számítható. Az MSZ EN 206-1:2002 az

$$E_{cm} = 22 * [(f_{cm})/10]^2$$

képlettel adja meg ezt az összefüggést. A képlet 150 mm-es próbakockára vonatkozik és jelen esetben a következőképpen módosul,

$$E_{cm} = 22 * [(f_{cm} \times \frac{f_{cmT}}{f_{cm20}})/10]^2.$$

ahol:

f_{cm} a beton 20 °C-on meghatározott nyomószilárdságának átlagértéke 20 °C-on tárolt, 150 mm élhosszúságú próbakocka esetén, (N/mm²)

f_{cmT} a beton 20 °C-on meghatározott nyomószilárdságának átlagértéke azonos sebességű felfűtésnek és ez után 1 órás T °C-os hőterhelésnek alávetett, majd lehűlt 75 mm élhosszúságú próbakocka esetén (N/mm²)

f_{cm20} a beton 20 °C-on meghatározott nyomószilárdságának átlagértéke 20 °C-on tárolt 75 mm élhosszúságú próbakocka esetén (N/mm²).

A második kísérletsorozatból származó kockákon mért nyomószilárdságokból átszámított értékeket ellenőrzésként összehasonlítottuk az azonos keverésből származó, hőterhelt hasábokon mért rugalmassági modulussal. Ha az eltérés megfelelően kismértékű, akkor feltételezhetően elegendő az egyszerűbb és kevésbé időigényes vizsgálatokat elvégezni (ez egyértelműen még nem jelenthető ki jelen kísérletsorozat alapján, ehhez további nagyszámú vizsgálatra van szükség, mely meghaladja egy diplomamunka terjedelmét). A mért és számított értékek adott hőmérsékleti határig megfelelően közelítették egymást, illetve konstans csökkentő tényező bevezetésével az említett határon túl is biztosítható a jó közelítés.

A réteges leválás oka alapvetően a beton húzószilárdságának lokális kimerülése. A hajlító-húzószilárdág vizsgálatokat központos hajlítással végeztük. A kapott húzószilárdsági értékek összevethetők az alagúttűz numerikus modelljéből kapott húzófeszültség értékekkel, így lehet következtetni a réteges leválás bekövetkezéséhez szükséges feszültségekre. Emellett a kevésbé roncsolódott próbatestek törési felületének szemrevételezésével információ szerezhető a beton hő hatására megváltozott struktúrájáról, ilyen például az átkristályosodott kvarc, a kontaktzóna tönkremenetele, a beton elszíneződése a keresztmetszet mentén.

A rugalmassági modulus méréseket, 70*70*250 mm-es hasábokon végeztük videoextenzométeres technológiával Instron 5989 típusú univerzális törőgépen *(6. ábra)*. Minden eredményt három próbatest mérési átlagaként határoztunk meg.

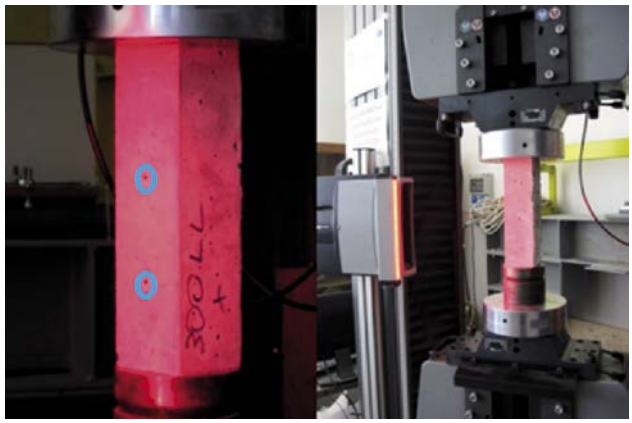

6 ábra *Rugalmassági modulus mérése videoextenzométerrel (mérési pontok a kék körökben)*
Fig. 6. *Testing of modulus of elasticity by video-extensometer (measuring points in blue circles)*

6. Kísérleti eredmények

A próbatestek és törési felületük szemrevételezéséből következtetni lehet a tönkremenetel módjára, a nem tönkrement beton károsodásának mértékére, illetve a végbement kémiai és fizikai változásokra. Az 1000 °C-on hőterhelt hasábok (összes típus) teljes szilárdságukat elvesztették, a cementkő kézzel morzsolhatóvá vált, a cementkő és az adalékanyag váz közti kapcsolat megszűnt, a kvarc adalékanyag szemek eltörtek. Az 1000 °C-on hőterhelt próbakockák erősen megrepedeztek, sarkaik lepattantak, a felületen lévő adalékszemek kiperegtek. Ezek oka, hogy 1000 °C-ig több szilárdságcsökkentő folyamat lejátszódik, a maradó szilárdság zérusnak tekinthető. A 800 °C-on hőterhelt LL és HS jelű próbatesteknél nyomó illetve hajlító-húzó szilárdsági vizsgálatok után az adalékszemek kifordultak a cementkőből. Ennek oka a kontaktzóna tönkremenetele, ami az adalékanyag és a cementkő magas hőmérsékleteken eltérő hőtágulása és a kvarckavics α-ból β módosulatba való kristályátalakulása miatt következik be. A kristályátalakulás 5,7%-os térfogat-növekedéssel jár *(Koch, Sztrókay , 1994)*. A hasábok törési felületén majdnem a teljes keresztmetszet mentén elszíneződött a cementkő, tehát a hő hatására átalakult a kristályszerkezet.

A 800 °C-os LL+ és HS+ jelű próbatesteknél vegyesen találtunk cementkőből kifordult és eltört adalékszemeket a szilárdsági vizsgálatok után. Ezek a próbatestek 800 °C-os hőterhelés után nagyobb maradó szilárdsággal rendelkeztek mit az LL és HS jelű próbatestek. A 20 °C-ról felmelegített próbatesteknél a kémiai átalakulások jobban végbe tudtak menni, mivel a próbatest adott hőmérsékleti intervallumok közt több időt töltött. Az a jelenség hogy az LL+ és HS+ jelű hőterhelési módon terhelt próbatestek nagyobb maradó szilárdsággal rendelkeznek mint a másik két terhelési mód esetén, csak 800°C-os hőterhelésnél volt tapasztalható, alacsonyabb és magasabb hőmérsékleteken nem. A 800 °C-on terhelt LL és HS próbakockák enyhén megrepedeztek, a sarkok és élek kis mértékben sérültek, néhány felületi adalékszem kipergett a próbatestekből, a felület elszíneződött. Ennek oka a kvarc átalakulása, az adalékanyag és cementkő eltérő hőtágulása és a cementkőben 800 °C-ig lejátszódó folyamatok összessége.

Az 500 és a 300 °C-on hőterhelt LL és HS jelű hasábok törésekor az adalékszemek kifordultak a cementkőből, ennek oka az lehet, hogy egyenletes felfűtés során az adalékszemek nem repedtek el, így az eltérő hőtágulásból származó feszültségek a cementkő és az adalékanyag határán összpontosultak, tönkretéve a tapadást. Az LL+ és HS+ hasáboknál szintén láthatóak a hirtelen hőmérsékletemelkedés hatására elpattant adalékszemek, ami csökkenti a beton próbatest integritását. A hasábok törési felületén látszik, hogy a keresztmetszet kisebb része színeződött el, mint magasabb hőmérsékleteken, tehát csak a felülethez közeli részeken alakult át a cementkő kristályszerkezete. A próbakockák felületén nem látható nagyobb mértékű elváltozás, néhány, a kontaktzóna környezetében lévő, kisebb repedésen és kisebb felületi elszíneződésen kívül.

A mérési eredmények igazolták, hogy a négy hőmérsékleti lépcsőből három esetén a legkedvezőtlenebb hatást a betonra a gyors lehűtés gyakorolja egy esetben azonban, a 800°C-on elvégzett terhelések esetén az LL és HS hőterhelési módokból származtak a legkisebb mért értékek *(7. ábra)*. A hőterhelési lépcsőkön a maradó szilárdság értékeket összehasonlítottuk az *MSZ EN 1991-1-2:2005* által javasolt csökkentő tényezőkkel *(7.* ábra), alacsonyabb hőmérsékleti tartományban (300 °C) a szabvány szerinti csökkentő tényező túlbecsli a valós értéket, így szabvány szerinti szilárdságcsökkenés mellett, akár még a felületen hagyható a sérült beton. Ezt a nagyobb, valós szilárdságcsökkenés miatt nem érdemes a felületen hagyni, mert csökkenti a megerősítő beton vastagságát, és nagy valószínűséggel a sérült beton tapadószilárdsága is nagyobb mértékben csökken, ezzel rontva a megerősítés minőségét. Az eltérés oka az lehet, hogy ezek a csökkentő tényezők szabványos tűzgörbére (nem szénhidrogén tűzgörbére) lettek maghatározva, jelen esetben viszont a felfűtés sebessége gyorsabb volt mindkettő fajta felfűtési módnál. Ezen felül eltérést okozhat az, hogy az EC felhevült állapotban vizsgálja a szilárdságcsökkenést, esetemben viszont lehűlt próbatestekről van szó, amelyeknek általában nagyobb a szilárdságcsökkenése, mint a még nem visszahűlt próbatesteké, amit a lehűlés során kialakuló repedések magyaráznak. 300 °C felett a szabvány által megadott csökkentő tényezők a biztonság javára közelítenek.

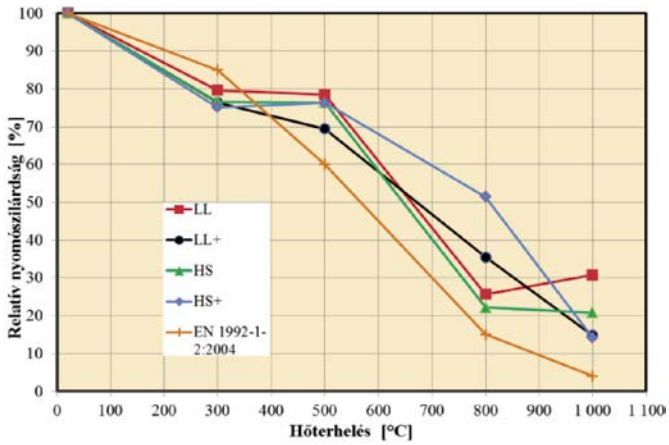

7. ábra *Az első betonösszetételből származó próbakockák relatív nyomószilárdsága a hőmérséklet függvényében*
Fig. 7. *Relative residual compressive strength of specimens from the first concrete mixture as a function of temperature of heat loading*

A második betonösszetételből kapott relatív szilárdsági értékeket szintén összehasonlítottuk a szabvány által javasolt csökkentő tényezőkkel. Itt a mért és javasolt maradó szilárdságok valamivel jobban közelítették egymást, mint az első betonkeverék esetén. Az előbbiekben említett okok mellett a szabvány és a kísérleti görbék eltérése abból is adódik, hogy a beton struktúrája erősen roncsolódik a hősokk miatt. Az 1000 °C-on hőterhelt próbatestek már a kemencében felrobbantak, erősen megrepedeztek vagy a lehűtés során veszítették el teljesen a szilárdságukat, így ezeknél a próbatesteknél 0-nak tekinthetjük a szilárdságot *(8. ábra)*.

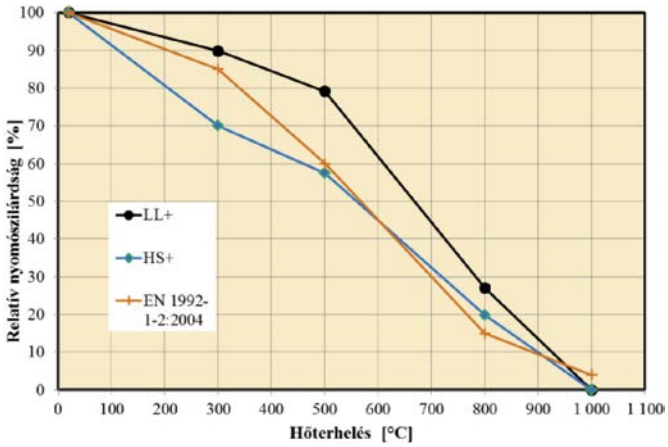

8. ábra *A második betonösszetételből származó próbakockák relatív nyomószilárdsága a hőmérséklet függvényében*
Fig. 8. *Relative residual compressive strength of specimens from the second concrete mixture as a function of temperature of heat loading*

Az első betonkeverék rugalmassági modulusának változását mind a négy fajta próbatesten vizsgáltuk *(9. ábra)*. A második keverékből származóknak csak az LL+,HS+ változatain mértünk rugalmassági modulust. A hasábokon mért rugalmassági modulus eredmények 300 °C és 500 °C estében az LL+ jelű próbatesteknél 94-96%-ban megegyeztek a próbakockák nyomószilárdságából számított értékekkel, a HS+ jelű próbatesteknél ez az arány csak 85-87%-os. Itt a hősokk során a hirtelen térfogatváltozások miatt sérül a cementkőváz és a kontaktzóna szerkezete, amit a szabvány képlete jelenlegi formájában nem tud figyelembe venni. Az LL+ jelű testeknél így az eltérés 10%-on belül marad, ez megengedhető pontatlanság, viszont a HS+ jelű próbatestek számított eredményeire érdemes bevezetni egy 0,85-ös korrekciós tényezőt (az általunk modellezett hőterhelés esetén).

800°C-on hőterhelt próbatesteknél a nyomószilárdságból számított rugalmassági modulus és a mért értékek között nagyságrendi eltérések voltak. Mire a próbatestek elérik a 800 °C-ot addigra a cementkőben végbemenő kémiai átalakulások teljesen lezajlanak, ami jelentősen gyengíti azt, ezenfelül a kvarckavics adalékanyag térfogatváltozáson megy keresztül, ami nagymértékben roncsolja a kontaktzónát. A rugalmassági modulus 800°C-on a kezdeti értékhez képest (20 °C) 10% alá esik vissza, ezeket az értékeket érdemes (a biztonság javára) zérusnak tekinteni. A rugalmassági modulusokat a kezdeti értékhez viszonyítottuk (relatív rugalmassági modulus), így jobban érzékelhető a beton folyamatos tönkremenetelének mértéke *(10. és 11. ábra)*.

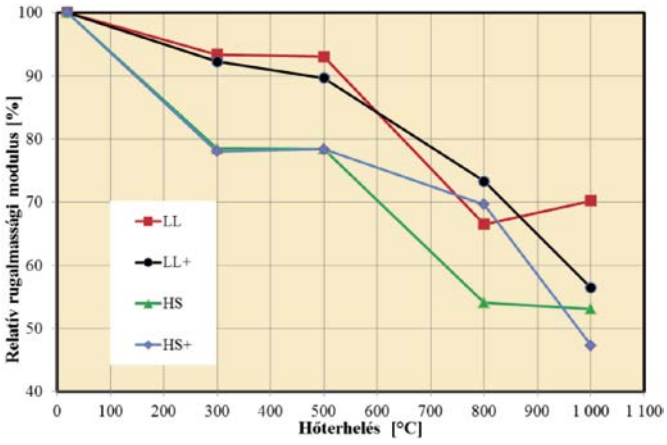

9. ábra *Az első keverésből származó próbatestek mért relatív rugalmassági modulusának változása a hőmérséklet függvényében*
Fig. 9 *Relative residual Young's modulus of specimens from the first concrete mixture as a function of temperature of heat loading*

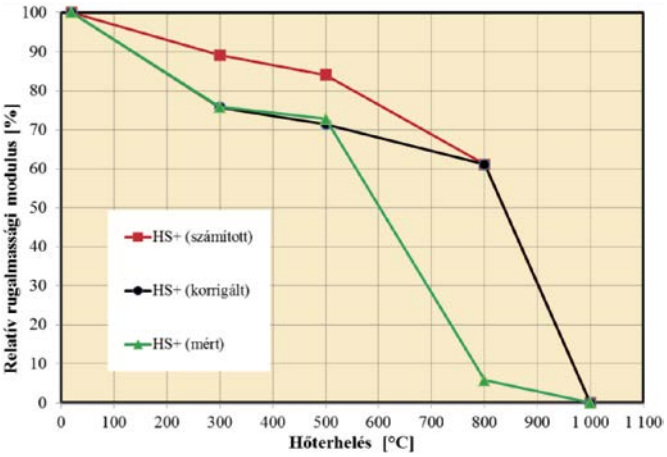

10. ábra *A második keverésből származó HS+ jelű próbatestek relatív rugalmassági modulusának változása a hőmérséklet függvényében, számított, korrigált és mért értékek*
Fig. 10 *Relative residual Young's modulus of HS+ specimens from the second mixture as a function of temperature, calculated, corrected and measured values*

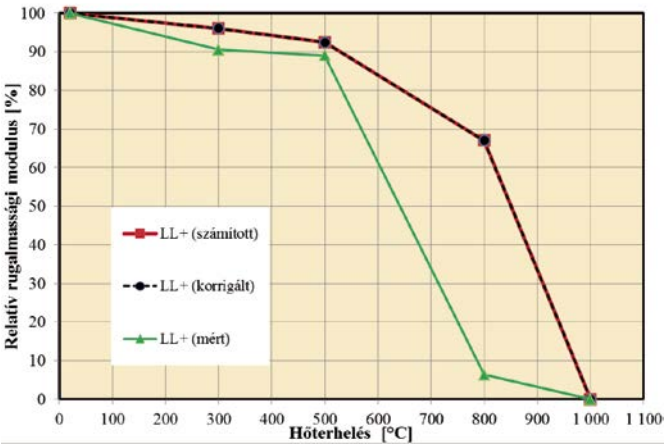

11. ábra *A második keverésből származó LL+ jelű próbatestek relatív rugalmassági modulusának változása a hőmérséklet függvényében, a számított, korrigált és mért értékek*
Fig. 11. *Relative residual Young's modulus of LL+ specimens from the second mixture as a function of temperature, calculated, corrected and measured values*

A laborvizsgálatokból kapott eredményeket később felhasználtuk erőtani számításokhoz alagútfalazat numerikus 2D és 3D modelljeihez. Ezek alkalmazását és eredményeit cikkünk 2. részében tárgyaljuk.

7. Megállapítások

Vasbeton alagútfalazatot modellező beton próbatestek anyagtulajdonságainak változását mértük hőteher hatására, visszahűlt állapotban. Két, CEM I 42,5 N típusú cementből és kvarckavics adalékanyaggal készült, C55/67 szilárdsági osztályú betonkeveréket vizsgáltunk. Felfűtés és lehűtés szempontjából négy eltérő hőterhelési módot alkalmaztunk. A próbatestek nyomószilárdságát, hajlító-húzó szilárdságát és rugalmassági modulusát mértük. A kapott relatív nyomószilárdsági értékeket összehasonlítottuk a *MSZ EN 1991-1-2:2005* által javasolt különböző hőmérsékleti lépcsőkhöz tartozó csökkentő tényezőkkel. Majd azt vizsgáltuk, hogy a hőterhelt, kisméretű próbakockákon mért nyomószilárdsági értékekből (relatív nyomószilárdság használatával) az *MSZ EN 206-1:2002* által megadott képlettel számított rugalmassági modulusok milyen mértékben közelítik meg a hőterhelt hasábokon mért, valós rugalmassági modulus értékét. Mind a szilárdsági, mind a rugalmassági modulus görbék közti eltéréseknél elemeztük azok lehetséges okait. Megfigyeléseink és a kísérleti eredmények alapján a következő megállapítások tehetők:

- a négy hőmérsékleti lépcsőből három esetén nyomószilárdság és rugalmassági modulus csökkenés szempontjából is a gyors felmelegítésű és lehűtésű próbatestekből származtak a legkisebb értékek.
- Ez alól a 800 °C-os hőlépcső kivétel, itt a lassabban, 20°C-ról felmelegített próbatesteknél nagyobb szilárdság és rugalmassági modulus csökkenést tapasztaltunk, mint a gyors felmelegítésű és lehűtésű próbatesteknél. Ezek a próbatestek adott hőmérsékleti intervallumok közt több időt töltöttek, így a kémiai átalakulások és az ezzel járó térfogatváltozások jobban végbe tudtak menni és kifejteni károsító hatásukat.
- Az *MSZ EN 1991-1-2:2005* szabványban megadott diagramok és csökkentő tényezők csak korlátozottan alkalmasak a szilárdságcsökkenés becslésére az általunk modellezett alagúttűz esetén. Ennek oka, hogy több tényezőt nem vesznek figyelembe (lehűlés során keletkező repedések, hősokk (oltás) közben sérülő kontaktzóna, stb.) és, hogy szabványos tűzgörbére lettek meghatározva.
- Vizsgálataink alapján nem elég egyfajta csökkentő tényező-hőmérséklet görbét alkalmazni tűzesetek utáni modellezéshez, hanem több eltérő görbe használata indokolt, felmelegítési és lehűtési sebességek kombinációjától függően, vagy összetettebb, a hőmérsékletváltozásra és annak sebességére érzékenyebben reagáló tapasztalati összefüggések szükségesek. Ezek megfelelő minőségű elkészítéséhez nagy volumenű vizsgálatokra van szükség.
- A laborlevegőn lehűlt próbatestek nyomószilárdságaiból számított rugalmassági modulus értékek 500 °C-os hőterhelésig közel esnek (az eltérés 10%-on belüli) a mért értékekhez. A hősokkolt próbatesteknél egy 0,85 értékű csökkentő tényezővel szintén hasonló egyezés érhető el.
- 800 °C eléréséig az általunk vizsgált beton már olyan átalakulásokon és roncsolódáson megy keresztül, amit a képlet nem tud figyelembe venni, ezért a mért és számított értékek eltávolodnak egymástól. Több hőmérsékleti lépcső esetén pontosabban megállapítható az a pont, ahol a számított és mért görbék különbsége már túl nagy lesz.
- 800 °C feletti hőterhelés esetén a maradó rugalmassági modulus 0-nak tekinthető, ezért a számított és mért rugalmassági modulus eltérése nincs hatással a későbbi erőtani számításokra.

Megemlítendő, hogy a kis mintaszám miatt a jelen kutatási eredményeket, nagyobb próbatestszám mellett ellenőrizni kell a megfelelő pontosság elérése érdekében.

Irodalomjegyzék

[1] Gál, E. – Görög, P. (2013): Lőttbetonos alagútfalazat és kőzet kapcsolatának vizsgálata gránitos kőzetkörnyezetben, In: Török Á, Görög P, Vásárhelyi B (szerk.), *Mérnökgeológia-Kőzetmechanika* 2013. 366 p. Budapest: Hantken Kiadó, 2013. pp. 165-176., Mérnökgeológia-Kőzetmechanika Kiskönyvtár; 16., ISBN:978-615-5086-06-9

[2] Görög, P. (2007a): Characterization and the mechanical properties of the eocene buda marl, CENTRAL EUROPEAN GEOLOGY 50:(3) pp. 241-258., Print ISSN: 1788-2281 Online ISSN: 1789-3348, https://doi.org/10.1556/CEuGeol.50.2007.3.4

[3] Görög, P. (2007b): Engineering geologic properties of the Oligocene Kiscell Clay, CENTRAL EUROPEAN GEOLOGY 50:(4) pp. 313-329. Print ISSN: 1788-2281 Online ISSN: 1789-3348, https://doi.org/10.1556/CEuGeol.50.2007.4.2

[4] Hertz, K. D. (2003): Limits of spalling of fire-exposed concrete, *Fire Safety Journal*, 38, pp103–116, ISSN: 0379-7112, https://doi.org/10.1016/S0379-7112(02)00051-6

[5] Horiguchi, T. – Suhaendi, S. L. (2005): Fiber-reinforced High-strength Concrete Under Elevated Temperature, Effect Of Fibers On Residual Properties (Conference), *Fire Safety Science*, pp. 271-278., https://doi.org/10.3801/IAFSS.FSS.8-271

[6] Koch, S. – Sztrókay, K. I. (1994): „Ásványtan II.", Budapest, Nemzeti Tankönyvkiadó, 5. kiadás, 566–581.o., ISBN 963 18 5973 8

[7] Lublóy, É. (2008): Tűz hatása betonszerkezetek anyagaira, Doktori disszertáció, Budapesti Műszaki és Gazdaságtudományi Egyetem, Budapest

[8] Lublóy, É. (2016): „Szálerősítésű betonok alkalmazása a tűzvédelemben", *Védelem tudomány: Katasztrófavédelmi online tudományos folyóirat*, I :2„ pp. 518-535. , ISSN 2498-6194

[9] Mörth, W. – Haberland, Ch. – Horvath, J. – Mayer, A. (2005): „Behaviour of Optimized Tunnel Concrete with Special Aggregates at High Temperature", *Proceedings of Central European Congress on Concrete Engineering*, Graz, pp. 41-50.

[10] MSZ EN 1991-1-2:2005, (2005), Eurocode 1: A tartószerkezeteket érő hatások. 1-2. rész: Általános hatások. A tűznek kitett szerkezeteket érő hatások

[11] MSZ EN 1992-1-1:2010, (2010), Eurocode 2: Betonszerkezetek tervezése. 1-1. rész: Általános és az épületekre vonatkozó szabályok

[12] MSZ EN 1992-1-2:2013, (2013) Eurocode 2: Betonszerkezetek tervezése. 1-2. rész: Általános szabályok. Szerkezetek tervezése tűzhatásra

[13] MSZ EN 206-1:2002, (2002) Beton. 1. rész: Műszaki feltételek, teljesítőképesség, készítés és megfelelőség

[14] Oreste, P. P. (2003): Analysis of structural interaction in tunnels using the covergence–confinement approach, *Tunnelling and Underground Space Technology 18*, pp347–363. ISSN: 0886-7798, *https://doi.org/10.1016/S0886-7798(03)00004-X*

[15] Parkinson, G. – Ékes, Cs. (2008): Ground Penetrating Radar Evaluation of Concrete Tunnel Linings, *Proceedings of 12th International Conference on Ground Penetrating Radar*, June 16-19, 2008, Birmingham, UK, ISBN: 978-1-4244-2111-4

[16] Rideg, D. (2014): „Hőmérsékletváltozás hatása a Nemzeti Radioaktívhulladék-tároló vágataira", Diplomamunka, Budapesti Műszaki és Gazdaságtudományi Egyetem, Budapest

[17] Sarma, L. P. – Ramana, Y. V. (1979): „Thermal expansion of a few indian granitic rocks", *Physics of the Earth and Planetary Interiors*, Vol. 22, Issue 1, April 1980, pp 36-41, https://doi.org/10.1016/0031-9201(80)90098-9 , ISSN: 0031-9201

[18] Török, A. – Török, Á. (2013): Gránitos kőzetkörnyezetben hő hatására bekövetkező kőzetfizikai változások, *Mérnökgeológia-Kőzetmechanika konferencia*, pp. 205-210, BME, Budapest, ISBN 978-963-420-933-1

[19] Török A. – Török Á. – Görög P. (2015): „The effect of temperature on the physical properties of Mauthausen Granite (Austria)", In: MG Winter, DM Smith, PJL Eldred, DG Toll (szerk.), Geotechnical Engineering for Infrastructure and Development: XVI European Conference on Soil Mechanics and Geotechnical Engineering. 4800 p., Edinburgh, Skócia, 2015.09.13-2015.09.17. London: ICE Publishing, 2015. pp. 3401-3406., ISBN: 9780727760678

[20] Walter, R. – Kari, H. – Kusterle, W. – Lindlubauer, W. (2005): „Analysis of the Load-bearing Capacity of Fibre Reinforced Concrete During Fire", *Proceedings of Central European Congress on Concrete Engineering* 8-9 Sept. 2005, (Ed. Pauser, M.), Graz, pp. 54-59., ISBN 963 420 837

[21] Winterberg, R. – Dietze, R. (2004): Efficient passive fire protection systems for high performance, More Engineering Developments: Proceeding for the Second International Conference on Engineering Developments in Shotcrete, Cairnis, Australia, pp. 275-290., https://doi.org/10.1201/9780203023389.ch31

Ref.:
Csanády Dániel – **Fenyvesi** Olivér – **Lublóy** Éva Eszter – **Megyeri** Tamás: *Alagúttüzek hatása az alagútfalazat és kőzetkörnyezet teherbírására*
Építőanyag – Journal of Silicate Based and Composite Materials, Vol. 70, No. 2 (2018), 54–61. p.
https://doi.org/10.14382/epitoanyag-jsbcm.2018.11

Influencing factors of the plate glass columns on the load bearing capacity

András JAKAB ▪ BME Department of Construction Materials and Technologies ▪ jakab.andras@epito.bme.hu

Salem Georges NEHME ▪ BME Department of Construction Materials and Technologies ▪ sgnehme@yahoo.com

Érkezett: 2018. 03. 21. ▪ Received: 21. 03. 2018. ▪ https://doi.org/10.14382/epitoanyag-jsbcm.2018.12

Abstract

The initial imperfection of the structural elements must be taken into account in case of the modern building designing. These imperfections are local or overall defects of the glass elements. These defects are able to reduce significantly the load bearing capacity and the stability limits as well. The initial curvature and the imperfections of the elements are taken into account at the stability designing in case of the general building materials. The applied limits depended on the cross-section of the structural elements. Glass designing for load bearing elements has been applied since a few decades, however there are limits for initial imperfections. More than 240 small scaled I-shaped glass columns were loaded until fracture under laboratory conditions. The lateral buckling was investigated based on the individual experimental procedure. One of the most important properties of the glass columns are the initial imperfections. The higher overall bow and roller wave values can cause disadvantages at the load bearing capacity of the glass columns; however, the roller waves also can increase the critical buckling force according to Euler. These specific factors of the glass specimens were measured by a new measurement method to analyse the effects of the imperfections on the load bearing capacity in case of a small amount of the specimens. The new method contains a Reference Point System and it is able to detect these imperfections in high accuracy. The new measurement method is also able to provide information about the glass manufacturing effects on the plate glass shape.

Keywords: glass, flexural buckling factors, own shape, tin-air side, reference point system

András JAKAB
PhD student at the BME, MSc Civil Engineer. Fields of interests: glass construction, glass columns, non-destructive testing methods, point-fixed glasses construction technology and management.

Salem Georges NEHME
MSc Civil Engineer, PhD, Associate Professor at the Department of Construction Materials and Engineering Geology, Budapest University of Technology and Economics (BME). Member of the Technical committee of Glass Working Group (MSZT/MB 112) of Hungarian Standardization Institute; Hungarian Group of fib; Hungarian engineer chamber (MMK: 01-9159). Fields of interests: concrete technology, mass concrete, self-compacting concrete, fibre reinforced concrete, quality control of building materials, non-destructive testing, reinforced concrete structures, recycling of building materials.

1. Introduction

Despite the fact that there are a lot of negative criticism about the glass materials as load bearing material, the number of the enthusiastic researchers increases every year. Therefore, the material develops at high speed from many aspects. The stability issues of the glass structures are very popular topics nowadays. In the present paper the stability of the plate glass columns and their designing parameters are investigated.

The ideal central loading, the buckling phenomenon and the classical critical load have been known since Euler (*Fig. 1*, *Eq. 1*). The calculation method was just developed for different materials. In the last few years the researchers started to develop and modify the formulas for glasses as well. The imperfection of the glass can highly influence the buckling resistance. Therefore, it is preferred to take into account an initial "w_o" displacement. Jan Belis et al. [1] already investigated the initial imperfections. Mean values were determined based on numerous large-scaled specimens and different measurement method. Products of different glass factories were tested, where differences were found, however measured values complied with the values of standards. The European standards set requirements [2,3]. The question is, which parameters are necessary or useless in the real formulas? Chiara Bedon and Claudio Amadio investigated a long time ago the possibility of design of glass structures with application of VEM models and laboratory experiments [4,5]. Roman Kalamar [6] investigated the load bearing capacity of glass hollow box columns. These researches demonstrate that the designing of glass columns – rather the designing of glass materials - became one of the most investigated topics.

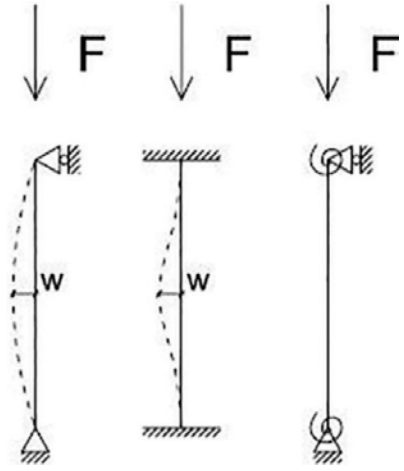

Fig. 1. Basic model for buckling of imperfect glass columns in case of pinned, fixed and flexible support
1. ábra Alap kihajlási modellek imperfect üvegoszlopk esetén csuklós, fix és rugalmas megtámasztással

$$N_{cr} = \frac{\pi^2 EI}{L^2} \quad (1)$$

where:
N_{cr} – critical buckling force
EI – bending stiffness
L – the freely rotated length of the columns

The stability issues of plate glass columns are investigated by the authors since 2012 on small-scaled specimens. In former researches the load bearing capacity, the typical crack patterns,

the buckling phenomenon were determined [5,6,7]. The influence factors of w_0 initial imperfection are investigated in the present paper. The design buckling curves formulas contain the a_{imp} and a_0 factors in the *Eq. 2* [8]. The initial imperfections are decisive point of the calculations the a_{imp} factor contains it (w_0).

$$\Phi = 0{,}5[1 + \alpha_{imp}\left(\bar{\lambda} - \alpha_0\right) + \bar{\lambda}^2] \quad (2)$$

where:

- Φ – buckling parameter of the buckling reduction factor (χ)
- α_{imp} and α_0 – shape factors
- $\bar{\lambda}$ – slenderness

2. Experimental test set-up and parameters

Laboratory experiments were carried out in order to study the buckling behaviour of single and laminated glass columns. Specimens were examined with the application of Instron 5989 testing machine. The scales of the geometry of specimens (height, thickness, width) were selected based on existing glass columns from international and Hungarian realized projects. Test parameters of glass specimens were selected as the following:

Constants: test arrangement; support type; interlayer material (EVA foil with thickness of 0.38 mm); edgework with polished edges; temperature (+23 ± 5 °C). Support: Height of fixing: 95 mm; rubber plate (Shore A 80) was used between the steel supports and the glass.

Variables: type of glass layers: heat strengthened glass (HSG) / non heat-treated float glass (annealed glass); height of specimens: 1000 mm, 920 mm, 840 mm; number of glass layers and the thickness of specimens: single layer: 8 mm, 12 mm, 19 mm; laminated glasses consisted of the following layers: 4.4 mm, 6.6 mm, 8.4 mm, 8.8 mm, 10.10 mm, 4.4.4 mm; glass width: 80 mm, 100 mm, 120 mm; The rate of loading: 0.5 mm/min; 1 mm/min.

Fig. 2. The laboratory test set-up
2. ábra A kísérleti elrendezés

Simplified designations are used to distinguish between the studied specimens, these are e.g. H_2(4.4)_2_920_0.5: ~ H, F: Type of glass: H – HSG; F – non heat-treated float glass; 2(4.4): Number of glass layers ex.: 4.4 mm laminated glass; 2: The number of specimen; 920: Nominate height of specimen [mm]; 0.5: Rate of loading [mm/min]. Abbreviations were used for the float laminated glass VG and for heat-strengthened laminated glass VSG. Although laminated glass with PVB interlayer foil and fully tempered glass (FTG) were not the part of the test parameters, a few pieces of these were tested as well.

The load and vertical displacement of the upper cross-head of the Instron 5989 universal testing machine were continuously measured. At three different heights the buckling displacement (horizontal displacement) of all specimens were continuously measured with HBM displacement transducers during the tests. Strains at center point on the surface of the glass panels were measured with HBM LY11-10/120 strain gauges. At least three specimens were tested at each testing combination. Laminated specimens were loaded until all glass layers were fractured (*Fig. 2*).

Until this moment more than 240 specimens were loaded until fracture, and more than 300 tests were carried out on these glasses including every type of tests: the axial vertical compressive tests until fracture or until the buckling phenomenon, compressive tests where the glasses were installed askew, specimens were loaded in horizontal direction at two different heights etc. The initial imperfections or own shape were measured in case of both sides of 22 glass specimens. These glasses were compressed twice. The ends of the glasses were not fixed in the steel shoes at the first test, when the specimen lost its stability, the test stopped. Both of the ends were fixed, so the area was filled out between the glass and the steel, at the second loading by the same specimen. At the second time the specimens were loaded until their fracture. The effects of the type of fixing can be studied on the buckling phenomenon without varying of the own shape of the specimen. Tin side detector was applied to determinate the types of sides in case of 102 specimens.

3.Previous results

3.1. Determined stages in the loading behaviour

Characteristic curves are presented in *Fig. 3.* as loading force vs. displacement (vertical, horizontal and deformations) diagrams to study the laboratory experimental results. Curves are categorized in three separate groups according to the numerous experimental results. Variation can be noticed in case of loading force vs. horizontal displacement diagrams. The characterization of the specimens depends on the stages of the loading history of the specimens. The name of stages are [7]:

- First stable stage
- Unstable stage
- Second stable stage

3.2. Grouping of the glass specimens

The first group contains all of the previously mentioned stages and in this group were experienced the highest bucking

forces when compared to the other groups results. Force reduction can be observed on the vertical displacement diagrams in the buckling moment. Specific buckling point cannot be determined in case of the second group, the unstable stage disappears and after a stable section, the buckling is gradual. Only one stable stage can be observed in case of the third group, so the ultimate force (that is equal with the critical buckling force according to Euler) can be determined, but the force cannot be determined which belongs to the starting of the buckling (it is called buckling force) [9].

The results of the specimens had to be distinguished depending on the groups of buckling at the comparison of the influence of the variables. All of three types of buckling can easily occur at one testing combination (one type of glass specimen). Despite the fact that different buckling types and different buckling forces are experienced at one testing combination, ultimate forces are equal as shown in *Fig. 3*. The HSG can reach higher horizontal displacements and higher ultimate forces than the annealed glasses. However, the buckling forces of annealed and HSG scatter in the same range. The ranges are different for each testing combination. It also demonstrates that the ultimate limit state depends rather on the glass surface defects and on the glass strength, which can be increased by the heat strengthening. Furthermore, the buckling force depends rather on the imperfections. These experimental results mean that the type of buckling does not influence significantly the value of the ultimate force. These statements are demonstrated at the modelled small-scaled specimens. Probably the first group does not occur in case of real sized glass fins, the second group and most of all the third group occur more frequently.

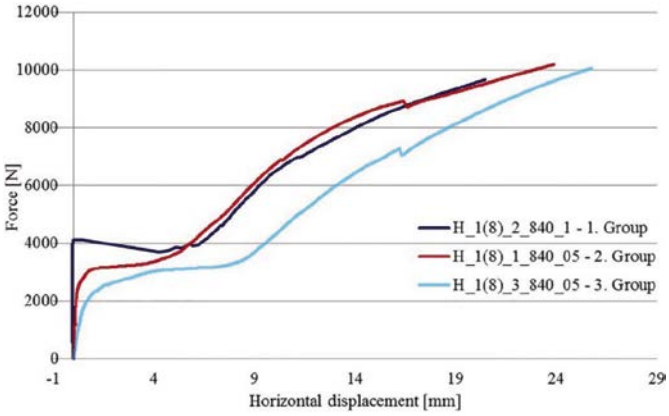

Fig. 3. The loading histories of glasses which belong to one testing combination
3. ábra Egy üvegcsoporthoz tartozó próbatestek különböző terhelési története

3.3. Standards and previous measurements of distortions

The distortion of glass influences heavily the stability and load bearing capacity of the load bearing elements. The influencing distortions are the overall bow, roller wave distortion, edge lift or twisted initial imperfection according to the standard EN 1863-1 [2]. The sinus wave (roller), the overall bow and the loading process are presented until buckling in *Fig. 4*. This standard does not recommend definitely adequate measurement methodology. For instance, the measurement of roller wave is the following: use a straight edge and place it at right angles to the roller wave and bridging from peak to peak of the wave. However, this measurement does not provide continuous information about the shape of the specimen. This methodology seems simple and inaccurate to measure distortion below 1 mm. The own shape initial imperfections need more information about the shape to take into account at the calculation of buckling. The shape of glass surface was measured by international researchers as well [1]. They applied the previous method and a continuous lineside methodology. The linear error meant the own shape of the auxiliary line structure, hence a displacement transducer was applied perpendicular to the surface, and it was moved along the glass.

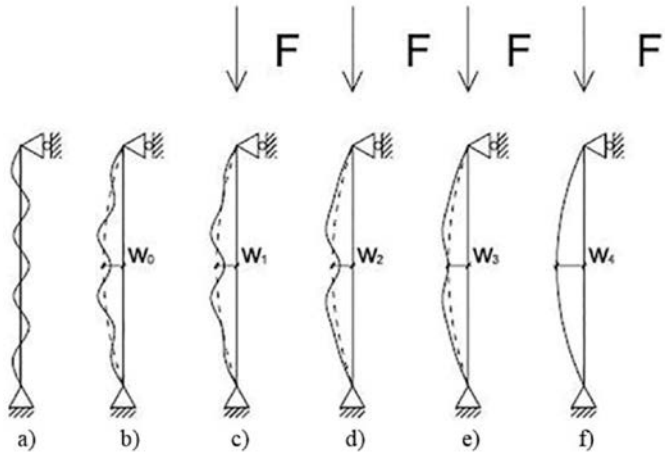

Fig. 4. Magnified roller wave and overall bow distortions of specimen. a) Unloaded specimen with sinus wave distortions b) unloaded specimen with sinus wave and overall bow distortions c-e) phenomenon of a compressed specimen before buckling f) buckled specimen $w_4=w_0+w_t$
4. ábra Nagyított szinusz hullámok és kezdeti kihajlások a) Tehermentes próbatest szinusz hullámai b) tehermentes próbatest szinusz hullámokkal és kezdeti kihajlással c-e) kihajlás előtti alakváltozás nyomóvizsgálat esetén f) kihajlott próbatest $w_4=w_0+w_t$

3.4. New measurement methodology

In our measurement methodology, the glass was fixed and the Wenzel LH 108 3D Coordinate Measuring Machine was moving above of the glass (*Fig. 5*). The glass lied one of its side on the machine. The Metrosoft CM software was applied and micrometer was measured in high accuracy. Reference Point System was the most accurate method for the measurement.

The measurement methodology was the following: Three points were chosen from the four corner points on the surface area of the glass [10]. These points were base points of the measurement and they determine a plane. The different distance between the determined plane and the fourth point was divided between the 4 corner points, so a new plane was determined, in which is an average plane according to the four corner points it is called bestfit method. Three additional different base points were added in the two other axis: two points were perpendicular to the longitudinal axis and one parallel to the longitudinal axis. These points were needed to place the glass in three dimensions. The machine measured the glass waves perpendicular to the surface. The own shape, twisting and the other distortions were determined with the application of this measurement. The measured points were placed in three different lines, two lines were placed 15 mm

from the edges in longitudinal direction. The third line was in the middle of the specimen. The measured points were placed 15 mm from each other in one line. The application of closer measuring point system does not increase the accuracy of the measuring only the measuring time. Three measured lines were applied in case of the 80 mm wide specimens.

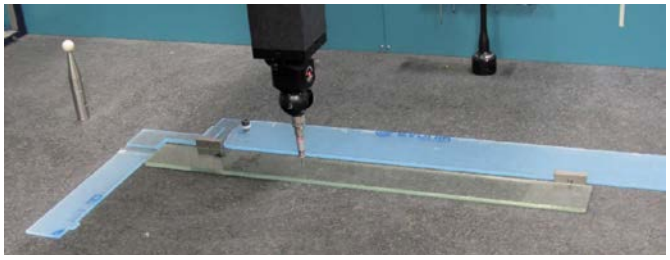

Fig. 5. Distortion measuring of glass specimen by the Wenzel LH 108 3D Coordinate Measuring Machine
5. ábra A Wenzel LH 108 3D Koordináta mérő műszerrel mért üvegek saját alak mérése

4. The results of the distortion measurement

4.1. Prediction of the buckling direction

The statements are drawn based on the distortion measurement results of 22 specimens. The measured points of the surface were integrated into different diagrams to show the own shape of the glasses. In general, the buckling direction of the specimens is occurred on the side where the higher values of sinus waves or overall bow were measured from the two sides. The statement proved to be true 8 and 6 times in case of the annealed glass and HSG. 3 and 5 times (annealed glass and HSG) the specimens buckled the other side where smaller measurement values were determined. The direction depends on the loading conditions and on the damping in the fixing area. In our laboratory test set-up, the last two conditions were constant, however the own shape of the specimens varied significantly at the tested specimens.

The reliability of the prediction of the buckling direction increased if the own shape is also taken into account next to the maximal overall bow and the mean sinus wave values. After the loading, the predicted direction was appropriate in case of 19 specimens from 22. These results indicate that the buckling direction is not predictable only based on the overall bow or sinus wave values. The whole shape of the glass should be known for the prediction of buckling direction.

4.2. Results of the sinus wave values

The applied sensitive measurement method enabled the authors to measure the smaller curves on the glass surfaces. It is already standardized that the heat strengthening procedure causes smaller curvatures which are called sinus waves (*Figs. 6* and *7*). The waves are formed when the heated glass plate – which was melted until the melting point - started to congeal and slightly formed on the ceramic rollers. The effect of the sinus wave can increase the buckling resistance in case of load bearing glass columns based on the basic Euler theory. Therefore, it is not easy to decide that altogether heat strengthened glasses are suitable materials for load bearing glass columns or not. Smaller curvatures can be observed in case of annealed glasses which cannot call sinus waves, because their distribution is unequal and their depth varied in larger range. The incidence of the smaller curvatures depends highly on the shape of the original glass plate (from where it was cut out) and the lamination procedure. Two glass plates, which had different own shapes, take on a new common shape after the lamination process, and this new common own shape will be independent. In *Figs. 6* and *7* the measured own shapes are drawn by blue sign, however it is needed to magnify to be evaluable that is sign by red colour.

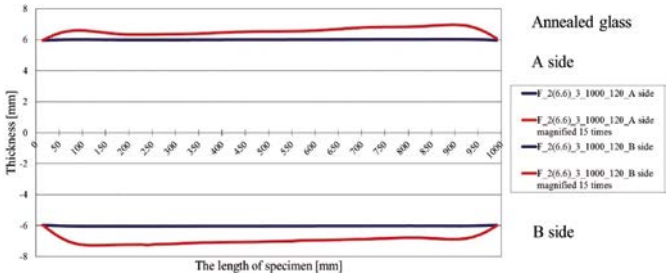

Fig. 6. Distortion measurement results in case of annealed laminated glass
6. ábra Egyrétegű float üveg saját alakja

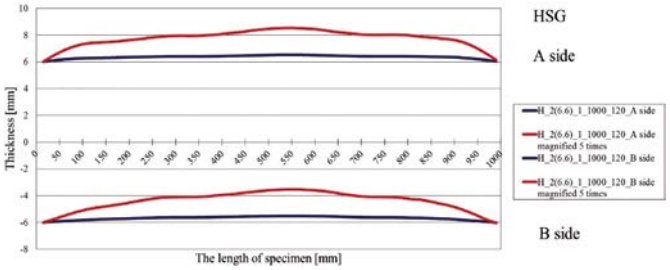

Fig. 7. Distortion measurement results in case of heat strengthened laminated glass
7. ábra Hőkezelt üveg saját alakja

In *Fig. 8* the absolute mean sinus wave values of the 120 mm width specimens can be observed. There were a few 80 mm width measured specimens as well. The values were measured on both sides of the glasses. Only 9 mean sinus wave values can be observed from 22 measurements in case of annealed glasses (the sinus wave of the annealed glass is not the typical wave phenomenon as in case of the HSG rather a similar surface property which is caused by the basic glass producing - floating - method). The mean sinus wave can be determined in all cases of the HSG. The depths of the sinus waves depend on the thickness (bending stiffness), heat strengthening and lamination process. The first conspicuous result is that the sinus wave values of the HSG are at least 3 times larger than the results of annealed glass. The maximal difference measured in case of the 80 mm width laminated glass consisted of two 6 mm layers where the sinus wave values of HSG were 17 times larger than the annealed glass. The number of the analysed specimens are not enough to determine accurate tendencies and correlations between the lamination, heat strengthening and the thickness. The conclusions need statistical evaluation as well due to the higher standard deviation of glass material. In former articles it was determined that the lamination process (also different lamination method) and heat strengthening increase the measured values, however that results cannot be seen due to the high standard deviation [10].

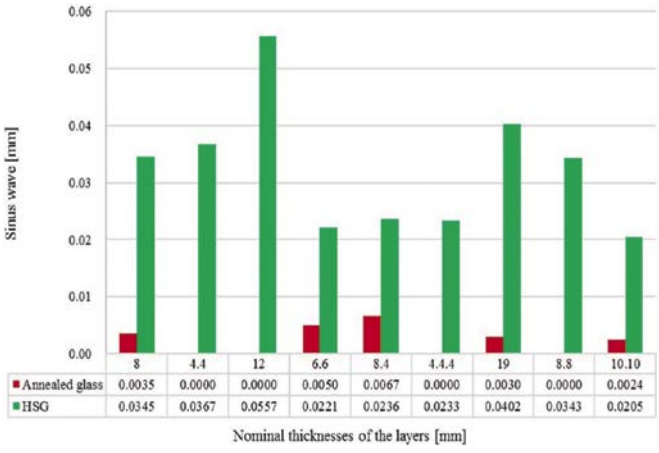

	8	4.4	12	6.6	8.4	4.4.4	19	8.8	10.10
Annealed glass	0.0035	0.0000	0.0000	0.0050	0.0067	0.0000	0.0030	0.0000	0.0024
HSG	0.0345	0.0367	0.0557	0.0221	0.0236	0.0233	0.0402	0.0343	0.0205

Fig. 8. Roller wave results in function of the nominal thicknesses of the layers
8. ábra Szinusz hullámok értékei a névleges vastagság függvényében

4.3. Own shape results

Between the specimens, there were similar and different figures based on the own shape results. Each own shape was compared to each other in the basic curvature. The own shapes of the annealed glasses were similar in 5 cases and different in 6 cases, while this ratio was 9 to 2 in case of the HSG. The effect of the heat strengthening procedure is that the own shape of glasses can be unified to a certain extent, however the overall bow and sinus wave values remain different, they cannot be unified due to the basic glass material differences (*Figs. 6* and *7*).

4.4. Closing of the end of laminated annealed glass plates

The two measured surfaces of a specimen were installed into one diagram, where it can be seen that the ends of the laminated glasses are closed in case of most of the annealed glasses, this phenomenon does not appear in case of HSG (*Figs. 6* and *7*). It can be observed in case of 6 annealed specimens and 1 HSG and it does not appear in case of 1 annealed and 6 HSG. The closing of the end of glass plates can be deduced to the lamination process. In the autoclave lamination system with EVA foil the pressure is generated by the air aspiration. It is interesting that the closing appears in case of annealed glasses but it cannot observe in case of HSG. Causes to be sought at the effect of the heat strengthening. The theoretical causes can be found at the unification glass plate by the heat strengthening which can fit better on each other and this fitting can be observed along the glass length while the own shape of annealed glass cannot fit on this low temperature and the applied pressure is only enough for the ending. The highest vacuum effect is at the glass edges, where the fitted HSG did not close in contrast to the annealed glass. The thickness of the specimens was measured by a calibrated calliper and a Bohle apparat (GlassBuddy Plus). The measured values did not show relevant differences between the devices, and differences cannot be observed between the HSG and annealed glass regarding the thicknesses.

4.5. Overall bow

The overall bow values can be seen in *Fig. 9*. These values are created from the average value of the maximal of the three measured lines. This average was necessary because the glass specimens had twisted own shape. The former wrote statements of the sinus wave are also true for the overall bow. Tendencies and correlations in function of the thickness and lamination cannot state that they are only predictable due to the high standard deviation of the glass material. It is also true that the overall bow values of the HSG glasses are general 10 times larger than the annealed glass values. The smallest difference was measured on laminated glasses which consisted two 4 mm thick glass layers, the value of the HSG specimen was 27% larger than the annealed specimen. The maximum overall bow of the HSG was 38 times larger than the annealed glass. The overall bow is influenced more by the own stresses of the specimens, the cutting out from the basic glass plate, the lamination process and the basic glass producing process. The overall bow is the highest if the specimen contains more HSG layers. It can be seen obviously that the lamination process increases the overall bow of the annealed glass, however this tendency cannot be observed in case of HSG due to the effect heat strengthening procedure. The effect of the lamination process caused at least 89% increasing based on the comparison of the measured overall bow values. The maximum difference was more than 6 times larger between the laminated and the single layered glass.

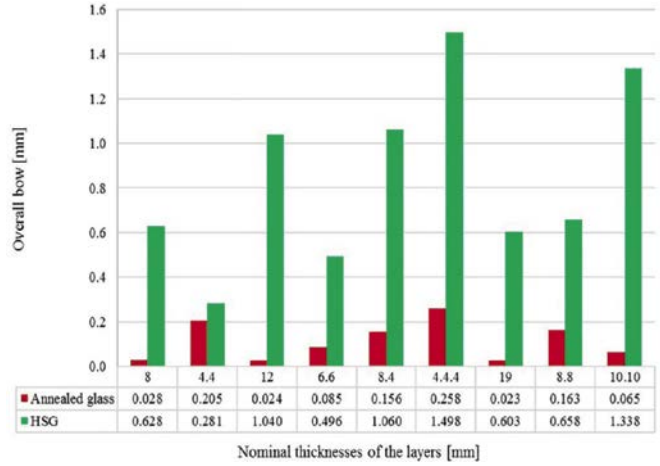

	8	4.4	12	6.6	8.4	4.4.4	19	8.8	10.10
Annealed glass	0.028	0.205	0.024	0.085	0.156	0.258	0.023	0.163	0.065
HSG	0.628	0.281	1.040	0.496	1.060	1.498	0.603	0.658	1.338

Fig. 9. Overall bow results in function of the nominal thicknesses of the layers
9. ábra Kezdeti kihajlások értékei a névleges vastagság függvényében

The overall bow and sinus wave values are given directly in mm/m unit as in the standards, because the common height of the measured specimens was 1000 mm [2,3]. Andreas Luible [11] provides in his thesis limits for initial deformation for annealed glass it was less 1/2500 while sinusoidal distortion of HSG can be 1/300 of the edge length L [11,12]. The size effect can also be caused by differences in the values if we compare the sinus wave and overall bow values which were measured by J. Belis et al. [1]. They determined L/400 initial imperfection when they analyzed different sized glasses with maximum length of 3000 mm for annealed glass and HSG. The limits of horizontally HSG are 3.0 mm/m for overall bow and 0.3 mm roller wave according the standard EN 1863-1:2012

[2]. However, our results reached only the half or less of these limits. The design parameters need sufficient safety factor, but the cost-effectiveness is also one of the most important goals in the building designing.

The maximal determined limits can be seen in *Table 1* based on the laboratory measurements. The experienced values are less than the measured values of the other researchers.

Type of distortions	Type of glasses	Single layer	Laminated consisted of two glass layers	Laminated consisted of three glass layers
Overall bow	Annealed glass	~L/35000	~L/4800	~L/3800
Overall bow	HSG	~L/960	~L/740	~L/660
Sinus wave	Annealed glass	~L/285000	~L/149000	no data
Sinus wave	HSG	~L/17900	~L/27200	~L/42900

Table 1. Maximal determined limits for overall bow and sinus wave distortions in function of the number of the layers without statistical analyzing
1. táblázat A kezdeti kihajlás és a szinusz hullámok legnagyobb mért határértékei a hőkezelés és a rétegszám függvényében statisztikai analízis nélkül

5. Influence of the initial imperfection on the load bearing capacity

5.1. The basic influence factors of buckling

The glass specimens were loaded by axial compression after their distortions have been measured. Thereby interesting conclusions can be drawn about the basic correlation between the measured own shape and the loading history including the buckling phenomenon. First of all, the key issue was: can the glass specimen be characterized by the sinus wave or by the overall bow for the buckling resistance design? If the answer is yes it means that few parameters are enough about the initial imperfection to design load bearing glass columns similarly as in case of the main construction materials (w_0 - limit). However, the answer is not based on the experimental results. The sinus wave and the overall bow are important data of the specimen, but the own shape provides relevant information about the glass specimen and for instance the buckling behaviour. The glasses consist of different waves, some are smaller and some are larger which seriously influence the buckling behaviour (*Fig. 4*). The buckling behaviour is also influenced by the stiffness of the fixing area, the bending stiffness of the glass and the skewness of the glass specimens. The human workers can also cause the reduction of the buckling resistance with mistakes at the adjusting. Therefore, the influencing factors are complex.

5.2. Numbers of analysed specimens

The buckling forces were determined in case of the first and second group based on the applied load vs. horizontal displacement diagrams. The maximal forces were easily determined if the specimens were loaded until fracture in case of all specimens. Further 44 specimens were tested next to the mentioned 22 specimens. Each type of specimen had two new pieces which were only compressed until fracture. The distortion measurement was done only on one specimen per groups and the most curved glasses were chosen with visual inspection from the groups. It means that the measured specimens are the most curved specimen with high probability. The selection was not random so the properties of rather curved glasses were investigated. The correlation can be nominated from this special aspect and newer conclusions can be drawn.

5.3. Maximal forces and buckling forces

The maximal forces were compared to each other in each type of groups. The maximal forces were close to each other in percentage, they varied between 82 – 125 %. It included the annealed glasses and HSG. However, the limit of these range is serviced by the annealed glass. The range is between 86 – 108 % for HSG. These ranges are very close to each other compared to the buckling force ranges. The range of buckling forces were between 45 – 302 % for annealed glass, and 28 – 217 % for HSG. The annealed glass values move in wider range, the minimal percentage is greater, than the HSG minimal value therefore, the annealed glass can be a better choice for glass columns material from the approach of reliability of the buckling force. The annealed glasses bear the design load with higher probability without stability losing than the HSG columns in case of buckling resistance design of the plate glass columns. This designing theory is slightly confused because the HSG has higher energy dissipation, toughness that is an advantage over the annealed glass.

5.4. Distortion effects on the maximal and the buckling forces

The maximal forces were independent from the overall bow and sinus wave values. These results are represented with the small range and despite the fact that the chosen glasses were the most curved specimens from each group the maximal forces were close to each other. The similar groups, where the difference was only the heat strengthening, have similar maximal forces. A ratio was calculated from the annealed glass and HSG maximal forces, where 9 groups results were between 97 – 104 % so in 7 % and about 12 % difference was determined at the further two groups. In case of the buckling forces the annealed glass results proved to be reliable. The range of the higher ratios is between 109 - 199 % this range included 9 groups results the mean percentage was 160 %. In two cases the HSG had higher buckling forces than the annealed with 75 and 91 %. The annealed glass has higher buckling force based on the experimental results, this statement verifies that the resistance of the annealed glass is better for plate glass columns.

From the basic theory of buckling the buckling force is less in case of a curved glass. Lower buckling force can be measured where higher overall bow was measured, which characterizes theoretically the initial imperfection. After all that the maximal forces did not present high differences between annealed and HSG therefore the effects of the overall bow and sinus wave values can be analysed on these specimens. As it has been introduced in *Figs. 8* to *9* the two types of distortions were about 10 times lower in case of annealed glass, where only the heat strengthening is the difference between the two types of glasses. It can be stated that the buckling force can be increased in case of lower overall bow and sinus wave values based on these

results. The rate of reduction cannot be determined because more data is needed about similar specimens which belong to one group. However, it is already stated that the own shape of the specimens (smaller - larger waves) has greater influence on the buckling behaviour. There were a few annealed specimens as exceptions where the measured buckling force was less despite of the less overall bow and sinus wave values in comparison of their HSG pairs. Theoretically the sinus waves can increase the critical buckling force but the unloaded axis of the glasses are not necessary linear shaped as it can be seen in *Fig. 4*. In these cases, the sinus wave does not influence the buckling force. If the overall bow could be kept on a low value for instance on the values of the annealed glass, and the glass has sinus waves it is imaginable that the specimen belongs to the first class of buckling phenomenon and has higher buckling force.

6. Experimental results and tin-air side correlations

6.1. Literature about tin-air side effects

Before the compression tests the tin side was detected on numerous glass specimens by LED technology. The applied measuring device is the Bohle TinCheck apparat. The properties of the glass surface are different depending on the tin side or atmospheric (air) side. The authors are interested that are there any influence of the types of sides on the buckling phenomenon as well? Are there any correlations between the buckling direction, the surface distortion and the types of sides? The question is justified because in most of the cases the type of sides can change the efficiency of the glass processing works. For instance, the adhesion on the atmospheric side is more efficient than on the tin side [13]. Higher compressive surface stress develops on the atmospheric side than on the tin side in case of the chemically strengthening [14].

6.2. Tin-air side effect on the buckling direction

In the research the tin-air side effect was also investigated. Clear correlation cannot be detected between the type of glass side and the buckling direction based on the experimental results of 119 specimens. The main curves of the specimens were determined visually before the compression test. The specimens were inserted into the testing machine so that the proved buckling direction carries left to protect the sensitive devices on the right side viewed from the front (*Fig. 2*). Therefore, it formed more left buckled results than right. The glass sides were also laminated randomly. There are not clear results and tendencies. The distribution of the specimens formed similar in case of the left and right buckling direction in *Table 2*.

Buckling direction	Air-air sides	Air-tin sides	Tin-air sides	Tin-tin sides
Left	12	10	10	11
Right	5	6	3	5

Table 2. The number of left and right buckling direction of tested specimens depending on the tin and air side of the laminated glass specimens consisted of two layers (Annealed glass and HSG together).
2. táblázat A jobbra és balra kihajlott próbatestek darabszáma az ónos és a levegős oldal függvényében

6.3. Tin-air side effect on the distortions

The effects of the tin and air side were analysed based on the distortion measurement results. The number of the analysed specimens were low because only the 22 specimens were proper to analyse the distortion measurement results. Only those specimens could be analysed which had different sides - the single layer glasses and some laminated glasses - and where sinus wave or overall bow results were measurable. *Table 3* introduces the number of specimens which had higher distortion results depending on the heat strengthening effect and the proper side. An example: the overall bow data of the tin side were larger than the results of air side in case of 2 annealed specimens. It can be seen that there is no clear result to decide the standard phenomenon. Probably, these effects are not enough to change significantly the overall bow and sinus wave values of glasses, despite the fact that differences of the surface properties can be detected between the tin or atmospherically side. The results vary randomly.

Type of glass	Overall bow and tin-side	Overall bow and air-side	Sinus wave and tin-side	Sinus wave and air-side
Annealed	2	3	1	1
HSG	4	4	6	2

Table 3. The number of the higher distortion values on the tin and air side in case of annealed glass and HSG.
3. táblázat A nagyobb felületi deformációkkal rendelkező próbatestek darabszáma az ónos vagy levegős oldalon az üvegek fajtájának függvényében

6.4. Tin-air side effect on the own shape

The own shapes of the right specimens – single layer or laminated glass with different type of sides - were analysed in function of the effects of the tin or air side. There were tendencies between the own shapes and the surfaces however the tendencies were caused rather by the heat strengthening and the lamination process. There was no phenomenon which is attributable to the tin-air effect, however it is possible that there are some effects at lower sizes which can influence the distortions of the specimens, but the extent of the effect is not measurable in the investigated range. It means that the role of tin-air effect is more important on the efficiency of lamination, adhesion and the surface strength of the glass structure designing than at the stability issues of glass columns.

7. Conclusions

Engineers have to calculate with the application of safe designing formulas and parameters which are serviced by the researchers in case of glass structures. The applied formulas and parameters have to be further developed to reduce the building costs. This approach helps the glass structures, designing and constructions to evolve unabated. New distortion measurement methodology was introduced to analyse the own shape, the sinus wave and overall bow values of plate glass columns. Both surfaces of 22 specimens were measured by the distortion measurement methodology which were also loaded by central compression until fracture. The measured results do

not reach the limits of the overall bow and sinus wave based on the standards. Moreover, most of the results were less than the half of limits in the standards and in the literature. The overall bow depends on the one hand on the glass producing method and on the other hand on the size effect. The increasing of the length of glass causes the larger overall bow values. The results of HSG were about 10 times larger than the values of annealed glass. The maximal load of plate glass columns can be estimated more safely over the buckling force, where the annealed glass had larger and more reliable results than the HSG. Therefore, it can be stated that annealed glasses are more suitable for plate glass columns than HSG. The influence of the sinus wave and overall bow on the buckling force is less than the own shape of the specimen which can influence the buckling resistance of glasses to a great extent. The maximal load is totally independent of the distortion results. Therefore, it is recommended to introduce other parameters (for example the individual own shape of glasses) at the critical buckling force designing instead of the overall bow. Despite that the tin-air effect causes differences on the properties of the glass sides it does not influence the buckling direction, the sinus wave, overall bow and the own shape results. Considering these statements, it can be concluded that the effect of the tin and air side is negligible at the load bearing capacity of glass columns and at the buckling force as well compared to the other factors which are more relevant: heat strengthening, the own shape of glass, gravity, the fixing area and the human impacts. The benefits of these results that engineers do not have to pay attention to the type of sides of glass plates during the designing and construction processes on the buckling point of view.

8. Acknowledgements

Authors express their gratitude to Rákosy Glass Ltd. for providing the specimens. Authors are thankful to the Department of Construction Materials and Technologies, BME for the technical support. The distortion measurement support is gratefully acknowledged to Balázs Petróczi, who is CAD Development engineer of Salgglas Ltd.

References

[1] Belis, J. – Mocibob, D. – Luible, A. – Vandebroek, M. (2011): On the size and shape of initial out-of-plane curvatures in structural glass components, *Construction and Building Materials* 25, 2700-2712. https://doi.org/10.1016/j.conbuildmat.2010.12.021

[2] EN 1863-1:2012, Glass in building – Heat strengthened soda lime silicate glass – Part 1: Definition and description.

[3] EN 572-2:2013, Glass in building – Basic soda lime silicate glass products – Part 2: Float glass.

[4] Amadio, C. – Bedon, C.(2010): An analytical model for buckling evaluation of laminated glass beams in bending and compression. *Proceedings of XXV. A.T.I.V. International Conference*. Glass, when Technology Meets Design.

[5] Bedon, C. – Amadio, C. (2012): Buckling Verification of Laminated Glass Elements in Compression. *JCES Volume 1*, Issue 3. pp. 90-101.

[6] Kalamar, R. – Bedon, C. – Eliasova, M. (2016): Experimental investigation for the structural performance assessment of square hollow glass columns. *Engineering Structures* 113. pp. 1-15. https://doi.org/10.1016/j.engstruct.2016.01.028

[7] Jakab, A. – Nehme, K. – Nehme, S.G. (2015): Laboratory Experiments of Centrally Loaded Glass Columns, GPD – *Glass Performances Days*. Tampere, Finland, ISBN: 978-952-5836-03-5, 117-121.

[8] Bedon, C. – Amadio, C. (2016): Design buckling curves for glass columns and beams. *Structures and Buildings*. Volume 168 Issue SB7. pp. 514-526. https://doi.org/10.1680/stbu.13.00113

[9] Jakab, A. – Nehme, K. – Nehme, S. G. (2015): Stability Questions of Centrally Loaded Glass Columns, *METNET Annual Seminar in Budapest*, Hungary, 7-17. ISBN 978-951-784-762-9

[10] Jakab, A. – Nehme, K. – Nehme, S. G. (2016): Classification of "I" – shaped glass columns, *CCC2016 Proceedings*. ISBN: 978-615-5270-24-6 pp. 78-83. https://doi.org/10.1016/j.proeng.2016.11.608

[11] Luible, A. (2004): Stabilitat von Tragelementen aus Glas, These EPFL 3014, Ecole polytechnique federale de Lausanne (EPFL), Lausanne

[12] Luible, A. (2005): Plate Buckling of Glass Panels, *GPD – Glass Performance Days*

[13] Mognato, E. – Schiavonato, M. – Pittoni, M. (2015): Chemically Strengthened Glass: correlation between Surface Compression, Potassium Profile, Mechanical Strength and production parameters, *GPD – Glass Performance Days*. Tampere, Finland, ISBN: 978-952-5836-03-5, pp.411-415.

[14] Stahldanke, C. – Sehati, P. – Sundberg, P. – Mattsson, L. – Siovall, P. – Albinsson, O. – Lundevall, A. (2015): The influence of surface composition and plasma treatment on adhesion, *GPD – Glass Performance Days*. Tampere, Finland, ISBN: 978-952-5836-03-5, pp. 266-269.

Ref.:
Jakab, András – **Nehme**, Salem Georges: *Influencing factors of the plate glass columns on the load bearing capacity*
Építőanyag – Journal of Silicate Based and Composite Materials, Vol. 70, No. 2 (2018), 62–69. p.
https://doi.org/10.14382/epitoanyag-jsbcm.2018.12

Sík lapokból álló üvegoszlopok teherbírását befolyásoló tényezők

A statikai számításokban figyelembe vesszük a tervezés során a szerkezeti elemek kezdeti imperfekcióját. Az üvegszerkezetek esetében kezdeti imperfeckiók lehetnek lokális vagy globális hibák, amik jelentősen tudják csökkenteni a teherbírási kapacitást és a használhatósági határállapotot. Az általános építőanyagok esetében a stabilitási tervezés tartalmazza a kezdeti görbületet és imperfekciót, amiknek a figyelembe vett értéke függ az elem keresztmetszetétől. A teherbíró üvegszerezetek tervezése még mindig újdonságnak számít, azonban alkalmazandó határértékeket már megfogalmaztak. Több mint 240 kisméretű „I" keresztmetszetű üvegpróbatest vizsgálatán alapuló kísérletben vizsgáljuk a rugalmas kihajlás tulajdonságait. A kísérletek során az egyik legfontosabb tényező volt a kezdeti imperfekció. A kezdeti kihajlás és a szinusz hullámok alapvetően kedvezőtlenül befolyásolják az üvegoszlopok teherbírását, azonban a szinusz hullámok hatása akár növelheti is az Euler-i kihajlási ellenállást a rúdban található szinusz hullámok számának növelésével. A kezdeti imperfekciókat és a vizsgált próbatestek saját alakját egy új mérési módszerrel vizsgáltuk, amiben referencia pontrendszert alkalmaztunk a lehető legnagyobb mérési pontosság érdekében. A méréssorozatban az üvegfeldolgozási munkák a próbatesteken végzett hatásait is vizsgáltuk.

Kulcsszavak: üveg, kihajlást befolyásoló tényezők, kezdeti alak, ónnal és levegővel érintkező felület, referencia pontrendszer

Conference ic-rmm3 – where science met five continents

Emese KUROVICS ▪ Bronislav KANEV ▪ Sergey SITKEVICH

The 3rd International Conference on Rheology and Modeling of Materials (ic-rmm3) was held in the marvelous historical palas Hotel PALOTA in the wonderful environment of Mountain Bükk (Hungary) in October 2-6, 2017.

In the conference have participated and made oral, short oral or poster presentation 122 scientists from 36 different countries of Asia, Europe, North- and South America, Africa and Australia. The largest delegations of scientists have arrived to Central Europe from Russian Federation, Czech Republic, China and Austria. The conference was opened by Prof. Sergey N Kulkov from Tomsk State University at 2:00 pm in Monday afternoon and after was continued in two different sections. In his opening speech Prof. Kulkov has welcomed the conference participants and mentioned by name Miss Siti Nadjiha from New Zeeland and Diego Genovese from Argentina, from the countries that are most distant from Hungary. He has specially greeted Prof. László A Gömze with the jubilee of 40 years teaching and research experiments in the University of Miskolc in September 2nd, 2017.

In the afternoon of October 3rd a part of participants had visited the monuments of city Miskolc including the old Castle of King Louis the Great, University of Miskolc and Thermal Cave Bath.

In October 4th the other part of the conference attendees have participated in a castle tour excursion in the Tokaj Wine Region including wine tastes in one of the cellars at Hercegkút which belong to the world heritage.

During the all 5 days of **ic-rmm3** conference the participants had opportunity to vote on the best posters and the best short oral presentation. The results of the votes were evaluated by the members of the International Scientific Advisory Board in each days. Finally in the poster session 2 posters were awarded as "**Best Poster**", one of them **Prof. Amirullah Mamedov** from the Bilket University, Turkey and the group of young authors **M Cvek, T Plachy, J Osicka, E Kutalkova, M Mrlik, M Sedlacik** from Tomas Bata University, Czech Republic. The "**Best Short Oral**" was awarded to Sara Lairah Mugabo from Swansea University, United Kingdom. The awards were handed by Prof. Anil Saigal Tufts University from USA, Prof. László A Gömze University of Miskolc, Hungary and Academician Prof. Valerii Kulichikhin the president of Vinogradov Society of Rheology from Russia.

Book of abstract and more information about conference you can find: www.ic-rmm3.eu.

Conference program you can download by http://www.ic-rmm3.eu/icrmm3_program0928.pdf.


ne New DISCOVERY
YBRID RHEOMETER
The 3rd Internatio

GUIDELINE FOR AUTHORS

The manuscript must contain the followings: title; author's name, workplace, e-mail address; abstract, keywords; main text; acknowledgement (optional)**; references; figures, photos with notes; tables with notes; short biography** (information on the scientific works of the authors).

The full manuscript should not be more than 6 pages including figures, photos and tables. Settings of the word document are: 3 cm margin up and down, 2,5 cm margin left and right. Paper size: A4. Letter size 10 pt, type: Times New Roman. Lines: simple, justified.

TITLE, AUTHOR

The title of the article should be short and objective.

Under the title the name of the author(s), workplace, e-mail address.

If the text originally was a presentation or poster at a conference, it should be marked.

ABSTRACT, KEYWORDS

The abstract is a short summary of the manuscript, about a half page size. The author should give keywords to the text, which are the most important elements of the article.

MAIN TEXT

Contains: materials and experimental procedure (or something similar), results and discussion (or something similar), conclusions.

REFERENCES

References are marked with numbers, e.g. [6], and a bibliography is made by the reference's order. References should be provided together with the DOI if available.

Examples:

Journals:

[6] Mohamed, K. R. – El-Rashidy, Z. M. – Salama, A. A.: In vitro properties of nano-hydroxyapatite/chitosan biocomposites. *Ceramics International.* 37(8), December 2011, pp. 3265–3271, http://dx.doi.org/10.1016/j.ceramint.2011.05.121

Books:

[6] Mehta, P. K. – Monteiro, P. J. M.: Concrete. Microstructure, properties, and materials. *McGraw-Hill*, 2006, 659 p.

FIGURES, TABLES

All drawings, diagrams and photos are figures. The **text should contain references to all figures and tables**. This shows the place of the figure in the text. Please send all the figures in attached files, and not as a part of the text. **All figures and tables should have a title**.

Authors are asked to submit color figures by submission. Black and white figures are suggested to be avoided, however, acceptable.

The figures should be: tiff, jpg or eps files, 300 dpi at least, photos are 600 dpi at least.

BIOGRAPHY

Max. 500 character size professional biography of the author(s).

CHECKING

The editing board checks the articles and informs the authors about suggested modifications. Since the author is responsible for the content of the article, the author is not liable to accept them.

CONTACT

Please send the manuscript in electronic format to the following e-mail address: femgomze@uni-miskolc.hu and epitoanyag@szte.org.hu or by post: Scientific Society of the Silicate Industry, Budapest, Bécsi út 122–124., H-1034, HUNGARY

We kindly ask the authors to give their e-mail address and phone number on behalf of the quick conciliation.

Építőanyag – *Journal of Silicate Based and Composite Materials*, Quarterly peer-reviewed periodical of the Hungarian Scientific Society of the Silicate Industry, SZTE.
http://epitoanyag.org.hu

About EGU

EGU, the European Geosciences Union, is Europe's premier geosciences union, dedicated to the pursuit of excellence in the Earth, planetary, and space sciences for the benefit of humanity, worldwide. It was established in September 2002 as a merger of the European Geophysical Society (EGS) and the European Union of Geosciences (EUG), and has headquarters in Munich, Germany.

It is a non-profit international union of scientists with about 15,000 members from all over the world. Membership is open to individuals who are professionally engaged in or associated with geosciences and planetary and space sciences and related studies, including students and retired seniors.

The EGU publishes a number of diverse scientific journals, which use an innovative open access format, and organises a number of topical meetings, and education and outreach activities. It also honours scientists with a number of awards and medals. The annual EGU General Assembly is the largest and most prominent European geosciences event, attracting over 14,000 scientists from all over the world in recent years. The meeting's sessions cover a wide range of topics, including volcanology, planetary exploration, the Earth's internal structure and atmosphere, climate, as well as energy and resources.

www.egu.eu

Association Européenne pour la Protection Passive contre l'Incendie
Europäischer Verband für Passiven Brandschutz
European Association for Passive Fire Protection

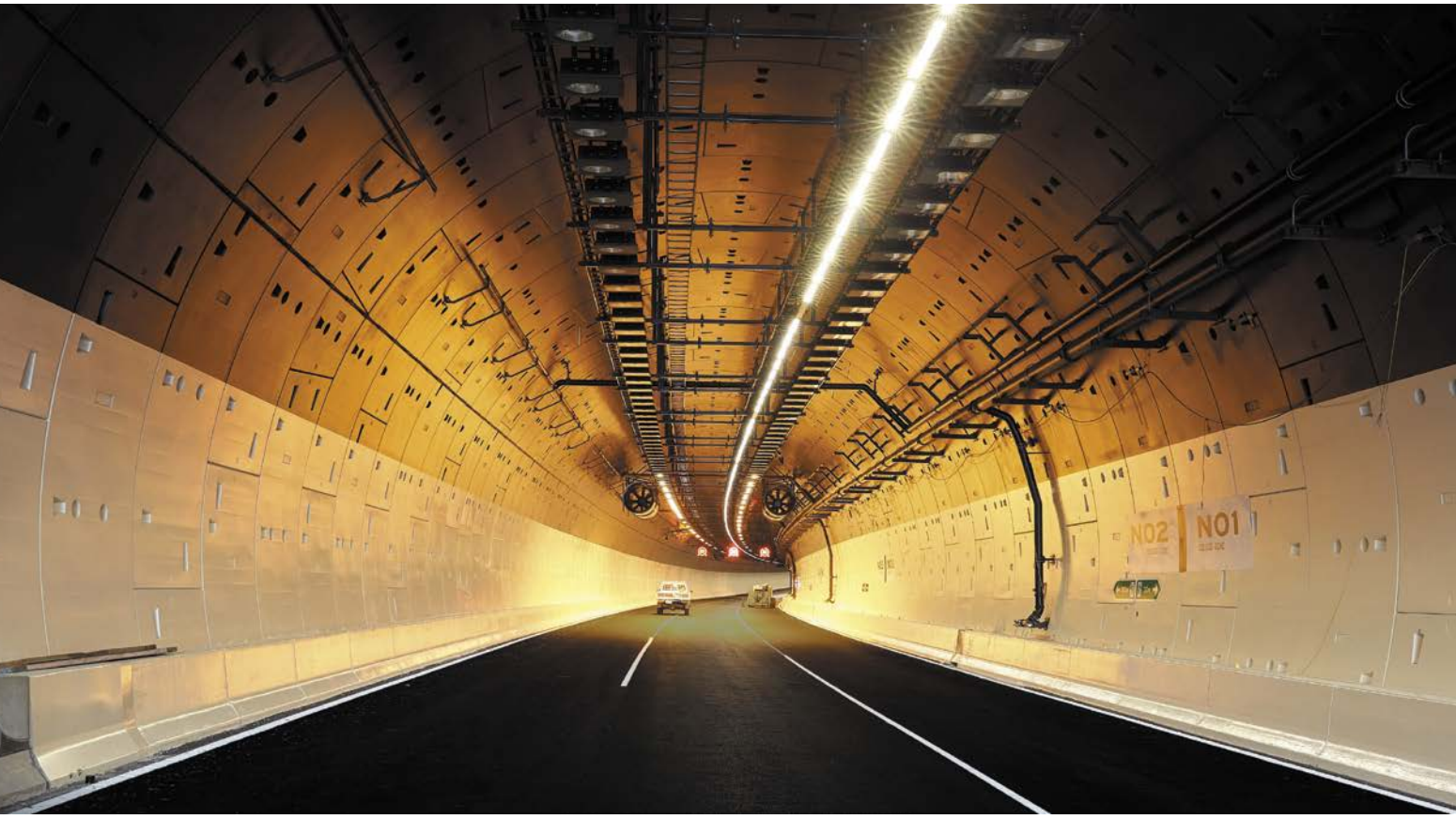

EAPFP was formed in 1988 to act as a “European” voice on behalf of national associations representing manufacturers, contractors and other institutions involved in fire protection to steelwork, timber, and other passive fire protection applications, including penetration seals and ductwork.

EAPFP has representation on CEN TC 127, the Technical Committee dealing with the harmonisation of standards for fire safety buildings. Close liaison is maintained with EGOLF the European Organisation for Fire Testing Laboratories. Joint Conferences have been held down the years. The last event was held at Jean Monnet Building Luxembourg entitled “Revising the Construction Products Directive - The impact on construction products with a fire performance”

Meetings of the Association are held on a regular basis at venues throughout Europe to update members on technical issues and to develop closer commercial contacts.

EAPFP, Kingsley House, Ganders Business Park, Kingsley, Bordon, Hampshire GU11 2LL
www.eapfp.com